PONTIFÍCIA UNIVERSIDADE CATÓLICA
DO RIO DE JANEIRO

Alexandr Zhemchuzhnikov

Influence of clay content and suction on the strength of compressed earth blocks

TESE DE DOUTORADO

Thesis presented to the Programa de Pós-Graduação em Engenharia Civil of the Departamento de Engenharia Civil, PUC-Rio as a partial fulfillment of the requirements for the degree of Doutor em Engenharia Civil

Advisor: Profª. Michéle Dal Toé Casagrande
Co-Advisor: Prof. Khosrow Ghavami

Rio de Janeiro
December 2015

Alexandr Zhemchuzhnikov

Influence of clay content and suction on the strength of compressed earth blocks

Thesis presented to the Programa de Pós-Graduação em Engenharia Civil of the Departamento de Engenharia Civil do Centro Técnico Científico da PUC-Rio as partial fulfillment of the requirements for the degree of Doutor.

Profª. Michéle Dal Toé Casagrande
Advisor
Departamento de Engenharia Civil — PUC–Rio

Prof. Khosrow Ghavami
Co-Advisor
Departamento de Engenharia Civil – PUC-Rio

Prof. Celso Romanel
Departamento de Engenharia Civil – PUC-Rio

Prof.ª Raquel Quadros Velloso
Departamento de Engenharia Civil – PUC-Rio

Prof. Conrado de Souza Rodrigues
Centro Federal de Educação Tecnológica de Minas Gerais

Prof. Romildo Dias Toledo Filho
Universidade Federal do Rio de Janeiro

Prof. Fathi Aref Ibrahim Darwish
Universidade Federal Fluminense

Prof. Márcio da Silveira Carvalho
Coordinator of the Centro Técnico Científico da PUC-Rio

Rio de Janeiro, 17th December 2015.

Alexandr Zhemchuzhnikov

The author is graduated in Mining Engineering from Peoples' Friendship University of Russia in 2009. Received MSc in Geotechnical Engineering at Pontifícia Universidade Católica do Rio de Janeiro in 2009. In 2011 joined PhD programme at the same university to research the use of soil as a construction material.

Bibliographic Data

Aknowledgements

Abstract

Zhemchuzhnikov, Alexandr; Dal Toé Casagrande, Michéle; Ghavami, Khosrow. **Influence of clay content and suction on the strength of compressed earth blocks.** Rio de Janeiro, 2015. 157 p. PhD Thesis – Departamento de Engenharia Civil, Pontifícia Universidade Católica do Rio de Janeiro

Soil is a sustainable construction material that has been used traditionally for thousands of years. In general, earth construction specifications are based on common knowledge. Existing recommendations tend to be supported by a limited number of studies and depend on local materials, climatic conditions and historical background. The lack of understanding of compacted soil behavior, in particularly its strength, may have prevented a wider application of earthen construction materials in housing. Understanding of the soil properties and parameters that influence its performance when used in walls and columns is essential for interpretation of experimental data. Recently a number of studies have analyzed rammed earth considering unsaturated soil mechanics, which suggest loss of strength following decrease in suction values, for example provoked by the increase in relative humidity. However, there is a lack of such research pertaining to compressed earth blocks (CEBs). The objective of this study was to verify the influence of clay content, density and suction on the strength of CEBs. Four soil mixes consisting of sand, quartz powder and kaolinitic clay were used. For each soil mix statically compacted samples with densities corresponding to optimum and dry of optimum moisture contents were tested for a range of suctions. Unlike reported in the literature, the results showed loss of strength following increase in suction values, while only small variations were registered for suctions corresponding to a wide range of RH and temperature conditions. The findings can be of use for specifications relating to construction of sustainable housing using CEBs.

Keywords

Resumo

Zhemchuzhnikov, Alexandr; Dal Toé Casagrande, Michéle; Ghavami, Khosrow. **Influência do teor de argila e da sucção na resistência dos blocos de solo compactado.** Rio de Janeiro, 2015. 157 p. Tese de Doutorado – Departamento de Engenharia Civil, Pontifícia Universidade Católica do Rio de Janeiro

Solo é um material de construção sustentável que tem sido utilizado por milhares de anos. As normas técnicas e recomendações existentes referente à construção de terra são baseadas em número limitado de estudos e dependem de materiais, condições climáticas e tradições locais. A compreensão dos parâmetros que influenciam o comportamento do solo compactado quando o mesmo utilizado em paredes e colunaas é essencial para a interpretação dos dados experimentais. Diversos estudos recentes analizaram taipa de pilão do ponto de vista da mecanica de solos nçao saturados, observando o decrescimo da resistência com a diminuição da sucção, causada por exemplo pelo aumento da humidade do ar. Porém, não hã uma pesquisa semelhante pertinente aos blocos de solo compactado. O objetivo do presente trabalho foi verificar a influência do teor de argila, dencidade e sucção na resistência dos blocos de solo compactado. Foram utiliazdas quatro dosagens de solo artificial que consistiu de areia, pó de quartzo e argila caulitinitca. Para cada dosagem, amostras estaticamente compactadas na umidade ótima e no ramo seco foram ensaiadas variando-se a sucção. Ao contrário dos resultados encontrados comunmente na literatura, a resistência das amostras diminuiu com o aumento da sucção, enquanto a influência das condições climáticas como umidade e temperatura foram mínimas. As conclusões feitas no presente trabalho podem ser utilizadas nos projetos de construção sustentável com emprego de blocos de solo compactado.

Palavras - chave

Bloco de solo compactado; Sucção; Argila; Resistência à compressão simples

Contents

List of figures

List of tables

List of abbreviations

CC	Clay content
CEB	Compressed earth block
EE	Embodied energy
EC	Embodied carbon
OMC	Optimum moisture content
PSD	Particle size distribution
PI	Plasticity index
PL	Plastic limit
RH	Relative humidity
RMSE	Root mean squared error
SC	Silt content
SWRC	Soil water retention curve
UCS	Unconfined compressive strength

List of symbols

A   Cross-sectional area

A_c Corrected cross-sectional area

A_i Initial cross-sectional area

B   Skempton's pore pressure coefficient

c   Drained compressibility of aggregated soil

c'   Effective cohesion

c_g Drained compressibility of the material forming the aggregates

C_c Coefficient of curvature

C_u Coefficient of uniformity

D   Maximum grain diameter

d   Specimen diameter

d_{10} Particle size for which 10% of soil is finer

d_{30} Particle size for which 30% of soil is finer

d_{60} Particle size for which 60% of soil is finer

e   Void ratio

E   Elastic modulus, energy

E_{vol} Energy density

f_i Predicted values

F   Force

G_s Specific gravity of solids

h   Water pressure head, height of rammer drop

I   Second order identity tensor

IDT   Tensile strength obtained by diametrical compression

k   Number of «subsystems» that form total pore distribution

L   Specimen length

LL   Liquid limit

m   Mass of the rammer

m_{wet} Wet mass of the specimen

m_{dry} Dry mass of the specimen

M_w Molecular mass of water

n	Porosity, grading coefficient
n_b	Number of blows
n_l	Number of layers
p	Proportion of grains of given diameter
Q(x)	Complementary cumulative normal distribution function
r_d	Displacement rate
R	Roundness, universal gas constant
R_C	The radius of the circumscribed circle centered at the center of mass
R_I	The radius of the inscribed circle
s	Suction
s_{air}	Air entry value
s_t	Total suction
S	Sphericity, degree of saturation
S_e	Effective saturation
t_f	Time to failure
T	Absolute temperature in kelvin
u_a	Pore air pressure
u_{ma}	Micropore air pressure
u_{mw}	Micropore water pressure
u_w	Pore water pressure
u_{Ma}	Macropore air pressure
u_{Mw}	Macropore water pressure
V	Volume of the specimen
V_i	Initial volume of the specimen
w	Water content
w_i	Weighing factor
x	Displacement
$\bar{y}$	Mean of the observed data
y_i	Measured values
σ_{rup}	Modulus of rupture
α	Fitting parameter, inverse of air entry value
α_m	Microscopic effective stress parameter of saturated double porous media

α_M	Macroscopic effective stress parameter of saturated double porous media
ε_a	Axial strain
ε_{vol}	Volumetric strain
λ	Pore size distribution index
ρ_d	Dry density of soil
σ	Total stress
σ'	Effective stress
σ_{C0}	Intergranular bonding stress
σ'_s	Suction stress
σ_t	Tensile strength
τ	Shear strength
θ	Volumetric water content
θ_s	Saturated volumetric water content
θ_r	Residual volumetric water content
φ'	Effective angle of internal friction
χ	Effective stress parameter
χ_M	Unsaturated effective stress parameter of macropores
χ_m	Unsaturated effective stress parameter of micropores

1
Introduction

The use of soil as a construction material dates back thousands of years. It is one of the first construction materials used by man. In the areas with no timber or stone available the dwellings were constructed entirely with earth. This provided a background for development of several construction techniques. Depending on local conditions and tradition, the earth was compacted by hand or with the aid of rammers, formed into walls or individual bricks of different shapes, mixed with straw and other natural fibers. A great number of historical structures that survived until nowadays reveals the variety of structures and complexity that could be achieved using soil as a construction material. Traditional earth construction techniques have been preserved through generations in some places, yet they have not been systematically registered.

As a result of industrial revolution, the use of concrete, steel and other industrialized materials became widespread and earth construction was mostly abandoned. As modern engineering was rapidly developing, a lot of research on these materials was carried out, numerous institutions dedicated to it appeared. Eventually, public opinion was formed in which traditional construction methods begun to be associated with poverty and underdeveloped urban and rural areas, whereas new industrialized materials - with science and progress.

In the 20th century it became evident that industrial development, in its current form, is accompanied by harmful consequences for the environment. Numerous ecological disasters, climate change, water and air pollution brought the necessity for sustainable development, making environmental concern a demand for any industry, of which construction is one of the most polluting. It operates with enormous volumes of material. Construction industry consumes almost 50% of world's raw material by weight (about 3000 Mt/year) [1]. The methods of obtaining raw materials cause strong environmental impact and their processing is inefficient. In 2000 mining raw material use was of 0.15%, thus generating huge amounts of waste which disposal is complex and often dangerous

[2]. Modern buildings are in many cases energetically inefficient and have poor thermal and acoustic insulation. This enforces the use of air conditioning, heating systems, and insulation materials. The downsides of such approach are high energy consumption and in many cases unfavorable indoor climate [1]. Thermal insulators generally are sophisticated products that involve polluting chemical processes in their production and in the case of fire emit toxic gases that cause the majority of fatalities in this kind of accidents [2]. After being demolished in the end of their life cycle, industrialized construction materials generate large amounts of waste, even though there is a certain degree of recycling. In the UK buildings are responsible for 50 per cent of primary energy consumption and generate 30 million tons of waste yearly [3].

To asses environmental impact of a material or structure the concept of embodied energy is aplied. It is essentially the energy used during construction process, production and transportation of construction materials [4]. Another indicator is embodied CO_2, as emission of carbon dioxide is viewed as a main driving force of climate change. The main source of CO_2 emission is the combustion of fossil fuels which is the process widely used in energy generation [5]. Table 1.1 shows the environmental impact assessment coefficients for some construction materials.

In order to reduce environmental impact caused by construction activities the materials used should be available locally to minimize energy consumption by transportation, produce little waste and be adequate for using in modern structures, e.g. be compatible with engineering standards.

Soil as a construction material offers a series of economic and environmental advantages. In most cases soil found on site can be used as a construction material, thus needing no transportation. Its strength allows constructing multi-story buildings, it has a good hygroscopic and thermal performance [6]–[11]. The indoor climate of the earthen buildings is favorable for human health thanks to humidity and temperature buffering of the material. Due to its hygroscopic and thermal characteristics, soil smoothes the peaks of temperature and humidity variation inside the building. In hot period of the day earthen homes stay cool, in cold period – warm. When it's too humid, extra moisture is absorbed, when too dry – released. Demolished unstabilized earthen structures generate no waste as the material can be reused or easily integrated into landscape. On the social

perspective, earth construction can stimulate the preservation of local traditions. In the areas with no access to modern technology or industrialized materials, building with earth can provide affordable dwelling.

Table 1.1 Embodied energy (EE) and embodied carbon (EC) coefficients of some construction materials [12]

Material	EE, MJ/kg	EC, kg CO$_2$/kg
Aggregate (gravel or crushed rock)	0.083	0.0048
Cement (average)	4.5	0.73
Cement stabilized soil (5% cement)	0.68	0.060
Common bricks	3.0	0.24
Concrete (1:1.5:3)	1.11	0.159
Expanded Polystyrene insulation	88.60	2.55
Glass fiber insulation (glass wool)	28.00	1.35
Iron	25	1.91
PVC	77.20	28.1
Rammed earth	0.45	0.023
Stabilized soil (8% cement, 2% lime)	0.83	0.082
Steel (recycled)	9.40	0.44
Steel (virgin)	35.40	2.71
Straw bale	0.91	-
Timber	10.00	0.72

The first use of soil as a construction material is estimated to date back 10000 years [13]. There is archaeological evidence of adobe houses built between 8000 and 6000 BC discovered in Turkmenistan [7]. In Mesopotamia the use earth construction dates back to 5000–4000 BC [14].

In the past, the development of earth construction was accompanied by and involved climatic architecture, rainwater collection systems, storage of ice to be used in hot part of the year, use of dove towers for production of fertilizers. In this context some ancient Persian structures can be cited: Yakhchal (Fig. 1.1a) – a building used for ice storage, its thick walls made of earth mixed with natural fibers and egg whites having thermal mass high enough to maintain indoor temperature below zero; Ab Anbar - underground water container used during drought; Badgir (Fig. 1.1b)– a windcatcher tower, that taakes advantage of high

wind currents in order to climatize urban dwellings [15]–[17]. These technologies can be adapted for modern use and combined with earth construction to make a substantial contribution for urban sustainable development.

Fig. 1.1 Persian traditional earth constructions: a) Yakhchal b) Ab Anbar with four Badgirs

Since 1980s there has been a growing interest for research and use of soil as a construction material. A number of conferences and research centers dedicated to earth architecture appeared during these years. There are some countries, such as Australia, New Zealand, US, Mexico, Brazil, that have technical norms, though often incomplete, that regulate earth construction. Australia is reported to have 20% of new buildings made of earth [18]. Non-load-bearing earthen masonry has become a popular option in western Europe, particularly in Germany [19], whereas USA is the greatest consumer of industrialized earth blocks [20]. The use of earth buildings proved helpful in reconstruction of the areas affected by modern conflicts in the Middle East and can provide a cheap housing solution for a growing number of refugees [21].

In spite of its advantages, especially concerning current environmental situation, most engineers are reluctant to use soil for construction. Big companies involved in the construction industry are not interested in promoting cheap materials that can reduce their profit. Besides prejudice and misinformation that are still persistent what prevents dissemination of earth construction is insufficient scientific research on the subject.

The study of soil from the engineering perspective started in the 19th century, an important benchmark being the publication of Terzaghi's «Erdbaumechanik» in 1925. Since the emergence of soil mechanics as a field of science, the progress of the research in foundation, earth dam and highway construction as well as other

geotechnical problems has been evident. However, the use of earth as a material for civil construction has not been studied to this same extent, although the existence of many great historical structures that survive until this day proves its potential. In spite of the advantages offered by soil as a construction material, its widespread application in civil engineering will not be possible without the existence of some generalized theory and commonly accepted standards and building codes. The properties of most construction materials have been studied during an extended period of time and are well known. Concrete, steel, aluminum, plastics and other industrial materials widely used in construction are produced to meet detailed specifications, which allow for little variation. The properties of natural materials, such as soils are not known in advance and depend on local conditions. Unlike concrete which demands normally only quality control tests on site, soils must be thoroughly characterized and a variety of tests should be performed prior to the inception of any engineering project.

2
Objectives

The strength of soil is an essential parameter that should be known to make any structure that implies its use possible. In order to establish this parameter, it is necessary to study the variables that influence it. When used as a construction material, soil is exposed to conditions different from its natural state and those generally studied by classic soil mechanics. The state of stress of soil in a structure demands an approach to material testing similar to one used in structural engineering. However, soil strength is strongly affected by its structure and composition and is susceptible to the influence of the environmental conditions such as temperature and humidity to a greater extent than industrialized materials. Classic soil mechanics deals with saturated soils, whether an earthen wall has a large contact area with atmosphere which allows evaporation. In this situation soil moisture eventually reaches en equilibrium depending on such conditions as relative humidity of air, temperature and pressure. It is argued that unsaturated soil behavior can explain the main mechanism that provides strength for earthen materials. Thus the approach to the study of soil as a construction material must encompass structural engineering as well as classic and unsaturated soil mechanics. Current work aims to combine the concepts of these fields of science to provide an insight into the behavior of earthen structures.

Recently a number of studies have analyzed rammed earth, i.e. dynamically compacted soil, considering unsaturated soil mechanics, which suggest loss of strength following decrease in suction values, for example provoked by the increase in relative humidity (RH). However there is a lack of such research pertaining to compressed earth blocks (CEBs), i.e. statically compacted soil.

The objective of this study was to verify the influence of clay content, density and suction on the unsaturated strength of CEBs. Four soil mixes consisting of sand, quartz powder and kaolinite were used. For each soil mix statically

compacted samples with densities corresponding to optimum and dry of optimum moisture contents were tested for a range of suctions in unconfined compression and diametrical compression. Soil water retention curves were also determined and drained consolidated triaxial tests performed in order to obtain saturated effective stress parameters. Using the experimental data, unsaturated effective stress parameter χ was determined and an attempt to predict the strength of the studied samples with respect to suction was made.

The first part of the present thesis contains the literature review of soil properties relevant to its use in construction, such as composition, classification and properties of different types of clay minerals, the principles of unsaturated soil behavior. Then the review of available research on earthen construction materials' testing and analysis of their performance is made. An experimental program is proposed in order to evaluate the influence of clay content, density and suction on unconfined compressive and tensile strength of statically compacted soil. Finally, the results of the tests carried out are presented and their implications are discussed.

3
Literature review

The following section presents literature review on the topics relevant to the behavior of soil when used as a construction material, criteria for soil selection and the phenomena related to unconfined soil strength. The review of the research on testing earth material strength is also presented.

3.1.
Soil composition

The first step in understanding soil behavior is defining its composition and structure. Soil composition can be described in terms of chemical compounds and their proportions, soil forming minerals, and textural terms such as the size of particles and percentage of material that belongs to certain grain size ranges. The particle size distribution is normally represented by granulometric curve.

Mineralogy is the primary factor controlling the size, shape, and properties of soil particles. If the properties of the minerals which compose the soil are known, it is possible to explain some important aspects of its behavior. Nonclay minerals are inert chemically and electrically, their interactions are defined by physical forces such as friction and gravitation. Soils consisting primarily of nonclay minerals are called granular, in terms of strength envelope they have a relatively high angle of internal friction and are cohesionless. Clay minerals are characterized by very small size, high specific surface, residual electric charge. They are responsible for plastic behavior of soil. Clay fraction has a major influence on soil properties, even when soil contains a greater percentage of granular material.

3.1.1.
Particle size and shape

Soil is frequently considered as consisting of the fractions of particles of different sizes: gravel, sand, silt and clay. The divisions between these fractions vary according to the classification used. The summary of the size limits adopted by different agencies is presented in Table 3.1. The most commonly used classification was proposed in MIT and divides soil into fractions as follows: gravel > 2 mm, coarse sand between 2 and 0.6 mm, medium sand between 0.6 and 0.2 mm, fine sand between 0.2 and 0.06 mm, silt between 0.06 and 0.002 mm, clay finer than 0.,002 mm. The division between sand and gravel at 2 mm can be explained as the point at which capillary effects are negligible and wet soil acts as individual particles, this being property-based distinction [22]. Particles smaller than about 200 mesh sieve size (0.074 mm), which is approximately the boundary between sand and silt, cannot be seen by the naked eye. The particle size of 2 μm that divides silt from clay can be explained by the fact that most clay minerals are smaller than that. However, the particles defined as clay on the basis of their size are not necessarily clay minerals. Fine particles of quartz, oxides and amorphous materials may be present in the clay fraction, behaving as inert material.

Particle size distribution (PSD) of a soil can be characterized by the parameters describing the shape of the the granulometric curve - C_u and C_c. Coefficient of uniformity C_u is defined as follows:

$$C_u = \frac{d_{60}}{d_{10}}$$

(3.1)

where d_{60} and d_{10} correspond to the sieve sizes that 60 and 10 percent of the particles by weight pass through. A soil with C_u from 5 to 10 is considered well-graded. Coefficient of curvature:

$$C_c = \frac{d_{30}^2}{d_{60} \cdot d_{10}}$$

(3.2)

where d_{30} corresponds to the particle size for which 30% of soil is finer. C_c is used to describe whether the soil is gap graded, i.e. if a certain size fraction is missing from particle size distribution. The soils with $C_c < 1$ or $C_c > 3$ are considered gap graded [23].

Table 3.1 Size limits of soil fractions according to different agencies [24]

Agency	Classification	Size limits, mm
U.S. Department of Agriculture (USDA)	Gravel Very coarse sand Coarse sand Medium sand Fine sand Very fine sand Silt Clay	> 2 2 - 1 1 – 0,5 0,5 - 0,25 0,25 - 0,1 0,1- 0,05 0,05 - 0,002 < 0,002
International Society of Soil Mechanics (ISSM)	Gravel Coarse sand Fine sand Silt Clay	> 2 2 - 0,2 0,2 - 0,02 0,02 - 0,002 < 0,002
Federal Aviation Agency (FAA)	Gravel Sand Silt Clay	> 2 2 - 0,075 0,075 - 0,005 < 0,005
Massachusetts Institute of Technology (MIT)	Gravel Coarse sand Medium sand Fine sand Silt Clay	> 2 2 - 0,6 0,6 - 0,2 0,2 – 0,06 0,06 - 0,002 < 0,002
American Association of State Highway and Transportation Officials (AASHTO)	Gravel Coarse sand Fine sand Silt Clay	76,2 - 2 2 – 0,425 0,425 – 0,075 0,075 – 0,002 < 0,002
Unified (U.S. Army Corps of Engineers, U.S. Bureau of Reclamation, and American Society for Testing and Materials)	Gravel Coarse sand Medium sand Fine sand Silt and clay (fines)	76,2 - 4,75 4,75 - 2 2 – 0,425 0,425 – 0,075 < 0,075

The smaller the range of the particles present in soil (the more uniform the soil), the narrower is the range of possible soil densities. A well graded granular soil can reach higher density with finer particles filling voids between coarser ones. At the same time, the particles comprising fine soil fraction frequently have

platy shape and are able to form loose fabric such as cardhouse one. Void ratio ranges of some granular soils can be found in Table 3.2.

Table 3.2 Maximum and minimum void ratios, porosities, and unit weights for several granular soils [25]

	Void ratio		Porosity, %		Dry unit weight, kN·m⁻³	
	e_{max}	e_{min}	n_{max}	n_{min}	$\gamma_{d\ min}$	$\gamma_{d\ max}$
Uniform spheres	0,91	0,35	47,6	26	-	-
Standard Ottawa sand	0,8	0,5	44	33	14,5	17,3
Clean uniform sand	1	0,4	50	29	13	18,5
Uniform inorganic silt	1,1	0,4	52	29	12,6	18,5
Silty sand	0,9	0,3	47	23	13,7	20
Fine to coarse sand	0,95	0,2	49	17	13,4	21,7
Micaceous sand	1,2	0,4	55	29	11,9	18,9
Silty sand and gravel	0,85	0,14	46	12	14	22,9

Particle shape is a characteristic that plays a major role in mechanical behavior of soils. Characterization of particle shape depends on scale. At larger scale the particle can be described as spherical, rounded, blocky, bulky, platy, elliptical, elongated, etc. At smaller scale, the characteristics of the particle surface, which reflect surface roughness, roundness of edges, corners, and asperities, are taken into account. Particle shape can be described by such parameters as sphericity (S), roundness (R), and roughness. There is a number of definitions of these parameters available. Sphericity can be quantified as the ratio of the radii of the largest inscribed and the smallest circumscribed spheres. Roundness can be quantified as the average radius of curvature of surface features relative to the radius of the maximum sphere that can be inscribed in the particle [26]. Sphericity of a particle is mostly dependent on elongation, whereas roundness is dependent on the sharpness of angular protrusions from the particle [27]. Mathematical definitions of sphericity and roundness can be given as follows [28]:

$$S = \frac{R_1}{R_C} \tag{3.3}$$

$$R = 4 \frac{A}{\pi L_{Major}^2} \tag{3.4}$$

where R_I is the radius of the inscribed circle and R_C is the radius of the circumscribed circle centered at the center of mass, A is cross-sectional area, and

L_{Major} is the length of the major axis.

It is possible to estimate sphericity and roundness by visual comparison with charts such as the one in Figure 3.1. Digital image processing, including Fourier analysis and fractal analysis, facilitates the systematic evaluation of mathematical descriptors of particle shape.
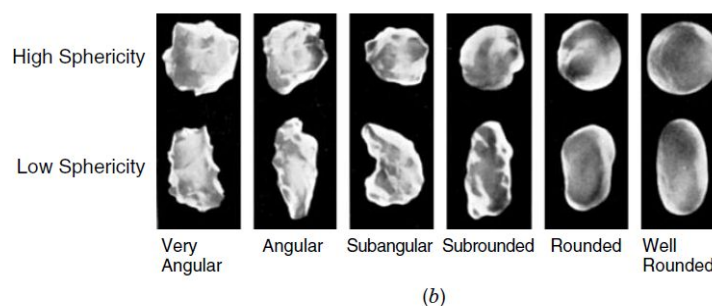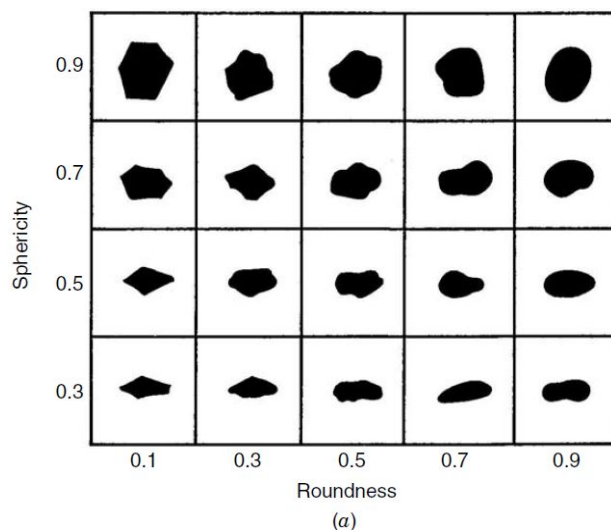
Fig. 3.1 Particle shape characterization: (a) Chart for visual estimation of roundness and sphericity (b) Examples of particle shape characterization [27]

3.1.2.
Inert minerals

Physical characteristics of soils consisting of nonclay (inert) minerals are determined mainly by particle shape, surface texture, and size distribution. The mineral composition is of importance primarily as it influences hardness, cleavage, and resistance to chemical attack. Most soil particles coarser than 2 μm are composed of nonclay minerals and are rock fragments or mineral grains.

The most abundant nonclay mineral found in soils is quartz, with feldspar and

mica present in smaller amounts. The pyroxenes and amphiboles are seldom found to any significant extent. Carbonate minerals, mainly calcite and dolomite, are also found in some soils and occur as bulky particles, shells, precipitates. Carbonates may dominate the composition of some deep sea sediments. Iron and aluminum oxides are abundant in residual soils of tropical regions [27].

Quartz is composed of silica tetrahedra grouped in a way that they form spirals, with all tetrahedral oxygens bonded to silicon. This kind of structure is very stable; there are no weakly bonded ions and cleavage planes. This explains high hardness and durability of quartz and its persistence in the nonclay fraction of soils.

Feldspars are silicate minerals that have a three-dimensional framework structure with silicon partly replaced by aluminum. The excess negative charge resulting from this replacement is balanced by cations such as potassium, calcium, sodium, etc. These cations are relatively large which results in low bond strength between structural units of the mineral. As a consequence, there are cleavage planes and hardness is moderate. Thus, feldspars are suspect to weathering which explains that they can be found in soils in less proportion then in rocks.

Mica has a sheet structure composed of tetrahedral and octahedral units. The sheets are stacked and bonded primarily by potassium ions that provide a bond of moderate strength, resulting in basal cleavage of the micas. As a consequence of the platy morphology of mica particles, sand and silts containing only a few percents of mica may form unstable fabric and exhibit both high compressibility and swelling.

The crystal structures and compositions of the amphiboles, pyroxene, and olivine are such that they are rapidly broken down by weathering, thus, they are absent from most soils.

The particles of quartz fall into two main size ranges: sand (2 mm - 60 μm) and silt (60 μm - 2 μm). There are specific geological processes behind both sand and silt formation. Sand nature is largely controlled by geochemical reactions, for example by cooling speed of magma, which defines mineral grain size. Eventually, these grains are released from mother rock by weathering action.

Large-scale formation of silt is thought to be essentially due to glacial grinding, or to intense weathering processes in high, cold, tectonically active

mountain regions [22]. Silt particles appear to be of a platy morphology, thus its behavior differs from that of extremely fine sand. A number of numerical studies showed that assuming that quartz silt particles are produced by high energy processes, such as grain crushing, the majority of them should have blade shapes with geometric proportions of 8:5:2 [22]. Considering this fact, the ability of silt to form metastable deposits with very open fabric, that collapse on loading or wetting, can be explained.

3.1.3.
Clay minerals

Clay can refer both to a size and to a class of minerals. As a size term, it refers to all constituents of a soil smaller than a particular size, usually 0,002 mm (2 μm) in engineering classifications. As a mineral term, it refers to specific clay minerals that are hydrous aluminum silicates, formed predominantly by chemical weathering of rocks. Not all clay particles are smaller than 2 μm, and not all nonclay particles are coarser than 2 μm; however, the amount of clay minerals in a soil is often closely approximated by the amount of material finer than 2 μm. Thus, the terms clay size and clay mineral content are frequently used. Clay minerals are characterized by:

- Small particle size;

- Negative electrical charge;

- Plasticity when mixed with water;

- High weathering resistance;

- Mostly platy particles, in some cases being tubular or needle shaped.

Magnesium or iron occupy part of the aluminum positions in some clay minerals, and alkalis (e.g. sodium, potassium) or alkaline earth metals (e.g. calcium, magnesium) are also present as essential constituents in some of them [29].

The clay minerals occur in particles of such small size that physicochemical interactions with each other and with the water-electrolyte phase of a soil may be strong; surface-area-to-mass ratio (specific surface area, SSA) being large either,

resulting in clay behavior highly influenced by surface forces [30].

The factors that are important for understanding the behavior of clay fraction are:

- The type and amount of clay minerals present;
- Non-clay mineral composition;
- The presence of organic material
- The type and amount of exchangeable ions and soluble salts;
- Fabric.

Very small amounts of certain clay minerals may have a large impact on the physical properties of soils.

3.1.4.
Structural units of clay minerals

The basic structural units ("building blocks") of clay minerals are the silicon-oxygen tetrahedra and the aluminum-hydroxyl or magnesium-hydroxyl octahedra, which have a net negative charge due to the valency imbalance of the individual atoms. These molecules combine to form strong sheet-like structures of silica $[SiO_4]_n$, gibbsite $[Al_2(OH)_6]_n$ or brucite $[Mg_3(OH)_6]_n$, where n denotes a large number of molecules. Cations within these sheets (i.e. Si^{4+}, Al^{3+} and Mg^{3+}) can be substituted for other cations depending on specific conditions. As a result of cation substitution (isomorphic substitution), sheet surface charges can become imbalanced so that additional cations are adsorbed onto the surface or held in suspension with water around the sheet. The tendency to adsorb or exchange cations is called the cation exchange capacity [30].

The octahedral sheet is comprised of closely packed oxygens and hydroxyls in which aluminum, iron, and magnesium atoms are arranged in octahedral coordination (Fig. 3.2a). When aluminum with a positive valence of three is the cation present in the octahedral sheet, only two-thirds of the possible positions are filled in order to balance the charges. When only two-thirds of the positions are filled, the mineral is termed dioctahedral. When magnesium with a positive charge of two is present, all three positions are filled to balance the structure and the mineral is termed trioctahedral.

The second structural unit is the silica tetrahedron which consist of four oxygens or possibly hydroxlys arranged in the form of a tetrahedron with the silicon atom in the center. These tetrahedra are arranged to form a hexagonal network repeated in two horizontal directions to form what is called the silica tetrahedral sheet (Fig. 3.2b).

The silica tetrahedral sheet and the octahedral sheet are joined by sharing the apical oxygens or hydroxyls to form the 1:1 clay mineral layer, e.g. kaolinite, or the 2:1 clay mineral layer, e.g. illite [31].
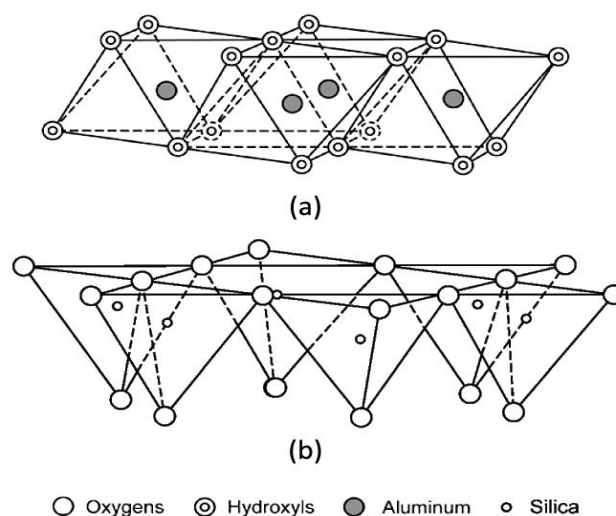
Fig. 3.2 Schematic representation of (a) octahedral sheet (b) tetrahedral sheet [31].

Clay minerals are formed by the combinations of two or more sheets and the type of clay mineral is determined by how combinations of these sheets are arranged. Although the intra-sheet bonding is strong, the inter-sheet bonding is relatively weak in some minerals, which gives insight into their distinct properties [32]. The most common clay minerals are kaolinite, illite and montmorillonite. The classification of clay minerals is presented in Table 3.3.

Table 3.3 Classification of clay minerals [29]

I. Amorphous	Allophane group	
II. Crystalline	A. Two-layer type (sheet structures composed of units of one layer of silica tetrahedrons and one layer of alumina octahedrons)	
	1. Equidimensional	Kaolinite group Kaolinite, dickite and nacrite
	2. Elongate	Halloysite
	B. Three-layer types (sheet structures composed of two layers of silica tetrahedrons and one central dioctahedral or trioctahedral layer)	
	1. Expanding lattice	a. Equidimensional Smectite group Sodium montmorillonite, calcium montmorillonite, and beidellite Vermiculite b. Elongate Smectite Nontronite, saponite, hectorite
	2. Non-expanding lattice	Illite group
	C. Regular mixed-layer types (ordered stacking of alternate layers of different types)	
		Chlorite group
	D. Chain-structure types (hornblende-like chains of silica tetrahedrons linked together by octahedral groups of oxygens and hydroxyls containing Al and Mg atoms)	
		Sepiolite Palygorskite (attapulgite)

3.1.5.
Kaolin minerals

The basic kaolin mineral structure comprising the minerals kaolinite, dickite, nacrite, and halloysite consists of a layer of a single tetrahedral sheet and a single octahedral sheet. These two sheets are combined to form a unit in which the tips of the silica tetrahedrons are joined with the octahedral sheet. All of the apical oxygens of the silica tetrahedrons point in the same direction so that these oxygens and/or hydroxyls, which may be present to balance the charges, are shared by the silicons in the tetrahedral sheet and the aluminum in the octahedral sheet (Fig. 3.3). The structural formula for kaolinite is $Al_4Si_4O_{10}(OH)_8$. Only two-

thirds of the octahedral positions are filled by an aluminum atom. The aluminum atoms are surrounded by four oxygens and eight hydroxyls [31].

The charges in the kaolinite structure are balanced. The minerals of the kaolin group, kaolinite, dickite, nacrite, and halloysite consist of the 1:1 layers of combined octahedral and tetrahedral sheets, which are continuous in the a- and b- axis directions and are stacked one above the other in the c-axis direction. The differences in the kaolin minerals are the manner in which the unit layers are stacked above each other. The thickness of the unit layer is 7.13 Å.

Kaolinite is the most important member of the group. It occurs in residually weathered material and is a common constituent of soil. Kaolinite particles appear in the form of hexagonal flakes [33] (Fig. 3.4), often with a noticeable elongation in one direction. The lateral dimensions of these flakes range from about 0.1 to 4 μm, and their thicknesses are about 0.05 to 2 μm. The degree of crystal perfection of the kaolinite affects its physical properties.
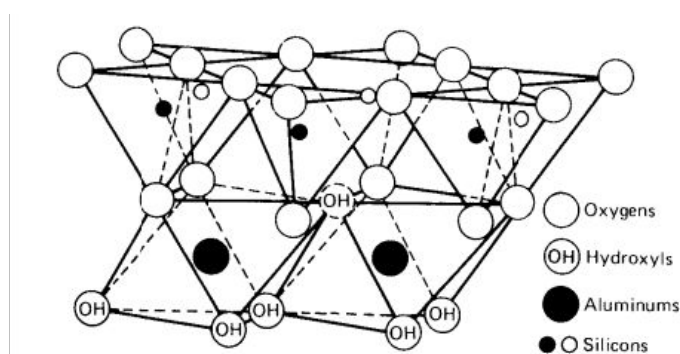
Fig. 3.3 Diagrammatic sketch of kaolinite structure [27].

The superficial charge of the kaolinite particles is very small due to little or no isomorphic substitution, broken bonds along the particle edges being principal place of electric charge concentration [34]. This combined with a relatively low surface area (8–15 m^2/g) explains kaolinite's low absorption and adsorbtion characteristics. Particles of kaolinite have a relatively broad size distribution. Other relevant physical and chemical properties are that kaolin is chemically inert over a relatively wide pH range (4–9), has low heat and electricity conductivity, is hydrophilic and disperses readily in water [31].
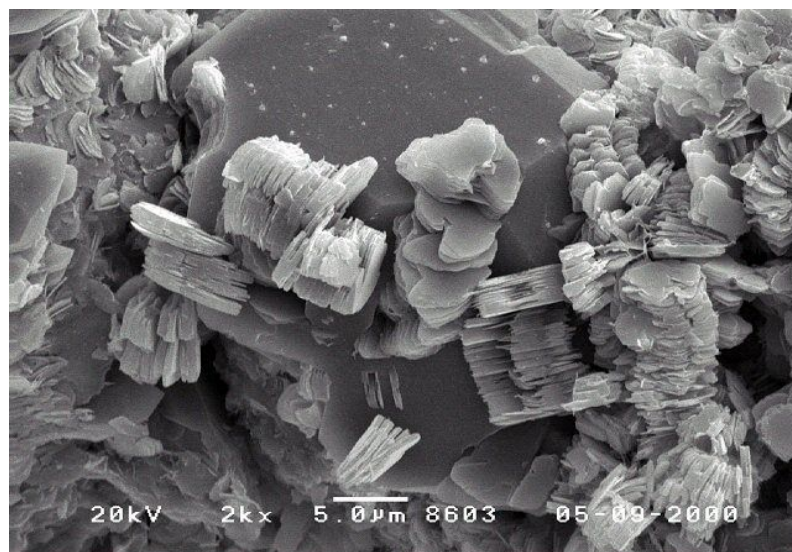
Fig. 3.4 Kaolinite plates covering a quartz grain. SEM image of a core sample [33]

In dickite, the unit cell consists of two unit layers and in nacrite, six unit layers. Halloysite occurs in two forms: hydrated, in which there is a layer of water molecules between the layers, and dehydrated. The hydrated form has a basal spacing of 10 Å and the dehydrated form - 7.2 Å. The particles of halloysite have elongate tubular shape (Fig. 3.5) [31], [35].
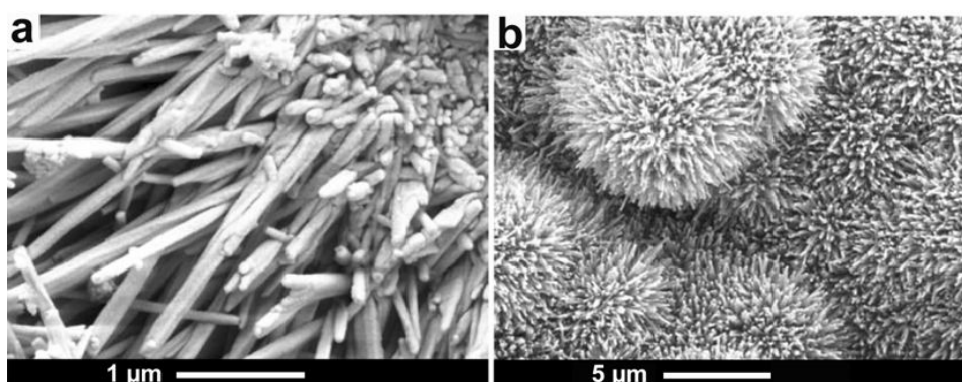
Fig. 3.5 Field emission scanning electron micrographs (FE-SEM) of halloysite (a) Spheroidal and short-tube morphologies growing on the edges of mica flakes (b) 0.2 - 0.3 µm halloysite particles on feldspar [35]

3.1.6.
Smectite minerals

Smectite minerals are composed of two silica tetrahedral sheets with a central octahedral sheet and are called 2:1 layer minerals (Fig. 3.6). Water molecules and

cations occupy the space between the 2:1 layers.

The theoretical formula is $(OH)_4Si_8Al_4O_{20} \cdot NH_2O$ (interlayer) and the theoretical composition without the interlayer material is SiO_2, 66,7%; Al_2O_3, 28.3%; and H_2O, 5%. In smectites, there is considerable substitution in the octahedral sheet and some in the tetrahedral sheet. In the tetrahedral sheet, there is substitution of aluminum for silicon up to 15% [29] and in the octahedral sheet, magnesium and iron for aluminum. This accounts for charge deficiency which is balanced by exchangeable cations adsorbed between the unit layers and on the particle edges. Substitution within the lattice is reported to cause about 80% of the total cation exchange capacity [34]. If the octahedral positions are mainly filled by aluminum, the smectite mineral is beidellite; if filled by magnesium, the mineral is saponite; and if by iron, the mineral is nontronite.
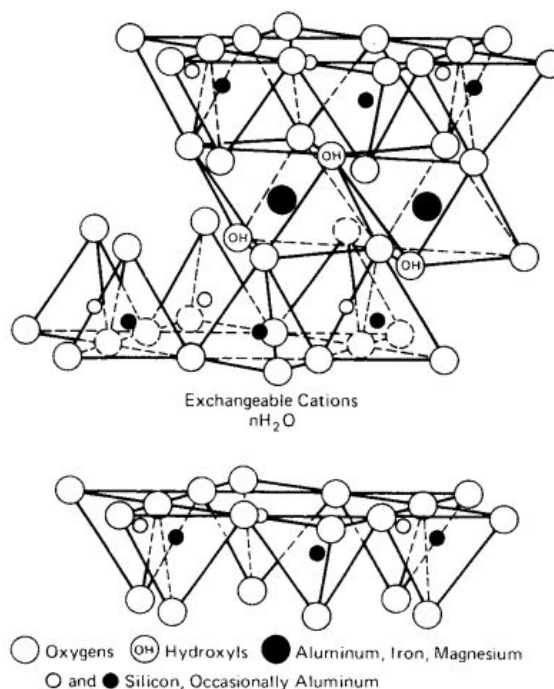
Fig. 3.6 Diagrammatic sketch of smectite structure [27]

Montmorillonite may occur as equidimensional flakes so thin that they appear to be films [36] (Fig. 3.7). Particles range in thickness from 1 nm unit layers to about 1/100 of the width. The long axis of the particle is usually less than 1 or 2 μm. When there is a large amount of substitution of iron or magnesium for aluminum, the particles may be lath or needle shaped [27].

The most common smectite minerals are calcium and sodium montmorillonites, which means that the layer charge deficiency is balanced by the

interlayer cations of calcium or sodium and water. The basal spacing of the calcium montmorillonite is 14.2 Å. Sodium montmorillonite has basal spacing of 12.2 Å. Calcium montmorillonites have two water layers in the interlayer position and sodium montmorillonites have one water layer [31]. Sodium montmorillonites have very high surface area of about 150–200 m^2/g which provides high sorptivity, high plasticity and high swelling capacity of the order of 10–15 times. Calcium montmorillonite is generally larger in particle size, has a lower surface area (50–80 m^2/g), a lower base exchange capacity, and a lower swelling index (2–3) [31].
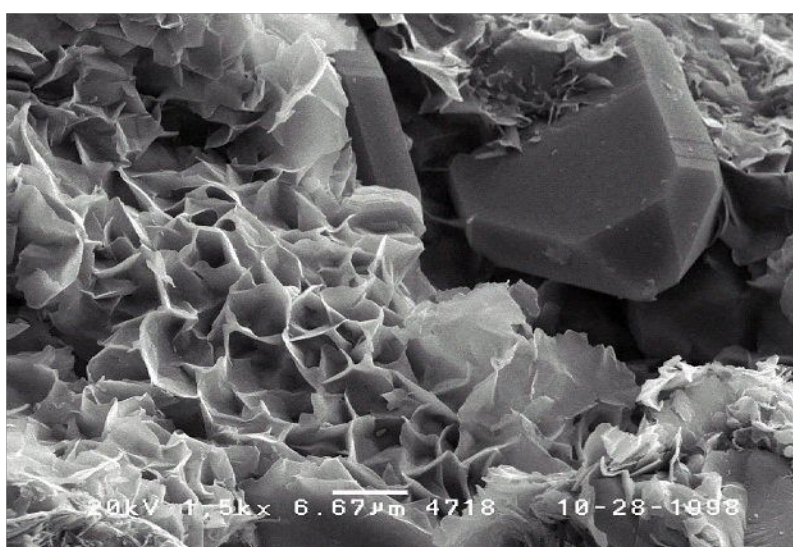
Fig. 3.7 Authigenic smectite (montmorillonite) overgrown on pore spaces of quartz grains in a sandstone. SEM image of a core sample [36]

3.1.7.
Illite

Illite is clay mineral mica. The structure is a 2:1 layer in which the interlayer cation is potassium. The size, charge, and coordination number of potassium gives the structure a strong interlocking ionic bond which holds the individual layers together and prevents water molecules from occupying the interlayer position as it does in the smectites. Illite differs from well-crystallized muscovite in that there is less substitution of Al^{3+} for Si^{4+} in the tetrahedral sheet. In muscovite, one-fourth of the Si^{4+} is replaced by Al^{3+}, whereas in illite only about one-sixth is replaced. Also, in the octahedral sheet, there may be some replacements of Al^{3+} by Mg^{2+} and

Fe^{2+}. The basal spacing of illite is 10 Å. The charge deficiency is about 1.30–1.50 for illite contrasted to 0.65 for smectite. The largest charge deficiency is in the tetrahedral sheet rather than in the octahedral sheet, which is opposite from smectite. Potassium binds the layers in a fixed position so that water and other polar compounds cannot readily enter the interlayer position and also the potassium ion is not readily exchangeable. Illite is commonly associated with many kaolins and smectites [31]. Electron micrographs of illite show small, poorly defined flakes commonly grouped together in irregular aggregates [37] (Fig. 3.8). Occasionally the flakes show hexagonal outlines [29].
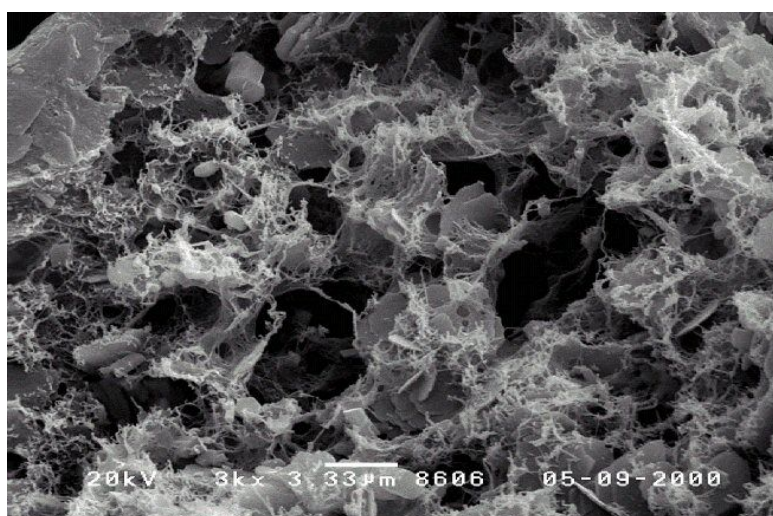
Fig. 3.8 SEM image of illite crystals filling a pore space in sandstone [37]

3.1.8.
Chlorite

Chlorite is commonly present in shales and also in clays associated with coal seams. Clay mineral chlorites are characterized by random stacking of the layers and some hydration. Chlorite is a 2:1 layer mineral with an interlayer brucite sheet ($Mg(OH)_2$). There a range of cation substitutions in chlorites, most commonly Mg^{2+}, Fe^{2+}, Al^{3+}, and Fe^{3+}.

The composition of chlorite can be described as $(OH)_4(SiAl)_8(MgFe)_6O_{20}$. There is considerable substitution of Al^{3+} by Fe^{3+}, Mg^{2+} by Fe^{2+}, and of Si^{4+} by Al^{3+}. The basal spacing of chlorite is about 14 Å. Chlorite is generally mixed with other clay minerals so it can be identified by the 14 Å basal spacing which does

not expand when treated with ethylene glycol or decrease to 10 Å upon heating [31]. SEM image of chlorite crystals can be seen in Fig. 3.9 [38].
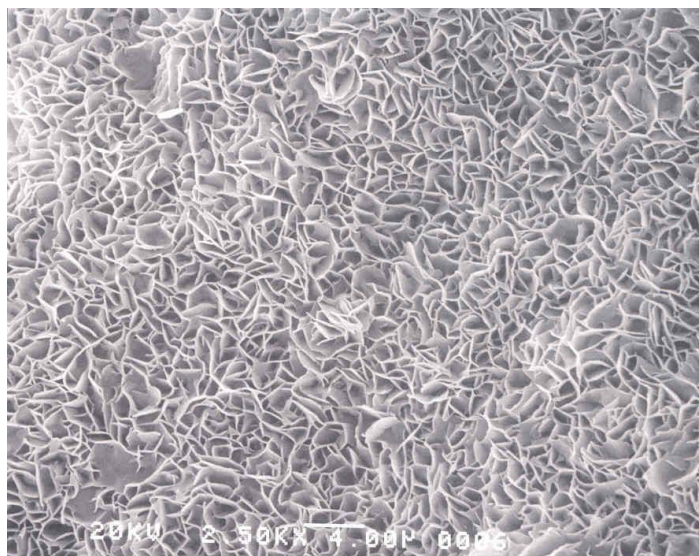
Fig. 3.9 Diagenetic chlorite crystals [38]

3.1.9.
Palygorskite, sepiolite

Palygorskite (attapulgite) and sepiolite are 2:1 layer minerals. Their tetrahedral sheets are linked in two dimensions. They are structurally different from other clay minerals in that the octahedral sheets are continuous in only one dimension and the tetrahedral sheets are divided into ribbons by the periodic inversion of rows of tetrahedrons.

The channels between ribbon strips are larger in sepiolite than in palygorskite. In palygorskite, the dimension of the channel is approximately 4 Å by 6 Å and in sepiolite, approximately 4 Å by 9.5 Å. Both of these clay minerals are magnesium silicates, but palygorskite has a higher alumina content. A general formula for palygorskite is $(OH_2)_4(OH_2)Mg_5Si_8O_{20}\cdot 4H_2O$. A general formula for sepiolite is $(OH_2)_4(OH)_4Mg_8Si_{12}O_{30}\cdot 8H_2O$. These two clay minerals contain two kinds of water, one coordinated to the octahedral cations and the other loosely bonded in the channels, which may also contain exchangeable cations.

Both palygorskite and sepiolite are elongate in shape and often occur as bundles of elongate and lath-like particles (Fig. 3.10). Usually, the sepiolite elongates are longer than palygorskite elongates (10–15 Å for sepiolite and >5 Å

for palygorskite) [31], [39].
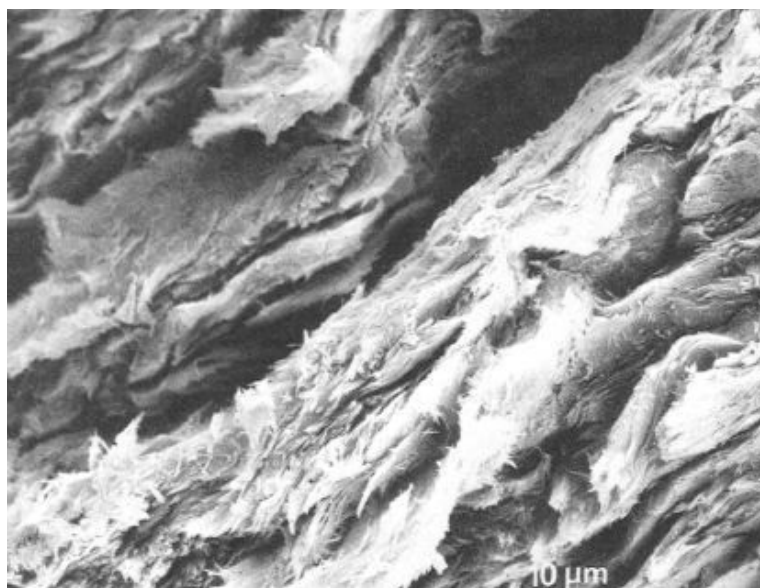
Fig. 3.10 Scanning electron micrograph of palygorskite forming mats of tightly interwoven fibers, Midra Shale [39]

3.2.
Soil fabric

Soil fabric can be defined as the appearance or pattern produced by various combinations of the relative size, shape and arrangement of the constituents, whether they occur as single grains or compound elements, and of the voids. Arrangement refers to the mutual spatial relationships of the constituent elements, including distribution patterns and packing [40]. The term structure is sometimes used interchangeably with fabric, but it is generally includes the effects of composition and interparticle forces.

Many soils are formed by deposition in water, therefore it is useful to study particle associations in clay suspensions, which can provide some understanding about a number of types of soil fabric (Fig. 3.11). They can be described as follows:

- Dispersed - no face-to-face associations of clay particles

- Aggregated - face-to-face association of several clay particles

- Flocculated - Edge-to-edge or edge-to-face association of aggregates

- Deflocculated - no association between aggregates.
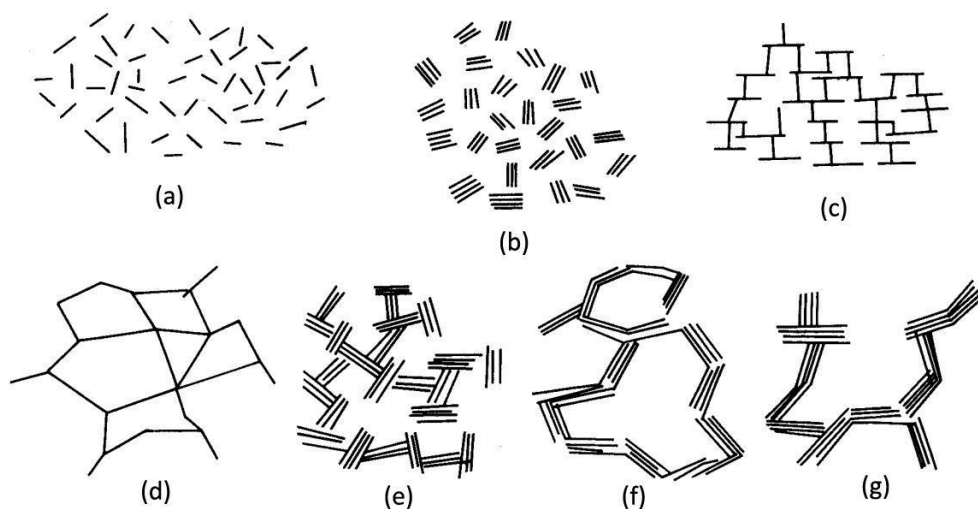
Fig. 3.11 Modes of particle associations in clay suspensions. (a) Dispersed and deflocculated, (b) aggregated but deflocculated (face-to-face association, or parallel or oriented aggregation), (c) edge-to-face flocculated but dispersed, (d) edge-to-edge flocculated but dispersed, (e) edge-to-face flocculated and aggregated, (*f*) edge-to-edge flocculated and aggregated, and (g) edge-to-face and edge-to-edge flocculated and aggregated [27].

The following elements of soil fabric can be distinguished [41]:

- **Elementary clay particles** represented by microcrystals of clay minerals, which are stable under mechanical and chemical action.

- **Ultramicroaggregates** are associations of several particles, generally having face-to-face interaction. They are most common in smectites and mixed layer clay minerals. Their dimensions are less than several microns.

- **Microaggregates** consist of associations of clay particles and ultramicroaggregates, which remain stable when immersed in water without physico-chemical dispersants. Microaggregates are main structural elements of natural clays. Their sizes range from several to dozens of micrometers. The most common microaggregates are those that consist of clay particles and ultramicroaggregates with face-to-face or edge-to-face contacts at small angles, which produces irregular assemblages of particles.

- **Aggregates** consist of several microaggregates or associations of microaggregates with silt or sand grains. Aggregates are generally less stable in contact with water. Their sizes range from dozens to

hundreds of micrometers. In contrast to microaggregates, aggregates generally have regular shape.

- **Grains of primary minerals** are represented by quartz crystals, mica, feldspar, and calcite debris. Mineral grains are frequently covered with coating of finer clayey particles.

Associations of fabric elements in soils have a variety of forms, but they are mainly related to the types of particle associations in clay dispersions. Figure 3.12 presents the basic types of particle interaction.
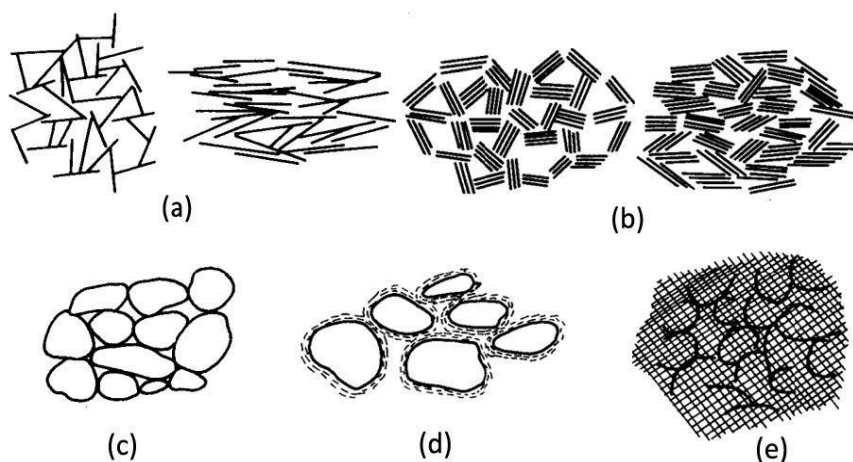
Fig. 3.12 Schematic representation of basic particle arrangements (a) interaction of individual clay plates, (b) clay platelet group interaction, (c) individual silt or sand particle interaction, (d) clothed silt or sand particle interaction, (e) partly discernible particle interaction [27]

Alternatively, some more types of assemblages of soils fabric elements can be identified:

- **Connectors** are assemblages which finer particles form between silt and sand grains and are sometimes referred to as clay bridges. Silt particles can be contained within the connecting material if space allows.

- **Interweaving bunches** are specific assemblages of fabric elements forming mesh-like structure as shown in Figure 3.13(h) and(i).

- **Particle matrices** are assemblages which form fine or granular homogeneous matrix of the fabric, and provide binding material for coarser elements. Clay particle matrices consist of clay and small silt particles with different clay particle arrangements. Granular particle matrices comprise silt and sand particles.
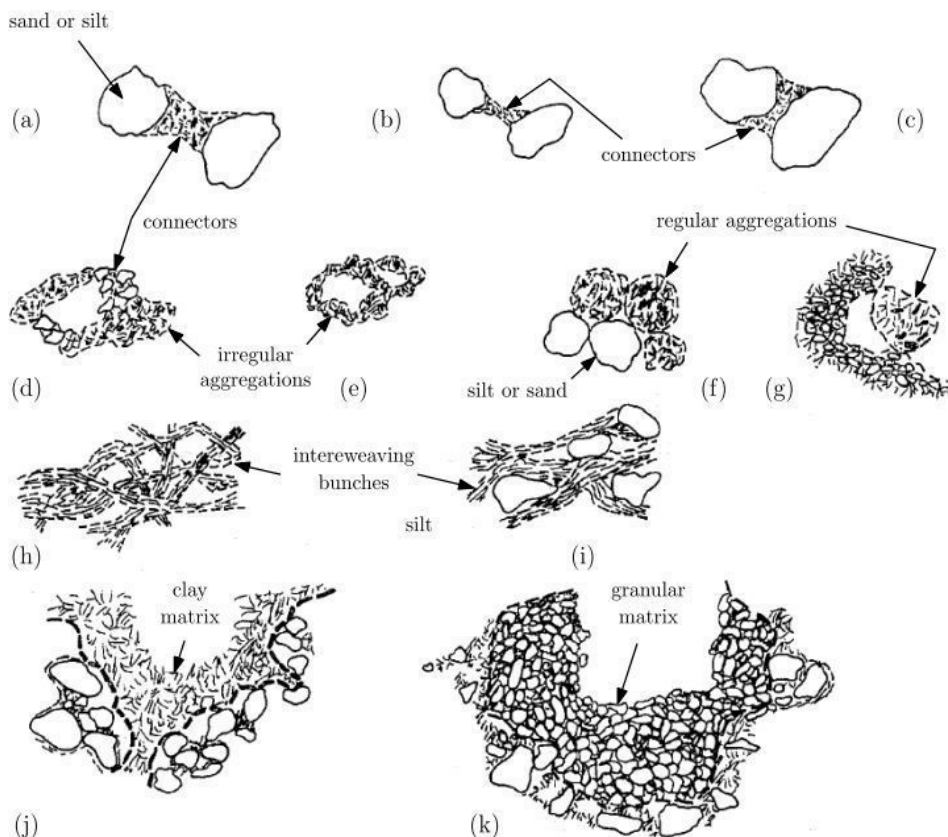
Fig. 3.13 Schematic representations of particle assemblages: (a) – (c) connectors, (d) irregular aggregations linked by connector assemblages, (e) irregular aggregations in a honeycomb arrangement, (f) regular aggregation interacting with particle matrix, (h) interweaving bunches of clay, (i) interweaving bunches of clay with silt inclusions, (j) clay particle matrix, and (k) granular particle matrix [27].

Another element of soil fabric is pore space. Pores or voids are limited by the boundaries of solid elements and can be classified as follows:

- **Intra-elemental pores** are those pores that occur within the elementary particle arrangements i.e. between individual particles or small groups of clay particles.

- **Intra-assemblage pores** occur within particle assemblages and are those pores that are present between elementary particle arrangements or between smaller particle assemblages within the larger assemblage.

- **Inter-assemblage** pores are those that occur between larger particle assemblages.

- **Trans-assemblage** pores occur between groups of particle assemblages or elementary particle arrangements or combinations of the two, so that their boundaries are not defined by the

aggregate type.
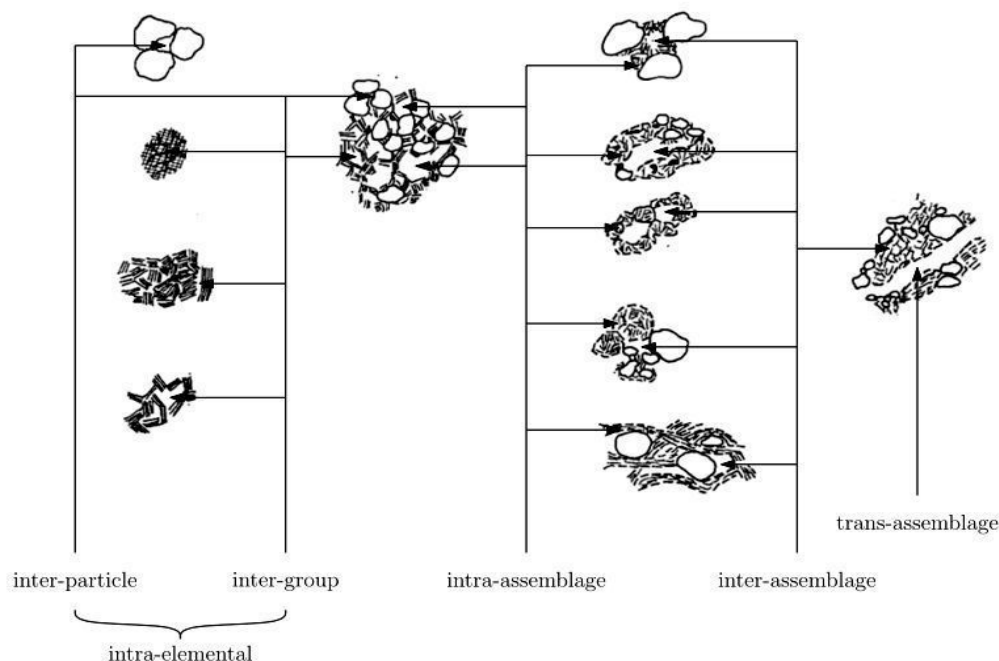
Fig. 3.14 Types of pores found in soils [27]

Pores can be classified according to their size, however this kind of division is usually quite arbitrary and depends on particular situation. Some authors proposed hydraulically motivated division of pore sizes into macropores, where capillary effects are the governing phenomena, and micropores, associated with interparticle distances or even intercrystalline spacing, where water is retained due to physico-chemical effects other than capillarity [42], [43]. However, the transition between these two pore types is difficult to be identified.

3.3.
Unconfined compressive strength of soil

In civil construction soil is used mostly to build walls and columns, therefore its behavior under unconfined compression is of major interest. Classic soil mechanics addresses soil mostly in confined and saturated state. The confining pressure depends on the depth of soil element considered. The strength of soil in most geotechnical problems depends on composition, stress history, confinement, drainage conditions and pore water pressure, that can be positive or negative, depending on whether soil specimen tends to contract or expand. There are other

relevant variables, such as temperature, rate of stress or strain, cyclic behavior, but they are rarely taken into consideration. Due to the state of soil when used as a construction material, other conditions determine its behavior. The surface of earthen walls and columns is in a direct contact with atmosphere, therefore the moisture retained by soil is free to evaporate until it is in hygroscopic equilibrium with surrounding air. While the temperature and moisture underground can be considered constant in many cases, atmospheric conditions may largely determine the behavior of earthen construction materials.

In geotechnical engineering, unconfined soil strength is termed true cohesion. There are two major components that contribute to it. The first is mechanical interaction (i.e. interparticle friction and interlock) and the second is the effect of suction in unsaturated soil, which is thought to be the main source of earthen construction materials' strength [30], [44]–[46].

The mechanical interaction between soil particles is a phenomenon that happens on a microscale. It is determined by geometric characteristics and frictional resistance of soil particles and their spatial configuration. External load applied to soil mass is transmitted via bonds between soil grains, which are small contact areas between the particles. The more bonds are developed, the more uniform is load dissipation and the higher is the strength. The way of increasing the number of bonds is to optimize the packing of the particles, thus increasing soil density. The variables that control the packing characteristics of soil are granulometry and grain shape. On the macroscale the friction between soil particles can be quantified by internal angle of friction and cohesion intercept (in most cases called cohesion) of the strength envelope. It is generally stated that a lower sphericity results in higher friction angles, as ellipsoidal particles can achieve denser packing, while for a given packing spherical particles develop more bonds, thus having higher cohesion [27], [47]. Surface roughness of grains is also reported to influence soil strength as rougher particles tend to interlock, thus forming more stable fabric. The internal angle of friction was shown to be influenced only by the largest soil particles whereas cohesion – by the whole particle size distribution. This is attributed to the fact that mostly large particles participate in stress distribution in granular soils [48].

The stress in soil mass is transmitted over chains of particles that form interconnected network, termed strong force network. With the aid of photoelastic

studies of loading of randomly packed spherical particles Santamarina [49] obtained a visual demonstration of this behavior (Fig. 3.15). The particles which are not a part of strong force network receive much smaller loads, forming weak clusters that have a size of 3 to 10 particle diameters [27].
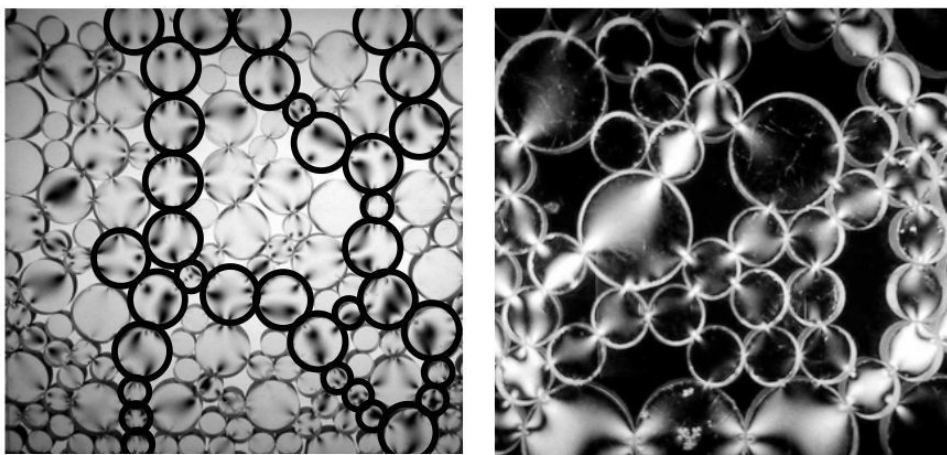
Fig. 3.15 Photoelastic study of strong force networks [49]

When loaded, soil fabric tends to rearrange to increase the number of bonds between the particles, thus large pores tend to collapse and new strong force networks are formed. At the same time, soil grains tend to rotate, which in granular systems is restrained only by the frictional forces between the particles. While in dense packings ellipsoidal grains tend to rotate less then spherical ones, fine particles of platy shape are able to form unstable "cardhouse" structures, which collapse abruptly on loading or wetting. This happens when intergranular bonds are mainly edge-to-edge or edge-to-face, where there is a very small contact area between the particles, which tends to increase when this loose structure collapses and face-to-face bonds are developed.

Dry granular soil specimens have zero unconfined strength as they collapse under their own weight. When a small amount of water is present in soil, so called liquid bridges are formed between the particles (Fig. 3.16). Their form depends on relative humidity (RH) of surrounding air and on the stage of wetting-drying cycle [50]. The liquid bridges are basically water menisci that have a tensile strength, so acting as kinematic constraints to particle sliding and rotation.
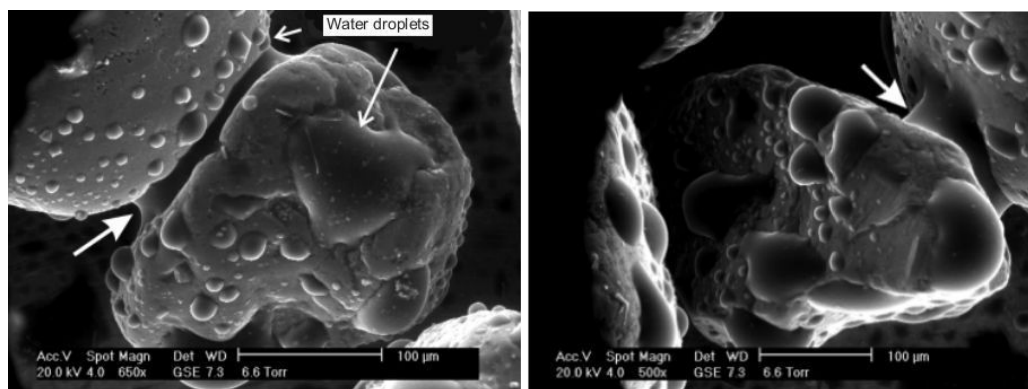
Fig. 3.16 Water menisci at the contacts of sand grains, RH 100% (bold arrows indicate liquid bridges) [50]

The described theory can be applied only to granular soils which consist of inert particles. Clay fraction has additional forces that contribute to its strength. It was shown that for particles less than 50 μm, cohesive forces, rather than gravitational, determine their behavior [47]. This is especially relevant for clay particles which size is less that 2 μm. Electrical forces and tension created by water films are major contributors to the behavior of clays. Due to electrical charges of clay particles, they attract water molecules and ions dissolved in water. Up to some extent the water adsorbed by clay remains in a rigid state and is called non-liquid water. The thickness of rigid water around a clay particle depends on the amount of its electrical charge, which can be estimated by the activity of clay. The thickness of water film around a clay particle increases gradually with further addition of water to the soil. The farther the water molecule from the surface of a clay particle, the weaker is the bonding between them. When added in excess of the amount that can be held in rigid state, water starts to have a lubricating effect, reducing cohesion and developing plasticity. Owing to low permeability and high specific surface of clay, it can take considerable amount of time for water to penetrate its micropores and form a film around each individual particle. Once clay hydration occurs, it doesn't lose its rigid water under normal conditions. Generally it takes temperatures up to 100°C to remove water present in clay without damaging the structure of clay minerals [29], [31]. Thus, the concept of dry soil should be specifically defined, as all water cannot be removed from a clayey soil under normal atmospheric conditions.

As it was stated earlier, clay minerals can be found in a soil as individual particles, as well as aggregates up to sand size range. Individual clay particles tend to form a coating around larger sand and silt grains. This can be seen in

numerous SEM images available in the literature. In the points of contact between sand and silt grains, clay particles tend to create wedges that hold them in place [51] and provide further kinematic constraints for the movement of larger soil grains. Furthermore, these clay wedges increase the area of stress transfer between soil particles in strong force networks, making stress distribution more uniform. Thus, any plane of weakness in soil structure receives less stress which reduces the probability of failure. When there are large clay aggregates present in soil, they occupy the places of sand and silt grains. These aggregates have significantly lower strength than any inert mineral, thus under stress they can be crushed provoking buckling of strong force networks, cracking and subsequent failure of earthen construction material (Fig. 3.17). To avoid this, soil should be mixed with water very thoroughly before compaction, including a period for moisture equilibration, which length will depend on the characteristics of particular clay minerals present.

| | sand grains | | clay coating and wedges | | clay aggregates |
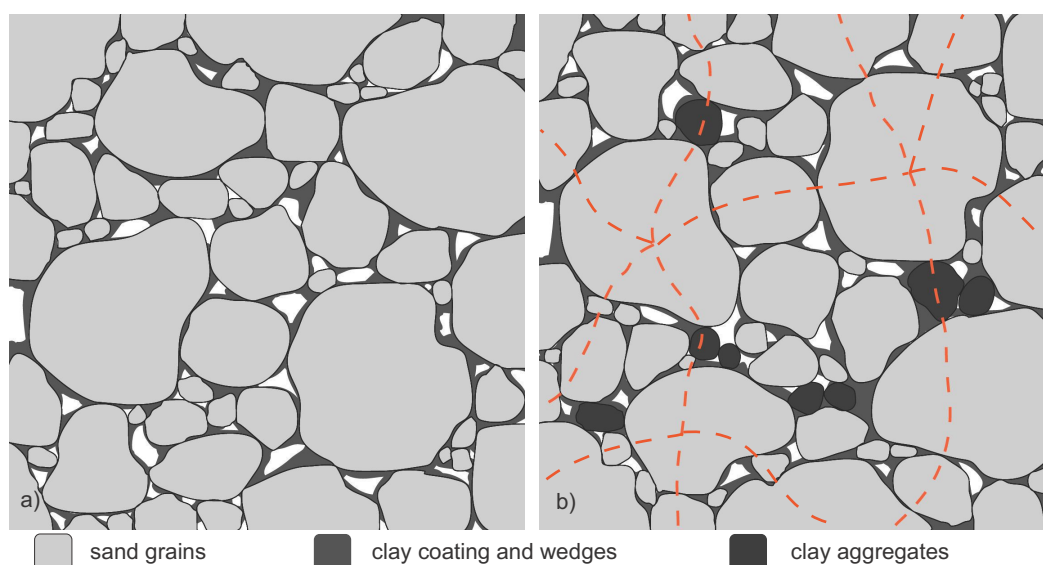
Fig. 3.17 a) Sand grains with clay coating and clay wedges b) Soil structure with clay aggregates (dashed line joins bonds between particles that form a hypothetical strong force network)

Grim [51] performed an extensive study on the bonding capacity of five different clays used in molding sands. Two types of montmorillonite clays, with exchangeable sodium and calcium cations, halloysite, kaolinite and illite clays were investigated. This includes most of common clay minerals present in soils. The following conclusions were made:

- Sands bonded with montmorillonite clays have high strength. This clays consist of extremely fine minerals that disaggregate

easily in water, therefore providing a uniform coating for sand grains. Kaolinites and illites have lower bonding capacity for their minerals are less active, they consist of larger particles and aggregates that are difficult to break. This results in non-uniform coating with numerous planes of weakness (Fig. 3.18);

- The amount of clay minerals present in clay influence the bonding properties of material, inert minerals present in clay phase reduce soil strength;

- The type of exchangeable cation adsorbed to clay particles affect the bonding capacity by determining the amount of rigid water that can be held by clay;

- It is hypothesized that the maximum strength of sand-clay mix is attained when all the water is held in a rigid state. It was possible to prove for montmorillonite clays, as water tends to penetrate this type of clay rapidly and form a rigid film around each particle. Eventually, the thickness of water film is possible to be calculated, being around 3 water molecules for the mineral studied. In kaolinites and illites this effect is difficult to be estimated as the particle sizes vary and water cannot penetrate fully all the clay aggregates. Thus, the strength of sand-clay mix for kaolinites and illites increases with time as water is adsorbed gradually by the clay particles. As the superficial charge of these minerals is much lower, they can hold less water in a rigid state;

- The strength of sand-kaolinite mixes increases when clay is subject to grinding in order to break the aggregates. The strength increases when more kaolinite is added to the mix, which increases the size of wedges in contact points of sand grains, thus reducing the planes of weakness.
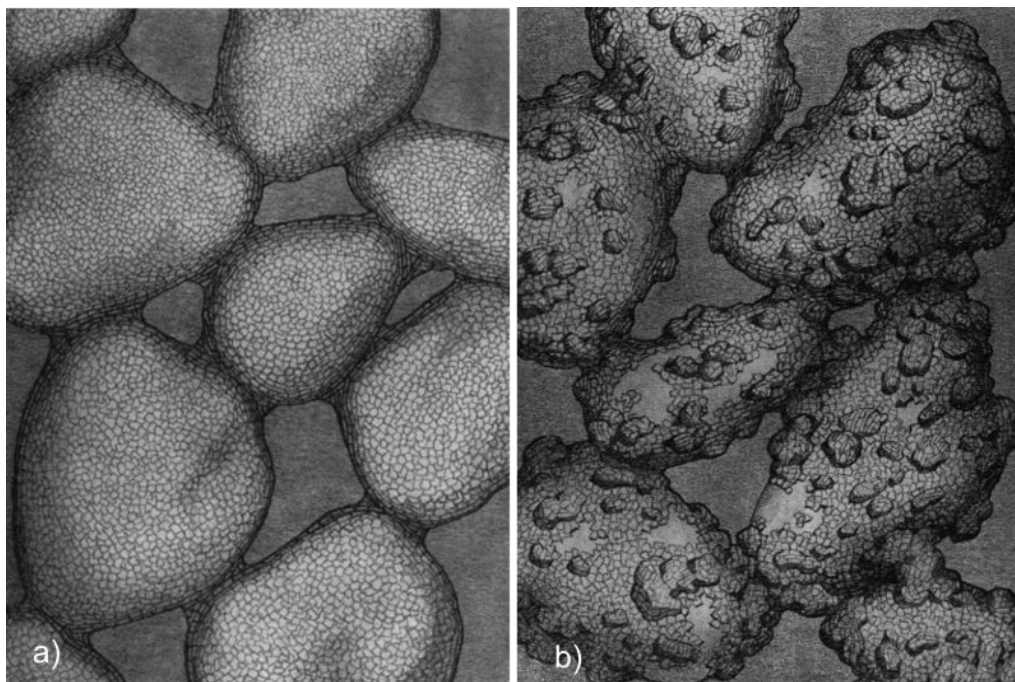
Fig. 3.18 Clay coating of sand grains: a) montmorillonite clay b) kaolinite clay [51].

These conclusions can be extrapolated to general soil behavior and give an insight into the mechanism behind unconfined soil strength. The two main soil phases, or fractions, behave in distinct ways. Inert minerals provide a skeleton through which a great part of the load is distributed. The denser is the grain packing, the more uniform is the load distribution. Active phase, represented by clay minerals, interact with moisture contained in soil attracting water molecules which bind clay particles together. Clay creates a layer of coating around larger soil grains and forms wedges in the points of contact between them. These clay wedges hold inert particles in place and help in load distribution.

3.4.
Unsaturated soil behavior

Soil that contains both liquid and gas phases is called unsaturated. All earthen materials are highly unsaturated as they are exposed to the atmosphere. The term «dry» is often used, however, as it was stated earlier, a soil always contains some amount of water at normal atmospheric conditions. As this water is found in the form of liquid bridges and adsorbed films, there is a significant contact area between liquid and gas phases in an unsaturated soil. The superficial layer of

water at the liquid-gas interface has tensile strength. The tension created by water menisci together with electrostatic forces in the water films around clay minerals cause negative pore pressure termed suction. Suction consists of two components: matric and osmotic. Matric suction is related to capillarity, relevant in coarse soils or in soils near saturation, and adsorbed water films, which predominate in the behavior of fine grained soils [52]. Osmotic suction occurs when soil water contains dissolved substances, such as salts. The higher the solute concentration, the higher is osmotic component of suction.

3.4.1.
Soil water retention

The relationship between soil suction and water content is defined by soil water retention curve (SWRC). It is normally represented as a graph in terms of suction vs. degree of saturation, gravimetric or volumetric water content. Some examples of SWRCs for different types of soils taken from [53] are shown in Fig. 3.19. The shape of SWRC depends on the soil mineralogy and structure, especially pore size distribution. For many soils SWRC presents hysteresis, as water content corresponding to the same suction can differ during wetting and drying. This effect is attributed to the changes in soil fabric and to different ways in which water enters or is expelled from pore space. For compacted soils, that have stable structure, the effect of hydraulic hysteresis is negligible [54].
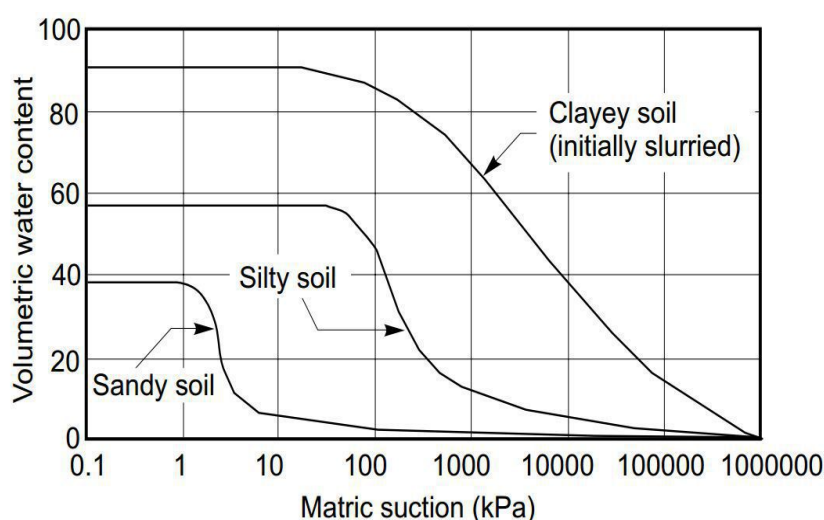
Fig. 3.19 Typical SWRCs for different types of soil [53]

An important parameter that characterizes unsaturated behavior of soils is air

entry value, also called air entry suction. Air entry value is defined as the matric suction that must be applied to a saturated soil before air enters into its pores. It can be identified on a SWRC by extending a constant slope part of the curve until it intersects a horizontal line passing through water content at saturation [55].

A soil can have more than one air entry value, a property called double or triple porosity (multimodal behavior). It is typical of aggregated soils, that have several distinctive pore size ranges, e.g. macropores, usually cracks or pore spaces between aggregates, and micropores, found inside the aggregates. When suction is applied to saturated soil with double porosity, air enters the macropores at the first air entry value, then after the macropores are almost dry and micropores still saturated, air starts to enter intra-aggregate pore space at the second air entry value.

After air entry value is reached, soil enters into transition zone, where water content decreases rapidly with the increase in suction. Eventually liquid phase becomes discontinuous and further increase in suction doesn't affect significantly degree of saturation. Residual value of saturation is a parameter that indicates boundary between transition and residual stages. Vanapalli et al. [55] proposed a graphic procedure for determination of residual saturation value. First, a tangent should be drawn through the inflection point of the straight portion of transition zone. Its intersection with the extension of the line passing through 1000 MPa along residual saturation zone indicates residual saturation value (Fig. 3.20). Frequently for purposes of modeling residual water content is defined as minimum humidity that a soil can contain at the highest possible suction, however this value cannot be precisely defined.
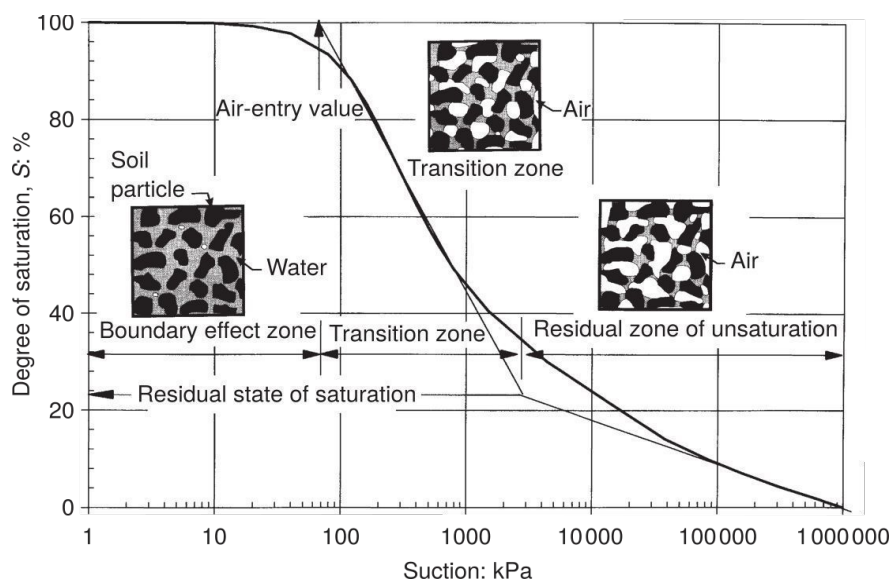
Fig. 3.20 Zones of desaturation of SWRC [55]

There is a number of functions that attempt to describe SWRC. Some of them are given below.

One of the first hydraulic functions describing SWRC was introduced by Brooks and Corey [56]:

$$\theta = \begin{cases} \theta_r + (\theta_s - \theta_r)(\alpha h)^{-\lambda} & for \quad \alpha h \geq 1 \\ \theta_s & for \quad \alpha h < 1 \end{cases} \qquad (3.5)$$

θ – volumetric water content,

θ_s – saturated volumetric water content,

θ_r – residual water content (minimum humidity in dry condition),

α – inverse of air entry value,

h – water pressure head,

λ – pore size distribution index.

A parameter called effective saturation (S_e) is frequently used in unsaturated soil mechanics:

$$S_e = \frac{\theta - \theta_r}{\theta_s - \theta_r} \qquad (3.6)$$

Equation 3.5 can be rewritten as:

$$S_e = \begin{cases} (\alpha h)^{-\lambda} & for \quad \alpha h \geq 1 \\ 1 & for \quad \alpha h < 1 \end{cases} \qquad (3.7)$$

Eq. 3.5 provides satisfactory results for granular soils with narrow PSD and for suctions above air entry value [53], [57].

One of the most widely used SWRC equations is the smooth function

introduced by van Genuchten [58]:

$$S_e = \frac{1}{(1+(\alpha h)^n)^m}$$

(3.8)

where α, n and m are are empirical constants (m = 1-1/n).

Kosugi [59] proposed a water retention function with the assumption of a lognormal pore size distribution:

$$S_e = Q\left(\frac{\ln\left(\frac{h}{h_m}\right)}{\sigma_h}\right)$$

(3.9)

h – capillary pressure head, related to pore radius,

ln(h_m) – mean deviation of ln(h),

σ_h – standard deviation of ln(h),

Q(x) – complementary cumulative normal distribution function.

$$Q(x) = \frac{1}{\sqrt{2\pi}} \int_x^\infty \exp\left(\frac{-t^2}{2}\right) dt$$

(3.10)

$$Q(x) = \frac{1}{2} erfc\left(\frac{x}{\sqrt{2}}\right)$$

(3.11)

Durner [60] developed a model based on Eq. 3.8 adapted for multimodal pore structure:

$$S_e = \sum_{i=1}^k w_i \left(\frac{1}{1+(\alpha_i h)^{n_i}}\right)^{m_i}$$

(3.12)

k – number of «subsystems» that form total pore distribution,

w_i – weighing factors for the subcurves, $0 < w_i < 1$ and $\Sigma w_i = 1$.

Recently a complete hydraulic model that combines both capillary and adsorptive water behavior, as well as hysteresis, has been proposed by Rudiyanto et al. [61]. A challenge remains to describe SWRC using physically meaningful parameters. An example of three different SWRC equations adjusted to experimental data for a sandy soil taken from Haverkamp and Parlange [62] is shown in Fig. 3.21. SWRCfit software [63] was used for data fitting.
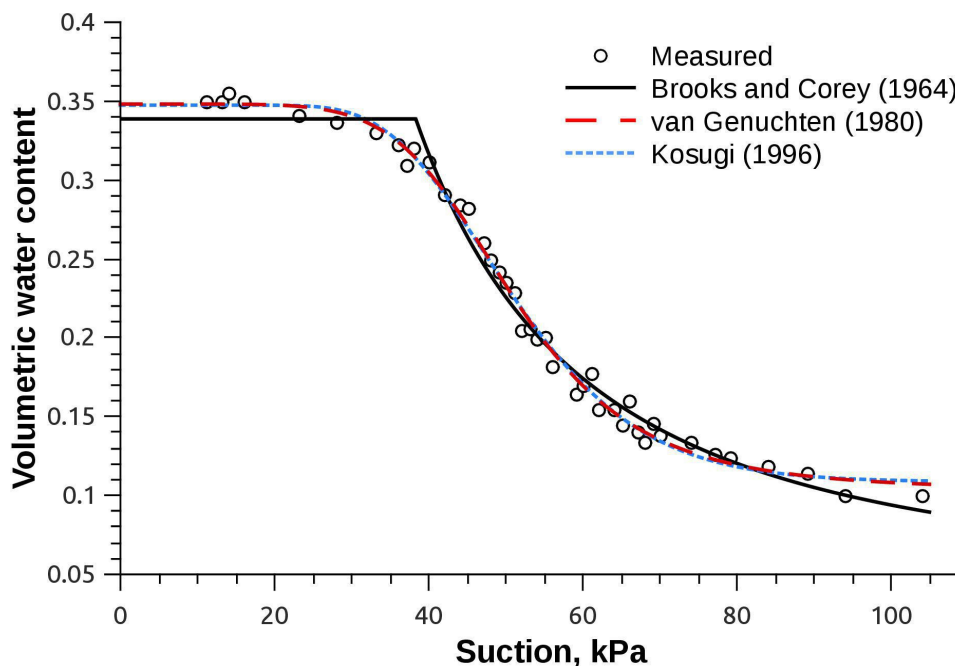
Fig. 3.21 Three equations used to fit SWRC of a sandy soil. Data taken from [62]

SWRC is useful for the analysis of earthen structures' behavior as it shows how much water the soil can store under different climatic conditions. By observing the variations of RH and temperature, soil suction can be calculated using Kelvin formula. During laboratory tests soil water content is a parameter relatively easy to control that is correlated with suction through SWRC. This enables the evaluation of soil characteristics under desired suction values. When a wet soil is exposed to the atmosphere, the water vapor pressure above the water surface, and the water vapor pressure in surrounding air tend to equilibrate. Thus the suction of the soil in this case depends on RH and temperature of the air. After moisture equilibrium between the soil and the environment is achieved, which happens through water vapor flow, soil suction can be calculated using Kelvin equation:

$$s_t = -\frac{RT}{M_w \rho_w} \ln(RH) \tag{3.13}$$

RH – relative humidity,

s_t – total suction,

M_w – molecular mass of water,

R – universal gas constant,

T – absolute temperature in kelvin.

The relationship between RH and suction at 10, 25 and 50º C derived from

Eq. 3.13 is shown in Fig. 3.22. It can be observed that suction is mostly affected by the changes in RH rather than temperature.

Earthen structures remain in complete contact with the atmosphere, so to estimate their suction, the ranges of temperature and RH variation on site should be known. The climatic conditions for the regions with reported use of rammed earth were presented by Beckett and Augarde [64] and are summarized in Table 3.4. Minimum and maximum possible suctions that can develop in soil under these conditions were added to the original data. Thus the rammed earth structures referred in the research work under suctions ranging from 1 MPa to 318 MPa.

Table 3.4 Minimum and maximum annual temperatures, relative humidities and suction values for rammed earth sites by region (modified from [64])

Region	t_{min}, °C	t_{max}, °C	RH_{min}, %	RH_{max}, %	s_{min}, MPa	s_{max}, MPa
Africa	4	38	36	90	13	147
Australia	3	32	23	91	12	207
Europe	-7	37	16	99	1	262
North America	-11	39	11	99	1	318
South America	8	31	15	97	4	266
South East Asia	-34	50	8	100	-	33
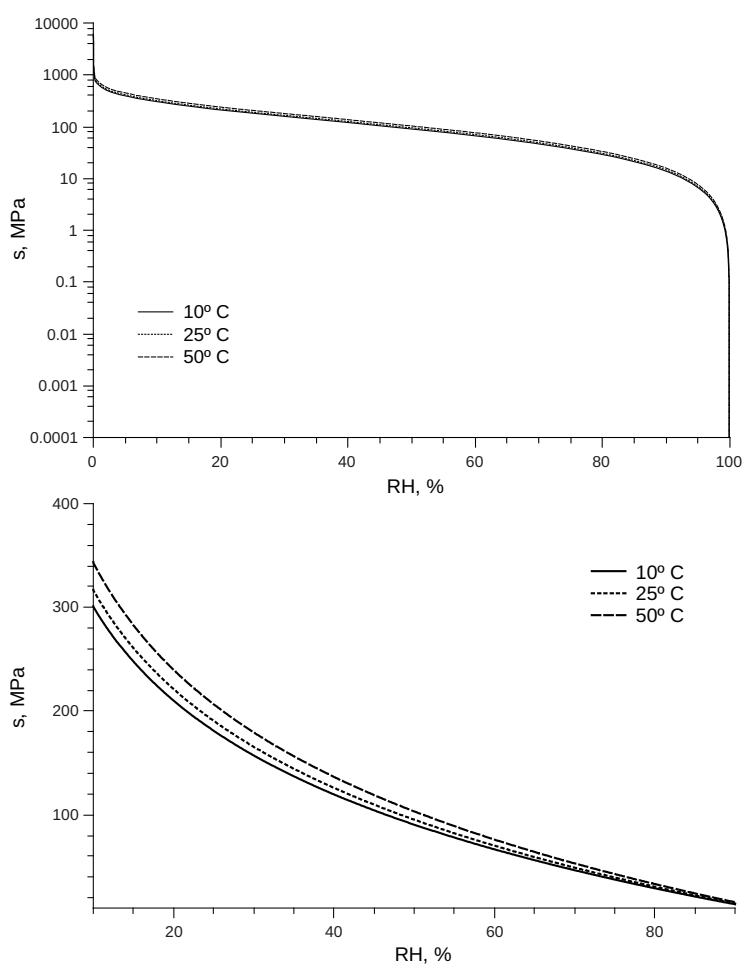
Fig. 3.22 The relationship between RH and suction for 10, 25 and 50° C

There is an uncertainty if changes in RH and temperature can significantly affect the strength of earthen construction materials. Particularly it is important to know if current changes in climate due to global warming can affect in a negative way existing historical structures built with earth. The influence of RH and temperature on rammed earth strength was studied by Beckett and Augarde [64]. The results showed that the unconfined strength of the specimens increased approximately 3 times when RH decreased from 90 to 30% and temperature increased from 20 to 40º C.

3.4.2.
Shear strength criteria for unsaturated soils

There are currently two main approaches to predicting shear strength of unsaturated soils: effective stress approach that involves one stress state variable

and independent state variables approach. The expression for the determination of effective stress in unsaturated soils was originally proposed by Bishop in 1959 [65]:

$$\sigma' = (\sigma - u_a) + \chi(u_a - u_w) \qquad (3.14)$$

$$\tau = c' + ((\sigma - u_a) + \chi(u_a - u_w))\tan\varphi' \qquad (3.15)$$

σ' – effective stress,

σ – total stress,

χ – effective stress parameter,

u_a – pore air pressure,

u_w – pore water pressure,

τ – shear strength,

c' – effective cohesion,

φ' – effective angle of internal friction.

$u_a - u_w$ – suction.

When χ is equal to 1, the Eq. 3.14 becomes Terzaghi's saturated effective stress equation. Initially attempts were made to correlate χ with the degree of saturation, but with limited success. Khalili and Khabbaz [66] analyzed experimental data of unsaturated strength tests reported in fourteen papers and concluded that χ can be estimated as:

$$\chi = \left(\frac{u_a - u_w}{(u_a - u_w)_b}\right)^{-0.55} \qquad (3.16)$$

where $(u_a - u_w)_b$ is air entry value (Fig 3.23). The authors conducted 17 unsaturated triaxial tests that successfully validated the proposed expression.
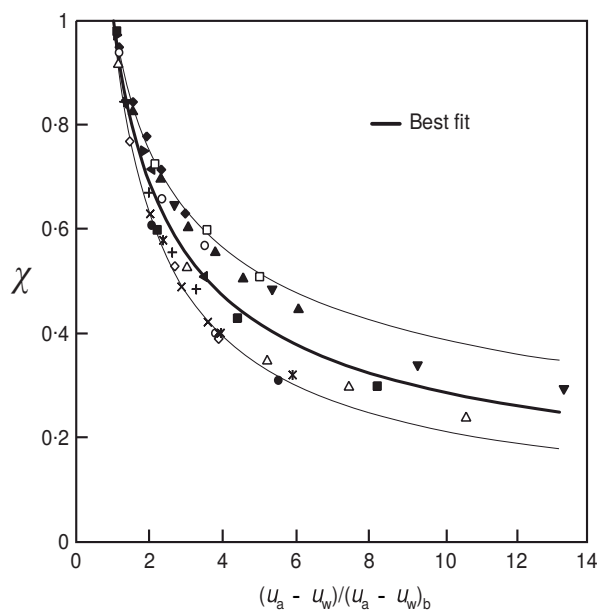
Fig. 3.23 Relationships between effective stress parameter and suction normalized by air entry value [66]

In 1978 Fredlund et al. [67] proposed the equation for predicting of shear strength of unsaturated soils in terms of two independent stress-state variables ($\sigma - u_a$) and ($u_a - u_w$), so the influence of each parameters on soil strength could be evaluated separately:

$$\tau = c' + (\sigma - u_a) \tan \varphi' + (u_a - u_w) \tan \varphi^b \qquad (3.17)$$

φ^b – the angle indicating the rate of increase in shear strength relative to matric suction. The value of φ^b can be estimated from triaxial tests as [68]:

$$\tan \varphi^b = \frac{\dfrac{\sigma_1 - \sigma_3}{2}(\cos \varphi' + \sin \varphi' \tan \varphi') - \left(\dfrac{\sigma_1 - \sigma_3}{2} + \sigma_3 - u_a\right) \tan \varphi' - c'}{u_a - u_w} \qquad (3.18)$$

And from unconfined compression tests (assuming a planar failure envelope):

$$\tan \varphi^b = \frac{\dfrac{\sigma_1}{2}(\cos \varphi' + \sin \varphi' \tan \varphi') - \dfrac{\sigma_1}{2} \tan \varphi' - c'}{u_a - u_w} \qquad (3.19)$$

Rewriting Eq. 3.15 in the form equivalent to Eq. 3.17, shear strength of unsaturated soil can be expressed as [54]:

$$\tau = c' + (\sigma - u_a) \tan \varphi' + \chi (u_a - u_w) \tan \varphi' \qquad (3.20)$$

Thus Bishop's effective stress parameter can related to Fredlund's φ^b as:

$$\chi = \frac{\tan \varphi^b}{\tan \varphi'} \qquad (3.21)$$

There are uncertainties associated with the application of both Eq. 3.15 and

3.17. χ depends on soil structure and stress path, thus its values obtained in different types of tests will differ. The values of φ^b were found to vary over wide ranges of soil saturation.

Some authors proposed correlations of SWRC with unsaturated soil strength. A formula that relates volumetric water content to unsaturated soil shear strength was introduced by Vanapalli et al. [68]:

$$\tau = c' + (u_a - u_w)\left(\frac{\theta}{\theta_s}\right)^\kappa \tan \varphi' \tag{3.22}$$

where κ is a fitting parameter. Vanapalli et al. [69] suggested a relationship between φ_b and effective saturation:

$$\tan \varphi^b = S_e \tan \varphi' \tag{3.23}$$

Lu and Likos [70] pointed out that there are forces that influence soil strength that are not explicitly included in abovementioned strength criteria. These forces include cementation and physicochemical phenomena such as van der Waals attraction and other electrical forces involved in the interaction between clay particles. The concept of suction stress that takes into consideration these factors was introduced:

$$\sigma' = \sigma - u_a + \sigma'_s + \sigma_{C0} \tag{3.24}$$

$\sigma'_s = f(\theta)$ – suction stress,

σ_{C0} – intergranular bonding stress that provides cohesion in saturated soil.

If Mohr-Coulomb criterion is considered σ_{C0} can be estimated as follows:

$$\sigma_{C0} = \frac{c'}{\tan \varphi'} \tag{3.25}$$

Li et al. [71] used the following equation to quantify effective stress in unsaturated soil:

$$\sigma' = (\sigma - u_a) - \sigma^s \tag{3.26}$$

where σ^s is suction stress, which can be described by:

$$\sigma^s = -(u_a - u_w) S_e \tag{3.27}$$

The authors validated Eq. 3.26 by using it to predict unconfined compressive strength and tensile strength of compacted soils via Brazilian test. The following equations were used:

$$IDT = \frac{m(\sigma^s + u_a) - b}{3.7 - 0.7\,m} \tag{3.28}$$

$$UCS = \frac{3\,m(\sigma^s + u_a) - 3\,b}{m - 3} \tag{3.29}$$

IDT – tensile strength obtained by diametrical compression,

UCS – unconfined compressive strength,

m – slope of mean effective stress vs. deviator stress plot,

b – intercept of mean effective stress vs. deviator stress plot.

Assouline [72] suggested, based on the experimental data from three soils, that both SWRC and rupture modulus (flexural strength) can be represented as a function of silt to clay ratio:

$$\sigma_{rup} = -0.06 + 0.37\left(\frac{SC}{CC}\right)^{-0.5} \tag{3.30}$$

where SC is silt content and CC is clay content.
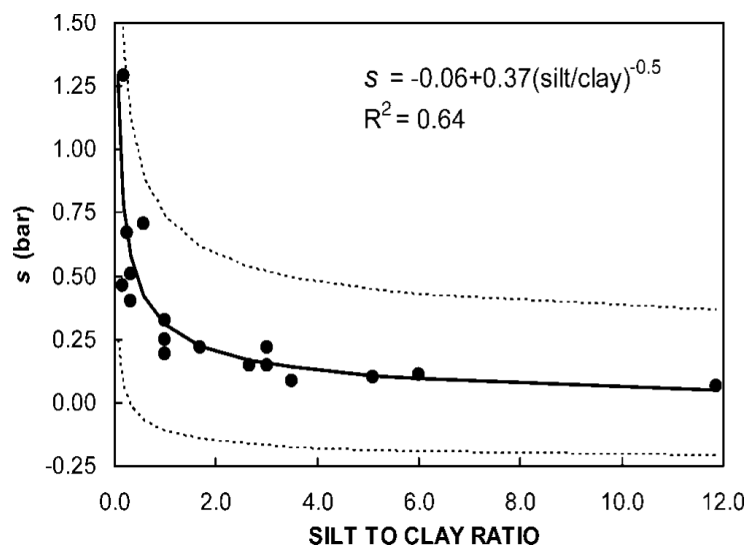
Fig. 3.24 Plot of the modulus of rupture (flexural strength), s, as a function of silt/clay content ratio and the fitted expression (Eq. (3.30)). The dashed line represent 95% confidence limits.

Khalili et al. [73] defined effective stress for the soils with double porosity:

$$\sigma' = \sigma - \alpha_M\left(\chi_M u_{Mw} + (1 - \chi_M)u_{Ma}\right)I - \alpha_m\left(\chi_m u_{mw} + (1 - \chi_m)u_{ma}\right)I \tag{3.31}$$

χ_M - unsaturated effective stress parameter of macropores,

χ_m - unsaturated effective stress parameter of micropores,

u_{Mw} - macropore water pressure,

u_{Ma} - micropore air pressure,

u_{mw} – micropore water pressure,

u_{ma} - micropore air pressure

I - second order identity tensor.

α_m and α_M are effective stress parameters of saturated double porous media:

$$a_m = \frac{c_g}{c} \tag{3.32}$$

$$a_M = 1 - \frac{c_g}{c} \tag{3.33}$$

c – drained compressibility of aggregated soil,

c_g - drained compressibility of the material forming the aggregates.

The influence of suction on the strength of unsaturated soil is not unlimited. It is expected to peak between saturation and completely dry state [74]. Lu and Likos [75] and Lu [76] argued that matric suction cannot wholly contribute to the state of stress in soil unless it is below air entry value, as water in transition and residual states of desaturation is no longer interconnected and acts on micro scale. Therefore, suction cannot be used together with net normal stress, which is macroscopic concept. Thus, uncertainties remain on the applicability of both effective stress and independent variables concepts to prediction of strength of unsaturated soil.

3.5.
Indoor climate of earthen buildings

Water retention properties of soils are directly related to the ability of earthen construction materials to regulate the quality of indoor air. Comfortable indoor climate comprises temperature and humidity fluctuations within certain limits that are favorable for human health. Excessive humidity can cause several problems such as mold formation and fast bacteria growth, whereas RH below 40% can cause respiratory diseases [2]. In poorly planned or houses built with inadequate materials there's a need for heating and air conditioning systems and eventual humidification. That leads to energy consumption that adds up to environmental impact of the structure. One of the most striking examples of bad indoor climate caused by improper use of construction materials can be found in South African poor urban areas, where the population lives in shacks built with corrugated steel. In such dwellings indoor temperature in summer can reach 45°C and in winter be

as low as 2°C [77], [78]. A solution of this problem might be inspired by Syrian beehive houses (Fig. 3.25), that due to their earthen walls and specific shape keep interior temperatures between 24° and 30° C, while outside noon-to-midnight extremes range from 15° to 60°C [79], [80].
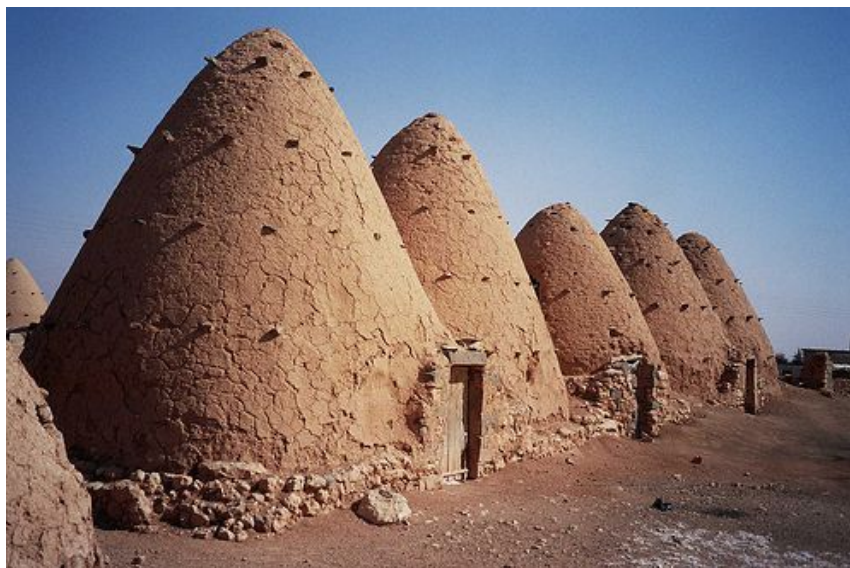
Fig. 3.25 Syrian beehive houses [80]

Minke conducted a series of experiments in order to analyze hygroscopic behavior of earthen walls, which showed humidity absorption characteristics 10 times better then burned brick and 50 times better then clinker brick, the absorption – desorption threshold being at 50% RH [7]. Morton et al [81] carried out extensive humidity and temperature readings in an earthen house every 15 minutes during one year and provided a detailed analysis that demonstrated a good performance of the construction material. Earth plaster showed to regulate short-term peaks, while the core wall material had influence on long term humidity fluctuations. In their book Bokalders and Block [82] also suggested that clay plasters are excellent materials when it comes to indoor climate regulation, helping to balance the effect of such activities as showering, laundering or cooking. Although control of RH generally is not considered in building design, there are cases when HVAC systems are used for temperature and humidity regulation. Earthen materials can reduce substantially energy consumption in these situations [83]. It was shown by Liuzzi et al. [84] that in air-conditioned environments that have lime stabilized earthen finishing there is significantly lower monthly energy demand as compared to common finishing materials -

acrylic stucco and gypsum plaster.

Earthen walls have high thermal storage capacity, not only because of their high mass but also because of the traditionally great thickness. It is particularly useful in the climates with significant daily temperature fluctuations, where it can absorb solar heat during the day and release it at night [52], [53]. Vega et al. [86] pointed out that the insulation capacity of earthen materials is lower than of those those currently in use, however the thermal conductivity of adobes can fall to two or three times below than that of industrialized masonry materials. Hall and Allinson [88] hypothesized that by controlling PSD and compaction energy it is be possible to create earthen materials with specific hygrothermal properties that would control evaporative drying and consequently indoor climate of the structures built with earth.

3.6.
Selection of soil for construction

In an ideal situation, the soil available on site should be used for construction so that it is possible to build walls with the material dug out during foundation works. This can minimize transportation costs and lower embodied energy of the structure. However, this soil has to comply with certain requirements such as have a desired strength, durability and shrinkage limit. The aim of soil selection is to evaluate if a given soil have the properties which allow achieving desired structural performance. This evaluation can be made by trail testing of compacted specimens, but ideally it should be possible to forecast earthen material performance analyzing the properties that can be determined through common soil characterization tests.

The recommendations for soil selection available in the literature are mostly based on empirical data and vary significantly. It is a challenging task to compare them conclusively due to different test conditions and lack of uniformity in the choice of used parameters. To a certain point, the selection of soil type depends on particular construction technique. Each technique implies a different type of compaction, such as dynamic - for rammed earth, static – for CEBs and kneading – for formed earth. There is generally a desired combination of clay and water content for a chosen compaction procedure to be effective. For example, adobe

production needs much more plastic soil, than rammed earth.

Delgado and Guerrero [88] made an exhaustive review of the normative documents and guidelines that determine the criteria of soil suitability. The common properties used for soil evaluation are:

- Particle size distribution;
- Consistency limits;
- Maximum shrinkage;
- Maximum content of salts and organic material.

Particle size distribution is the most cited property in soil selection recommendations. Some common assumptions that can be made are: there is a minimum quantity of clay needed for a soil to develop a resistance in unconfined compression, there is a maximum particle size limit that depends on the particular construction technique and equipment available. It is also stated by several authors, that well graded material is preferred due to the possibility to achieve higher densities thus increasing particle interlock and subsequently mechanical strength [13], [89]. The use of Fuller formula was proposed by Houben and Guillaud [13] to calculate the proportions of each particle fraction:

$$p = 100 \left(\frac{d}{D} \right)^n$$

(3.34)

p – the proportion of grains of given diameter;

d – the diameter of grains for the given value of p;

D – the maximum grain diameter;

n – the grading coefficient.

The grading coefficient of 0.2-0.25 is recommended for earth construction [13], however in highway engineering the values between 0.33 and 0.5 are preferred [90]. Fuller formula is only applicable for spherical particles, which is not the case for most soils and cannot be used for clay. All known models for packing of granular material are limited because they do not take into account geometric characteristics of particles, such as sphericity, roundness and surface roughness [47].

Though intuitive, the assumption that the material density is related to its unconfined compressive strength wasn't confirmed by the experiments available in the literature [46], [91]. As shown before, the type of clay has a major influence

on soil behavior, however, the recommendations based on granulometric distribution alone fail to take this into account. Fig. 3.26 presents recommended PSD ranges for adobe, rammed earth and CEBs found in technical norms and guidelines. If scientific papers are also considered, the data becomes more disperse, for example the proportions of different particle size fractions used for rammed earth can vary from 0 to 35% for clay, from 0 to 80% for silt and from 10 to 80% for sand [89].
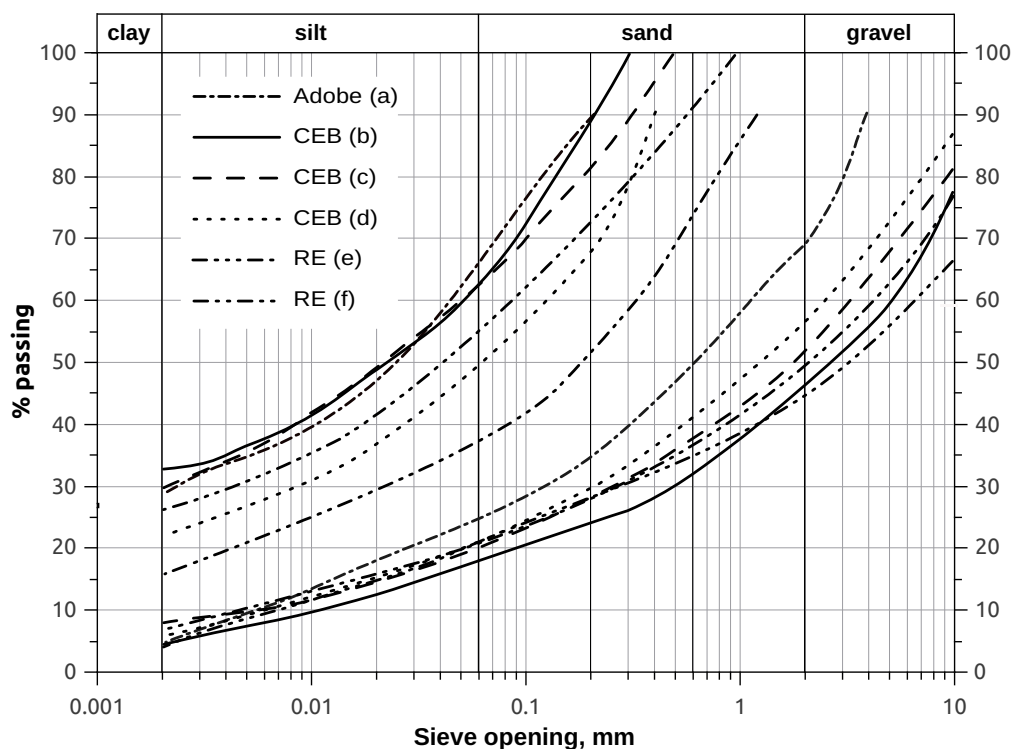
Fig. 3.26 Recommendations for PSD limits for different construction techniques (modified from [88]): a) [13] b) Spanish norm c) French norm d) [13] e) [13] f) Spanish norm

The type of clay minerals present in soil has major influence on its water adsorption properties and consequently on its strength and shrinkage. However, the activity of each particular clay mineral can vary significantly, depending on its level of crystallinity and isomorphic substitution. Liquid limit and plasticity index are properties that indicate the activity of soil and together with clay content can be a used as a parameter for evaluation of soil suitability. The existing recommendations on plasticity of earthen construction matrials are presented in the form of LL vs PI nomograms shown in Fig. 3.27.
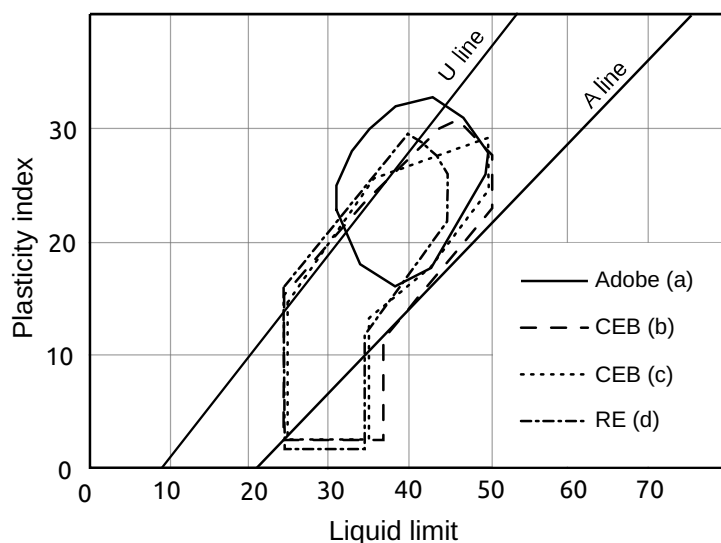
Fig. 3.27 Plasticity recommendations a) [13] b) [13] c) French norm d) [13]

Three of five references appear to share the same data from Houben and Guillaud [13], who offer no description of the experiments that were carried out to obtain it.

3.7.
Soil compaction

Compaction is a method of mechanical stabilization of soil which consists in material densification by reduction of air voids without changing water content. It is widely used for the improvement of the mechanical characteristics of soil for the construction of dams, embankments, fills, and in earthen buildings. There are different types of compaction, which are applied according to soil type, material characteristics to be achieved and the equipment available. Compaction generally increases the strength of soil, reduces its compressibility and permeability. The main variables that control compaction of a given soil are water content, type of compaction and compactive effort, which can be represented in terms of energy density in order to account for the size of compacted specimen. The following types of compaction can be named:

- Compaction by vibration;
- Dynamic, which is generally performed by dropping a weight on a soil

mass;

- Static, which consists in applying a static or quasi-static load to the whole area of a specimen;

- Kneading - applying a static load to a fraction of the area of a specimen.

Laboratory compaction test can provide a set of curves showing the relationships between water content and dry density for different energy levels, from which the values of optimum moisture contents (OMC), at which maximum dry density is achieved, can be obtained. When the soil compaction properties are known, it is possible to prepare samples in the laboratory for the determination of engineering characteristics representative of the material in the field.

First compaction test was introduced by Proctor in 1933 in order to determine the properties of soils used for the construction of dams. The test consists in compaction of a given soil in three layers in a cylindrical mold which has a volume of one liter. A rammer of 2.5 kg weight is dropped from the height of 30 cm in 26 blows for each of 3 layers. With the appearance of heavier equipment modified Proctor test, with the same principle, but higher energy input, was introduced.

Water content is the determinant variable in the process of compaction. Dry granular soils are best compacted by vibration. The aggregates of dry fine grained soils tend to be broken by compaction force, thus causing an increase in dry density. At low water content liquid bridges are formed between soil grains which restrains their rearrangement and provokes a decrease in dry density. With consequent increase in moisture content, water begins to act as a lubricant facilitating the movement of soil particles and increasing the plasticity of clay fraction. The dry density increases up to optimum moisture content. At that point the soil grains become as closely packed together as they can under the application of fixed compactive effort. Adding water above OMC reduces the efficiency of compaction. Air bubbles become trapped, excess water tends to hold soil particles apart and clay fraction swells. This continually reduces dry density as moisture content increases. At water contents above OMC the degree of saturation of soil remains practically constant. All air voids cannot be eliminated by compaction, but the degree of saturation can reach as high as 85-90%. At this condition the volume of soil remains nearly constant as water and solids are incompressible and air can be no longer expelled. Thus, when the compactor is

dropped upon soil surface (dynamic method) or inserted into soil mass (kneading), the soil around it tends to heave.

A different compaction curve can be plotted for each energy input. As compaction energy increases, maximum dry density becomes higher and OMC decreases, the curve moves up left and becomes narrower (see Fig. 3.28b). For dynamic compaction, the energy input can be elevated by using heavier rammer, increasing the quantity of blows and the hight of fall. For static compaction and kneading, the energy transmitted to the soil can be altered by changing applied pressure. When using automatic tampers it is convenient to use time as a parameter to regulate energy input. In geotechnical engineering the compaction energy is chosen according to the type of equipment used on site. In traditional rammed earth applications the soil is compacted until it "rings" [89], so the energy transmitted to the soil depends mostly on soil type. The energy used to produce CEBs depends on the press available, but the capacity of the equipment is mostly reported as maximum pressure that it can achieve. These pressures range from 2 MPa for manual presses up to 12 MPa for hydraulic units [92]. Although higher energies can yield higher densities of material, overcompaction is not recommended, especially for fine-grained soils, because it can lead to a type of soil structure which contributes to high water absorption rates, swelling and low strength [93]. The energy applied by dynamic compaction can be calculated as:

$$E = m \cdot g \cdot h \cdot n_b \cdot n_l \qquad (3.35)$$

m - mass of rammer;

h - the height of drop;

n_b - number of blows;

n_l - number of layers.

Unlike in Proctor test, the energy of static compaction depends on a number of variables, such as the type of soil and water content. It can be calculated through integration of force - displacement curve:

$$E = \int_{x_1}^{x_2} F(x)\,dx \qquad (3.36)$$

F(x) – applied force;

x - displacement.

However, compaction energy itself doesn't provide useful information, the same energy applied to different amount of soil yields different densities. To account for the volume of material, compaction effort can be represented in terms of energy density E_{vol}:

$$E_{vol} = \frac{E}{V} \tag{3.37}$$

E - energy applied to the soil;

V - the final volume of compacted sample.

To aid the interpretation of compaction curves, air voids lines can be plotted on the graph. Air voids line is a curve showing the relation between dry density and water content for a fixed percentage of air voids. The compaction curves can only be positioned to the left of zero air voids line. The equation that describes these lines is as follows:

$$\rho_d = \frac{G_s \rho_w}{1 + \dfrac{w G_s}{S}} \tag{3.38}$$

ρ_d - dry density of soil,

V_{air} - percentage of air voids,

G_s - specific gravity of solids,

w – water content,

S – degree of saturation.

Different types of soil have their characteristic compaction curves (see Fig. 3.28a). The curves for well graded sandy and silty soils show a clear peak, while uniform sand and clayey soils present no well-defined OMC. The compaction curve indicates soil sensitivity to water content change. Sand with a small fraction of clay undergoes considerable change in density with 2-3% variation in water content, while uniform sand, loamy gravel, plastic clay do not react significantly to small changes in water content [25].
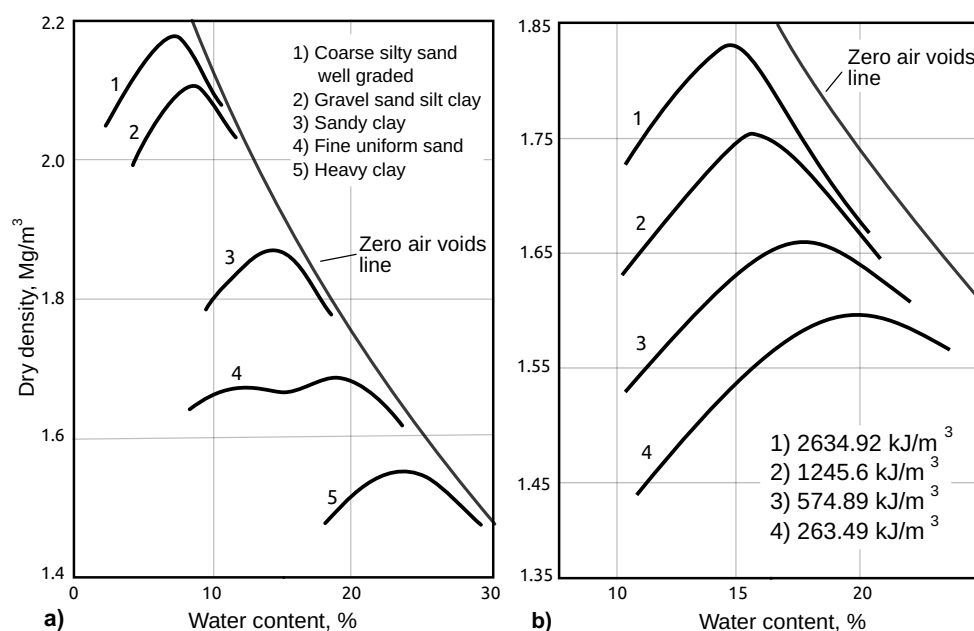
Fig. 3.28 Typical compaction curves for a) different types of soils [93] b) different energy inputs [25].

It was shown by a number of authors that certain structure is imposed on soil by compaction, which depends on soil type, compaction method and energy, and water content [25], [94], [95]. This effect can be observed on micrographs of compacted soil specimens [94]. During the process of compaction plate shaped and elongated particles tend to align perpendicularly to the direction of compaction force. The degree of particle arrangement varies and is more pronounced for soil compacted on the wet side of optimum. Fig. 3.29 shows schematically the soil structure at different regions of compaction curve. On the dry side of optimum the soil particles stay flocculated becoming more dispersed with the addition of water, see structure evolution along the points A-B-C. Increasing compactive effort also contributes to the dispersion of particles, see soil structure in points A vs. E and C vs. D. Thus particle dispersion and alignment increases with the increase of water content and compaction energy [25].
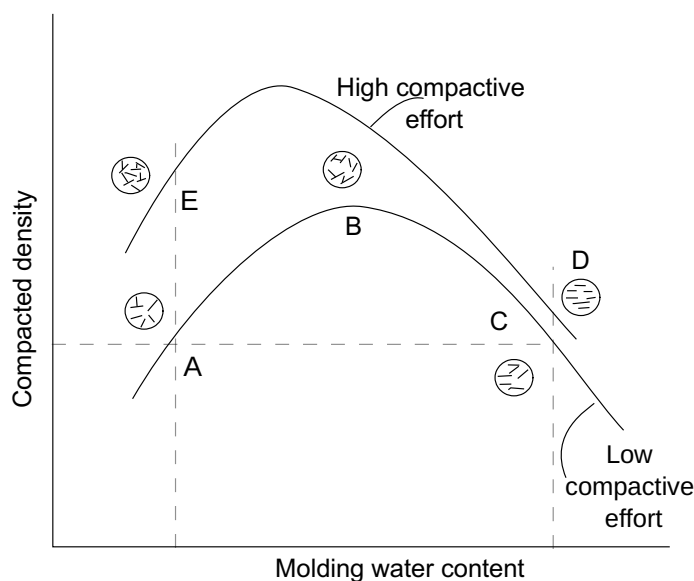
Fig. 3.29 Effect of compaction on soil structure [25]

Lambe [25] presented the effect of compaction on soil structure in terms of individual particles, while normally in soils fine fraction is found in form of aggregates of various sizes and as a coating of coarser particles, e.g. stacks of kaolin minerals in Fig. 3.4. Sloane and Kell [94] produced micrographs of the replicas of the sections of kaolinitic clay specimens compacted by impact, kneading and static pressure (Fig. 3.30). The authors observed almost no individual particles in edge-to-face or face-to-face contacts but rather packets of clay minerals with different degree of fabric orientation. It was concluded that on the dry side of optimum the particle arrangement was random for all types of compaction and above optimum the kaolin plates were aligned according to the direction of load application, the effect most visible for statically compacted specimens. Layers of oriented clay particles in the soil compacted on the wet side of optimum were also observed in the recent study by Oliveira [95].
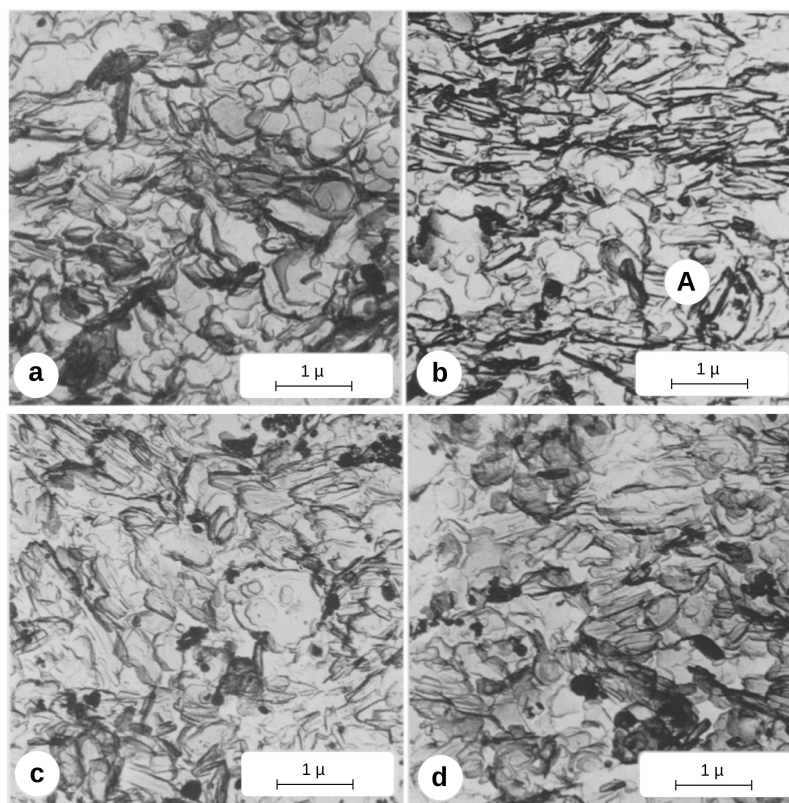
Fig. 3.30 The fabric of kaolinitic clay compacted by a) impact 3% below optimum b) impact 3% above optimum c) static pressure 3 % below optimum d) static pressure 3% above optimum. A) Packets oriented at steep angle due to soil shearing by compactor (from [94])

The differences in soil fabric obtained by compaction at different moisture contents affect permeability of compacted soil. This parameter is essential for durability of earthen materials. Theoretically, permeability depends on the average pore size of material. Thus, for a certain soil lower permeability can be achieved by breaking down as much particle aggregations as possible. This is done by increasing compaction energy and water content as soaked aggregates break down more easily. Bagherieh [96] suggested that soils compacted on the dry side of optimum tend to be aggregated, while Toll [97] argued that aggregation occurs as a result of compaction at degree of saturation below 90%. This fact was partially confirmed by Toll and Ong [98] who showed that residual sandy clay compacted wet of optimum had double porosity structure.

The type of compaction that provides the lowest permeability is kneading due to high values of shear applied. Traditionally soil used for construction is mixed with water by kneading, either stomping by feet or with the aid of a horse. The comparison of permeability of soil compacted statically and by kneading is shown

on Fig. 3.31, it can be noted that the increase only in water content and not in dry density leads to a drastic drop in permeability at high water contents. Tests on four different soils [99] revealed that minimum permeability is achieved at OMC, for predominantly granular soils is a function of density, but for fine-grained soils is not affected by water content change above optimum.
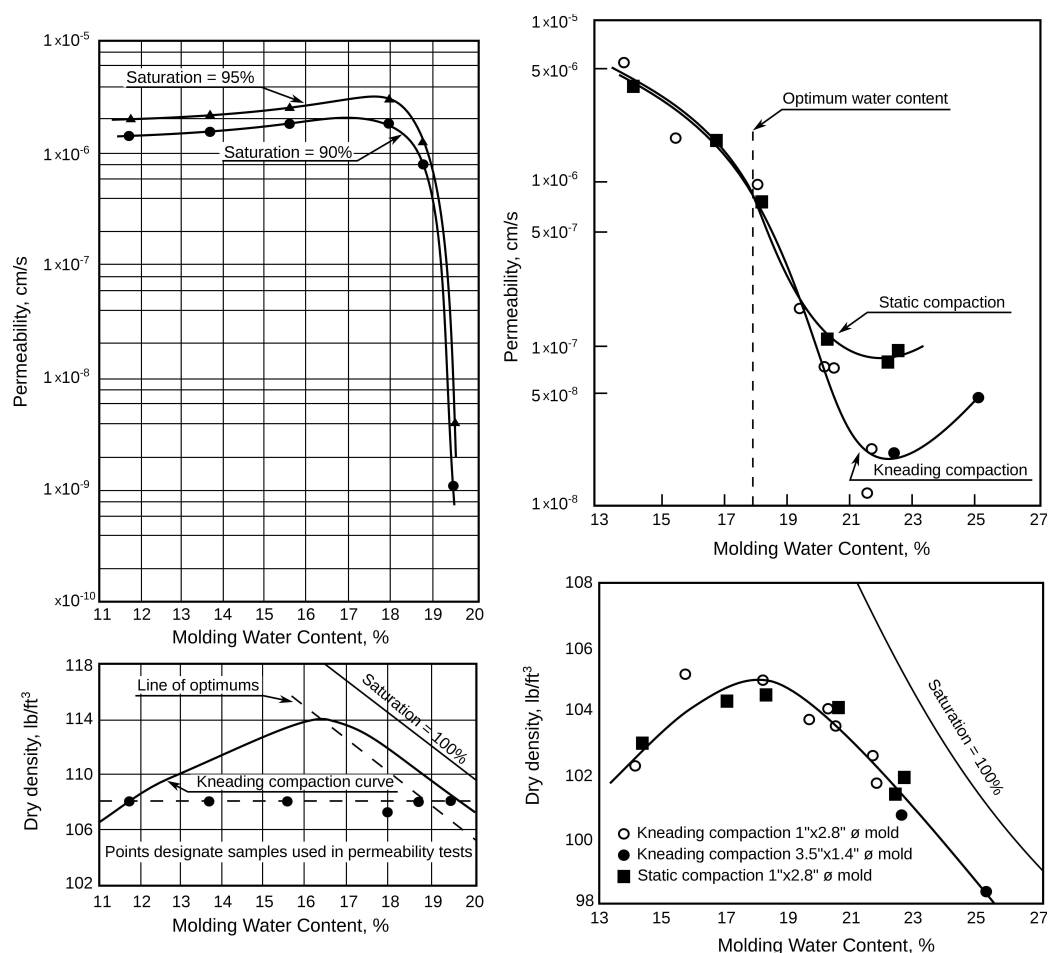
Fig. 3.31 Influence of compaction water content on soil permeability for constant and varying densities [27]

There are studies that present the influence of molding water content on soil strength [25], [100]. However, the tests were made on as-compacted specimens, so soil strength in this case is mostly affected by the value of suction than specific structure imposed by the process of densification.

3.7.1.
Static compaction

Proctor compaction test has been used to determine OMC of soil used both in

geotechnical structures and in earth construction. In case of rammed earth, where compaction method is dynamic as in Proctor test, it can provide adequate results. Modified Proctor test is often used for rammed earth OMC determination [46], [101]. As it was shown earlier, soil structure resulting from static, kneading and dynamic compaction is different. Static compaction is the process used in the fabrication of compressed earth blocks (CEBs). The static compaction curve differs from one obtained in Proctor test, so such parameter as OMC is also different.

When the soil is compacted statically, its volume decreases continually as the load is applied to the whole area of the sample. Depending on the characteristics of the equipment used, when water content approaches saturation and no more air can be expelled, either consolidation starts, i.e. water is drained from the soil, or, if there is no way for water to drain, pore pressure begins to grow at equal rate as the applied load, for water is relatively incompressible.

The parameter that in most cases is used to control static compaction is maximum stress rather than energy [10], [102]–[105], which can be calculated by integration of force-displacement curve. Unlike in Proctor test, where the energy transmitted to the soil is constant, the energy in static compaction test depends on water content. Consequently, static compaction curve plotted for constant maximum pressure and dynamic one, which is plotted for equal energy input cannot be compared directly. Static compaction test can be performed at constant rate of stress or constant rate of strain using either maximum force or maximum displacement as the limiting condition. High compaction speed can cause rapid increase in pore pressure especially in fine grained soils, although there is no recommendations available and the rates of strain that vary from 1.25 mm/min to 65 mm/min can be found in the literature [106], [107]. Maximum rate of stress of 0.25 MPa/s was recommended by Olivier [108].

One of the first studies of static compaction was presented by Turnbull ([103] in [25]). Moisture – dry density curves were produced for a silty clay compacted to different maximum stresses ranging from 1.379 MPa (200 psi) to 13.79 MPa (2000 psi). The pressure was applied from the top of the specimen and from both top and bottom. The curves obtained for a constant maximum pressure were compared to Proctor test data (constant energy input) and field compaction data. Olivier and Mesbah [102] argued that modified Proctor test, widely used in

earth construction, wasn't representative of the CEB fabrication conditions, as the energy transfered to the soil in dynamic test wasn't comparable to static pressure used for earth blocks. The authors developed a static compaction test that enabled the optimization of the parameters of the soil used for CEB production. The load was applied statically on the top of the soil placed into 110 mm diameter mold, the force being measured on the bottom of the sample. As a result, a set of curves for pressures from 1.2 MPa to 10 MPa was produced. The unconfined compressive strength (UCS) of the specimens compacted at different water contents was also determined, however their diameter-to-height ratio was equal to 1 and no shape correction factor was applied. More details of this study were provided in [108]. Some of the force-displacement curves were presented, from which it was clear that at moisture content equal to 10.5% the soil reached saturation at the static pressure of 2 MPa, as it was impossible to compact the soil further even increasing the stress up to 8 MPa (Fig 3.32d). The tests were carried out at a constant rate of stress. Both Turnbull [103] and Mesbah [102], [108] obtained compaction curves that resembled dynamic ones in shape, showing a peak dry density value corresponding to OMC (Fig 3.32a,b).
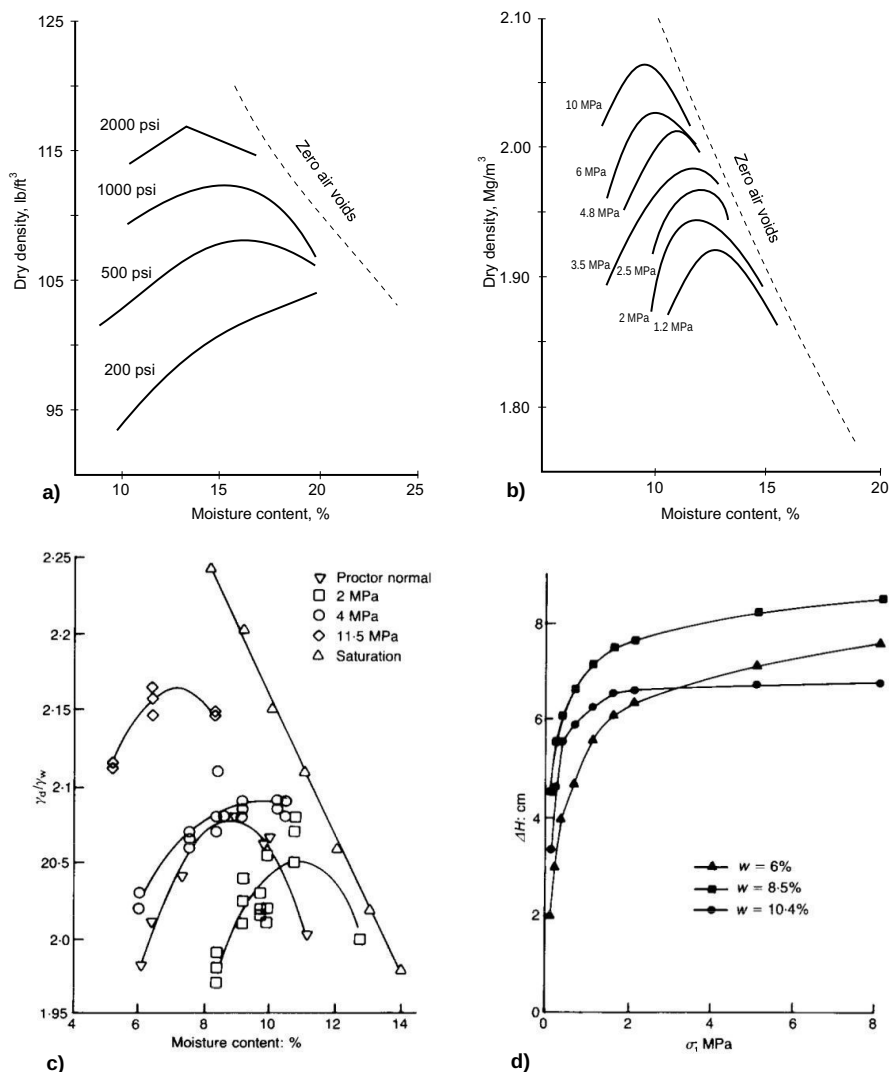
Fig. 3.32 The results of static compaction tests: a) Compaction curves from
[103] b) Compaction curves from [102] c) Compaction curves from [108] d)
Stress – displacement curves [108]

Reddy and Jagadish [106] performed static compaction of a silty clay at a
constant rate of strain of 1.25 mm/min. For each moisture content force-
displacement curves were obtained and energy density calculated. Compaction
curves were plotted for different energy inputs and compacted with the results of
Proctor test. The shape of static compaction curves was different from the
dynamic one and didn't show peak dry density value, instead OMC was found to
be at the point of the curve where water starts to be expelled from the soil and
consolidation starts. There was no particular saturation value that indicated OMC,
instead it was different for all the compaction curves presented (Fig. 3.33).
Similar results were obtained by Mesbah et al [109] and Tarantino and De Col
[110].
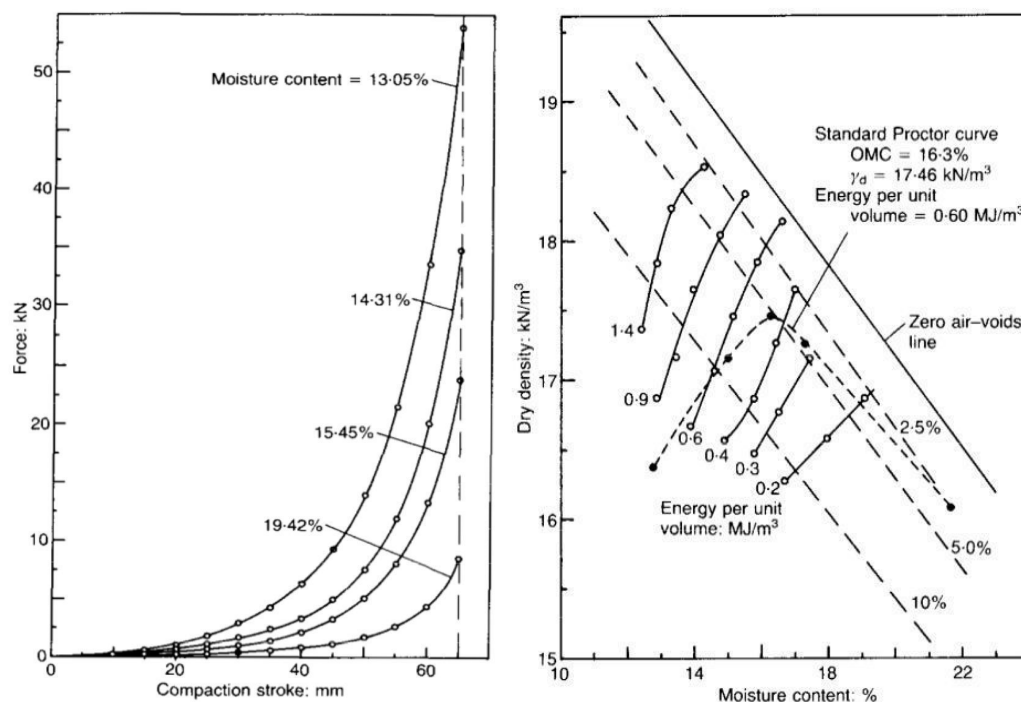
Fig. 3.33 Static compaction test data: force - displacement and moisture content - dry density curves for different energy inputs [106]

All the referred authors performed static compaction tests only on one type of soil each. It was recommended to investigate the behavior of different types of soil under this kind of test [109]. The effect of friction between compaction mold and the soil was mentioned by a number of researchers [10], [102], [106], [109], yet there are no quantitative results available, the same is for the influence of rate of stress or strain during the test.

3.8.
Strength testing of soil as a construction material

Determination of the strength characteristics of earthen materials is an essential part in any construction project. Presently there are no commonly accepted technical norms regulating earth material testing. There are earth building codes in New Zealand, Australia, Mexico, USA, but they differ significantly. Geotechnical standards are normally used for material characterization and concrete and masonry tests are adapted for strength determination.

Rammed earth is a monolithic construction technique, thus concrete testing procedures and terminology are often used, especially for stabilized material.

Rammed earth specimens are produced by dynamic compaction. Proctor test and its modifications are mainly used for this purpose. Standard proctor mold dimensions differ from ones recommended for unconfined strength tests. A variety of rammed earth specimen shapes can be found in the literature: cylindrical specimens of different sizes, cubic, prismatic ones, as well as full size walls and columns [91], [101], [111]. The lack of standardization of sample shape and size complicates the analysis and comparison of available research results and their application in construction projects.

Strength testing of compressed earth blocks and adobes normally follows the procedures developed for masonry. Examples of different test configurations can be found in the literature: individual blocks tested in uniaxial compression in different directions, two blocks with mortar or plywood between them, blocks cut in halves or quarters. There are also some studies in which cylindrical statically compacted soil samples are used in order to represent CEBs [10], [104], [105], [112], [113].

There is a very large number of soil types used in earth buildings. When the behavior of soil as a construction material needs to be analyzed, it is important to investigate the soil properties as thoroughly as possible. Particle size distribution or percentage of size fractions is presented in all the papers reviewed. Besides clay percentage, it is essential to know clay mineral type present in soil, for different clay minerals behave in completely different way. X ray diffraction analysis is considered the best way for clay mineral identification. If it is not available, simpler methods as methylene blue test can be applied. The activity of clay can indicate its behavior and it requires common Atterberg limits tests to be carried out. These are basic material properties that are often dismissed during earth construction research [91], [104], [105], [114].

Earthen materials should dry before their usage as load-bearing elements in structures. Relative humidity of the drying environment affects soil suction significantly. The soil drying conditions should be compatible with service conditions of the structure. It is not uncommon that earthen materials are tested after drying at 100º C, which removes all the water from the specimen and can damage the crystalline lattice of clay minerals, or after immersion in water, which is unrealistic and difficult to be quantified. In recent years a number of studies has appeared where rammed earth is treated from the point of view of unsaturated soil

mechanics, which has an adequate framework to account for all the variables that influence its behavior [30], [44], [45], [64], [74], [114], [115]. Currently there is no such research for CEBs or any other earth construction technique apart from rammed earth.

Ciancio et al [46] tested rammed 10 artificial soils consisting of kaolinitic clay, silica flour, white sand and gravel mixed in different proportions. The soils were compacted into 100 mm diameter and 200 mm height cylindrical samples with a jackhammer at OMC determined in Proctor test. The samples were dried for 28 days the laboratory where temperatures varied from 7 to 18ºC and mean RH equal to 67%. Prior to unconfined compression tests the samples were oven dried. All soils showed resistance below 2 MPa. The authors attributed low strength to total removal of water, this situation being unrealistic.

Lawson et al. [105] tested CEBs compacted at three different water contents: OMC-3%, OMC and OMC+3%, and two static pressures: 5.17 and 9.31 MPa. Although the blocks were compacted statically, OMC was determined in Proctor test. The CEBs were dried for 7 and 28 days at RH 60% and temperature of 16 ºC. Clay mineral present in the soil as well as dry density of the blocks were not reported. The authors stated that higher compactive effort produced stronger CEBs. The longer the drying period, i.e. the lower the moisture content, the higher was soil compressive strength. Flexural strength was found not to be affected by moisture.

Hall and Djerbib [91] used 10 artificial soil mixes with different proportions of clay, silt, sand and gravel compacted into 100 x 100 mm cubic samples. OMC was determined in proctor test and compaction was carried out according to New Zealand standard. Clay mineral used for mix production was not identified. The samples were dried for 28 days at 20º C and RH 75% prior to be tested in compression. The authors' hypothesis that dry density was the determinant factor for soil strength was not supported by experimental data. Instead, it was suggested that the binder/aggregate ratio was more important parameter in determining compressive strength values.

Koukau and Morel [104] tested CEBs produced with natural soil at 2 MPa static pressure. The blocks were compacted at four different water contents and dried at 22 ºC until reaching constant mass. The CEBs compacted at lower water contents had higher density and compressive strength.

Maniatidis and Walker [101] conducted large scale tests on rammed earth columns as well as prismatic and cylindrical small samples. Natural soil with illitic clay fraction was used. The strength of large columns was lower that of small specimens due to higher content of large aggregates and difference in compaction procedure.

Jaquin et al [44] tested unsaturated strength of rammed earth compacted by vibrating hammer for three soil mixes. Compressive strength was determined for the soil mix containing 26.2% of clay, 52.3% of silt and 21.5% of sand for high water contents (above 5%) to enable tensiometer suction measurements during the tests. Two other soil mixes with 10% increase in sand and 10% increase in clay content were tested in diametrical compression. Tensile strength was measured only for water contents below 5%. SWRCs were also defined for two later soil mixes based on 4-5 measurements.

Nowamooz and Chazallon [115] performed finite element analysis of a rammed earth wall with respect to different water contents. Uzan's non-linear elastic model was used, which was considered adequate for granular soil. The model parameters were determined in repeated load triaxial tests. SWRCs and effective stress parameters c' and φ' were also obtained.

Bui et al. [114] studied the effect of water content on the mechanical behavior of rammed earth produced with three soils, one of which was stabilized with natural hydraulic lime. SWRCs were obtained and unconfined compression tests conducted. It was found that soil strength and elastic modulus increased with decreasing water content.
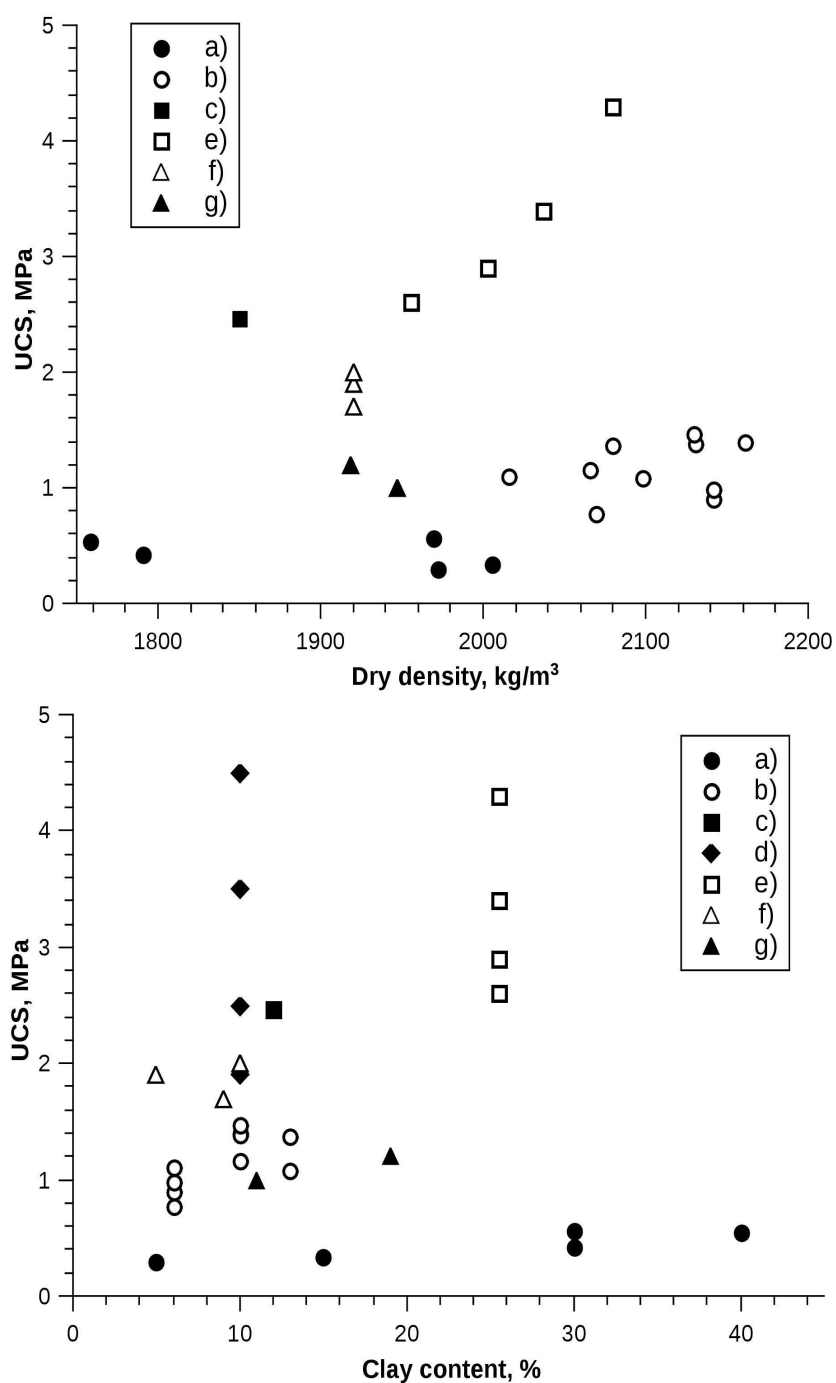
Fig. 3.34 Results of UCS tests on rammed earth and CEBs. Data from:
a)[46] b)[91] c)[101] d)[105] e)[104] f)[114] g)[64]

In Table 3.5 and Fig. 3.34 the data collected from the research on unstabilized earthen material strength available in the literature is presented. It can be noted that for the same soil increase in density leads to higher strength. However, due to great variability of testing procedures and missing information, it was not possible to make generalized conclusions on how dry density, soil composition or activity of fine fraction influence the strength of earthen construction materials.

Table 3.5 Details of soil tests from the reviewed references

Ref.	Nº	Clay, %	Silt, %	Sand, %	Gravel, %	Clay mineral	LL, %	PI, %	Compaction type or static pressure, MPa	Comp. water, %	Dry dens., kg/m³	UCS, MPa	Other information
[46]	1	5	25	50	20	Kaolinite	15.6	3.1	Modified Proctor	5.8	1971.76	0.3	Max. particle size = 10 mm Drying conditions: RH = 68% t = 7-18º C Specimens tested oven-dry
	2	30	0	50	20		26.1	13.8		8.3	1969.28	0.56	
	3	15	15	50	20		18	9.7		6.4	2005.35	0.34	
	4	30	20	40	10		24.8	13.4		7.4	1791.03	0.42	
	5	40	20	20	20		34.5	18.4		9.6	1758.13	0.54	
[91]	532	6	14	50	30	-	-	-	Proctor light	7-9	2141.83	0.9	Max. particle size = 10 mm Drying conditions: RH = 75% t = 20º C 28 days Clay was dried at 105º C prior to mixing
	622	6	14	60	20		-	-			2141.83	0.98	
	712	6	14	70	10		-	-			2069.89	0.77	
	802	6	14	80	0		-	-			2015.68	1.1	
	433	10	20	40	30		-	-			2160.87	1.4	
	523	10	20	50	20		-	-			2130.28	1.38	
	613	10	20	60	10		-	-			2129.74	1.47	
	703	10	20	70	0		-	-			2066.14	1.16	
	424	13	27	40	20		-	-			2079.94	1.37	
	514	13	27	50	10		-	-			2098.03	1.08	
[10]	Ic	28	16	56	0	Kaolinite	30	16	1.8	-	2055*	7.6	Max. particle size = 5 mm Specimens tested oven-dry Molding water content «same for all specimens» *Unrealistic value
									2.5		1932	13	
									5		1933	21.9	
									10		2000	25.2	
[101]		12	13	45	30	Illite	49	24	Modified Proctor	12.5	1850	2.46	Max. particle size = 20 mm Drying conditions: RH = 60%, t = 20º C, 28 days

Table 3.6 (cont.) Details of soil tests from the reviewed references

Ref.	Nº	Clay, %	Silt, %	Sand, %	Gravel, %	Clay mineral	LL, %	PI, %	Compac. type or static pressure, MPa	Comp. water, %	Dry dens., kg/m³	UCS, MPa	Other information
[105]	1	31		69		-	24	8	5.17	11	-	3.5*	Max. particle size = 4.75 mm Drying conditions: RH = 60%, t = 16º C, * 7 days, otherwise 28 days Proctor density = 1800 kg/m³ Proctor OMC = 11%
	2								9.31	11	-	3.1*	
	3								5.17	11	-	3.5	
	4								9.31	11	-	4.5	
	5								5.17	8	-	2*	
	6								9.31	8	-	2.1*	
	7								5.17	8	-	1.9	
	8								9.31	8	-	2.5	
	9								5.17	14	-	2.7*	
	10								9.31	14	-	3*	
	11								5.17	14	-	5.8	
	12								9.31	14	-	7	
[104]	1	25.5	30	44.5	-	-	38	18	2	14.7	2080	4.3	Drying conditions: RH = 60%, t = 22º C, 27 days
	2								2	16.4	2040	3.4	
	3								2	17.4	2000	2.9	
	4								2	20.7	1960	2.6	
[64]	514	19	18.1	50	10	Kaolinite	-	-	Proctor light	12	1918.1	1.2	Drying conditions: RH = 60%, t = 20º C, Clay was dried at 105º C before mix
	712	11	8.4	70	10					12	1947.5	1	

4
Materials and methods

The following section contains the information on the materials and equipment used in present study and the experimental program carried out.

4.1.
Materials

Natural soils can be heterogeneous, may contain organic matter and sometimes a number of minerals with complex properties. Locally available residual soils are characterized by specific behavior, can contain large percentage of clay aggregates and present a certain degree of cementation. In order to reduce the number of variables and to facilitate the control over soil granulometry and mineralogy it was decided to use artificial soil mixes. Commercially available building sand was used to represent coarse inert fraction. After preliminary granulometric analysis it was found that the sand had less than one percent of material finer than 0.075 mm. Thus, quartz powder passing through #200 sieve was used to represent silt. Kaolinitic clay was chosen as fine active soil fraction. Kaolinite is the most commonly used clay mineral for earth construction research [10], [46], [64], [116] as well as for structural applications [13], thus the results of present study could be more easily compared to those available in the literature.

There is an infinite number of possible combinations of soil fractions. Clay has an essential influence on soil behavior as it was stated earlier, so it was decided to produce different soil mixes with varying clay content and fixed inert fraction in order to reduce the number of variables. After plotting a different mix components combinations against the recommendations reviewed by Delgado and Guerrero [88], mix proportions were chosen so that two of the mixes fitted into the narrowest PSD limits indicated for CEBs. To investigate if the recommendations provided stronger material, two other mixes with clay contents above the indicated limit were produced. Sand and quartz powder were blended in

6 to 1 proportion by weight respectively. Then kaolinite was added to obtain four soil types with 10%, 20%, 30% and 40% of clay (particles < 0.002 mm) in dry mass, denominated K10, K20, K30 and K40 respectively.

4.2.
Experimental program

Literature research identified the following variables that influence the strength of compacted soil:

- Particle size distribution and geometric parameters of soil grains;
- Type of clay mineral present and its activity;
- Compaction method used – defines material density and structure;
- Compaction ware content– influences soil density and structure;
- Drying conditions of compacted specimens - determines soil suction;
- Shape of the specimens used for strength testing

In the present research the following variables were addressed: PSD, specifically clay content; molding water content, which determined dry density; water content of the specimens on testing, which determined suction. To investigate how these variable affect the strength of soil when it is used as a construction material, an experimental program shown in Table 4.1 was proposed.

After material characterization was made for all mix components and soil mixes and such properties as PSD, specific gravity and consistency limits were determined, the specimens for strength testing could be produced. Following the research of Pinto [107], cylindrical specimens 50 mm in diameter and 100 mm height were chosen to be used in this study. To minimize the effect of friction between mold and soil which can lead to inhomogeneous material, the specimens were compacted in three layers of equal thickness. At least 18 cylindrical specimens were produced for every soil mix. The effect of molding water content was studied by compacting half of the specimens at optimum moisture content and the other half at 2% below it, maintaining the same compaction pressure. For both molding water contents, three of the specimens were sheared in triaxial Bishop-Wesley chamber at different confining pressures. The results of the

triaxial tests allowed for strength envelope to be drawn and soil cohesion and angle of internal friction to be determined. The remaining six specimens were dried to a range of evenly distributed water contents and tested in unconfined compression. Smaller samples (50 mm diameter and 25 mm height) were produced for SWRC tests. After suction measurements, the samples were subject to diametrical compression in order to obtain a relation between soil suction and tensile strength. The stages of experimental program for one soil mix are schematically shown in Fig. 4.1.

Table 4.1 Experimental program

Type of test	Description
Characterization of materials	
Particle size distribution: • Wet sieving • Sedimentation	Determination of PSDs of sand, quartz powder and kaolin in order to calculate the proportions for the production of soil mixes
Atterberg limits (LL, PL)	Plasticity characteristics of soil mixes can be used for estimation of the activity of clay phase
Specific gravity (G_s)	Specific gravity of soil minerals is used to obtain the relations between solid, liquid and gas soil phases
Compaction tests	
Standard Proctor compaction tests	Moisture content – dry density relations for the four soil mixes to be compared with static compaction results
Static compaction tests	Determination of static compaction curves, used for sample production
Triaxial CD tests	Confined drained tests for determination of the parameters c' and φ' of compacted specimens
SWRC tests	Determination of SWRCs of compacted specimens
Brazilian tests	Relation between tensile strength of soil and water content/suction
Unconfined compression tests	Determination of compressive strength of the specimens as influenced by water content/suction
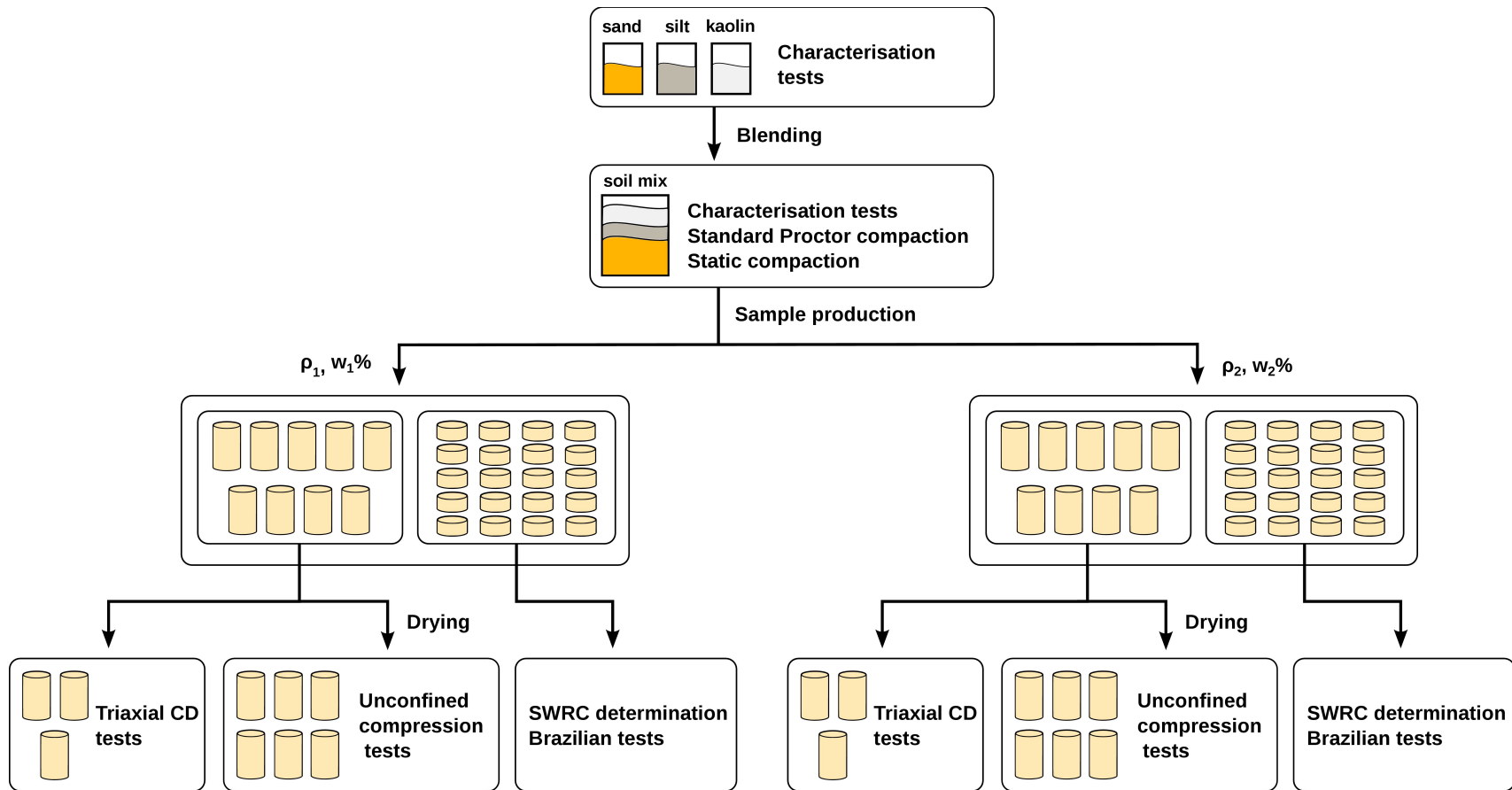
Fig. 4.1 Testing stages of one soil mix

4.3.
Static compaction tests

Universal testing machine (EMIC DL-3000) was used for the determination of static compaction curves and production of the specimens. The equipment was adapted by attaching a cylindrical steel compactor to the load cell and using a standard mini CBR mold which is 50 mm in diameter and 130 mm in height. The gap of 0.02 mm was ensured between the compactor and the mold to allow air to escape from the material during compaction, at the same time no soil was expelled. The schematic design of the equipment is shown in Fig. 4.2.
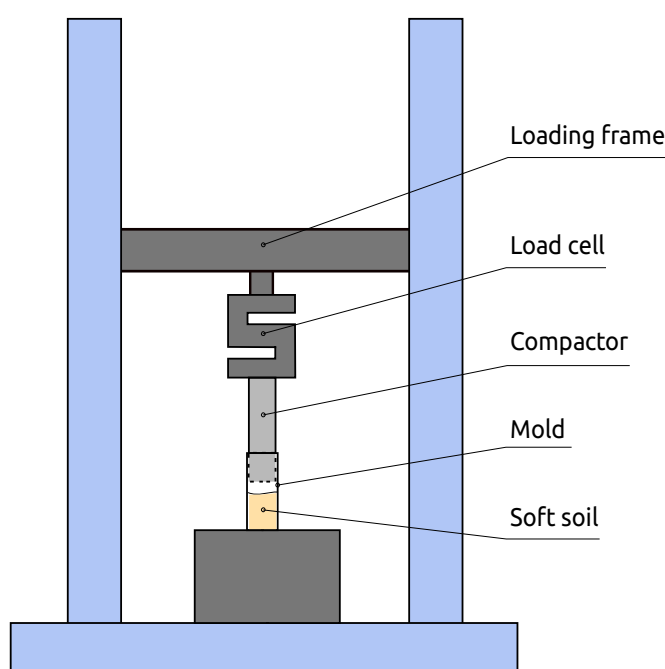
Fig. 4.2 Schematic drawing of the static compaction test configuration

The loading frame had maximum capacity of 30 kN, which could produce maximum pressure of approximately 15 MPa for 50 mm diameter specimens. This was considered adequate for current research purposes. The loading frame displacement and the load cell readings were recorded during the test with 1 Hz frequency. The equipment allowed for the control of displacement speed. The test data enabled generating load-displacement curves and subsequent determination of energy transferred to the soil as well as sample density. Typical pressure-displacement curve is presented in Fig. 4.3.

Before performing static compaction, displacement speeds ranging from 50

mm/min to 0.5 mm/min were tested. Different quantities of soil were compacted at these speeds and the resulting curves were compared. The displacement rate of 2 mm/min presented consistent, repeatable results, while being feasible, and was chosen to be used throughout this study.
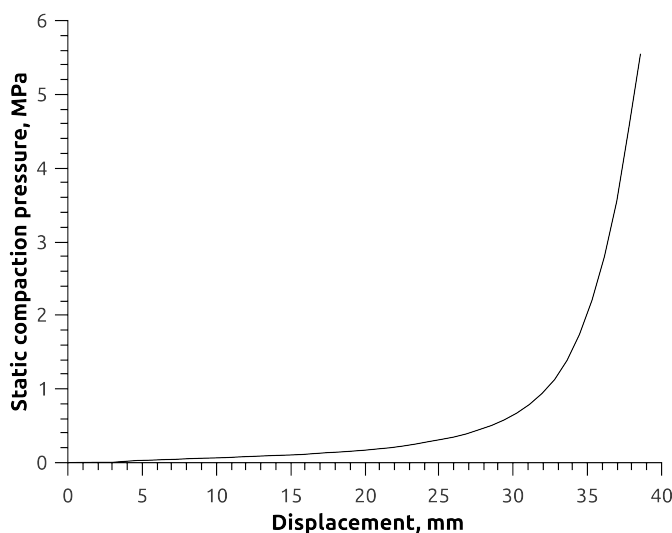
Fig. 4.3 Typical pressure-displacement curve obtained in static compaction test

Dry density was chosen as a control parameter for sample production. 50 x 100 mm samples were compacted in three layers to the desired dry density, which corresponded to OMC or to 2% drier than OMC (denominated OMC-2%). Each layer had the same mass and thickness. Scarification of soil surface was carried out in order to enhance the adherence between the layers. The specimens for SWRC determination and Brazilian tests were produced in the same manner, having only one 25 mm thick layer.

4.6.
Determination of soil water retention curves

Twenty specimens were used for SWRC determination for each soil density, which produced 10 points per curve. Filter paper and chilled mirror psychrometer (dewpoint potentiometer) methods were combined for the measurements of suction over the whole range of SWRCs. Both methods enable indirect soil suction determination.

Filter paper method is based on a correlation between soil suction and water

content of the paper with the aid of a calibration curve. The filter paper is placed in direct contact with soil sample for matric suction measurement or is suspended above it for total suction measurement. After moisture equilibrium between the paper and the specimen is achieved, which means that their suctions are equal, filter paper's water content is measured. Then a calibration curve is used to match water content with corresponding value of suction. This procedure is repeated for different soil water contents, so the complete SWRC can be drawn. In this study an adaptation of the method described in ASTM D5298-94 [117] was employed. Whatman nº 42 filter paper was used. The test setup is shown in Fig. 4.4.
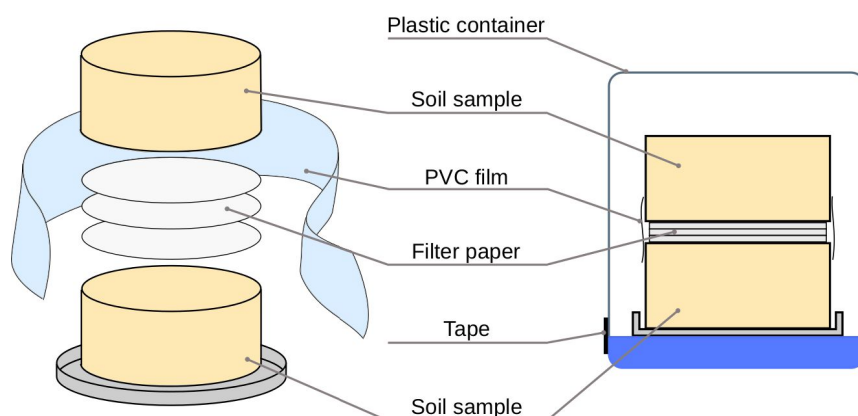
Fig. 4.4 Schematic drawing of matric suction test configuration

For every soil density 10 pairs of 50 x 25 mm samples were dried or wetted to different water contents evenly distributed between quasi saturation and air dry conditions. When a pair of specimens reached their target water content, three Whatman nº 42 filter papers were sandwiched between them and one layer of PVC film was wrapped around the specimens to ensure stability. The assembly was put into a plastic container and its lid was sealed with several wrappings of electric tape. Finally, the whole container was wrapped in PVC film. In order to minimize temperature fluctuations, all ten containers were left inside a Styrofoam cooler box for one-two weeks. One week is considered sufficient for moisture equilibrium to be achieved for most cases [118].

After suction equilibration period, the containers were opened and the middle filter paper weighed using a balance with 0.0001 g precision. One of the soil specimens was immediately tested for tensile strength in diametrical compression while the other one used for suction measurement with chilled mirror psychrometer. Only a small part of the sample was necessary for dewpoint potentiometer test, the rest of the material was used for water content

determination. After measurement of the wet mass of filter papers, they were dried in an oven at 105º C for 2.5 hours. Filter paper absorbs and looses humidity easily, so its change in mass was recorded during two minutes for either wet and dry conditions. The following sigmoidal function was applied to interpolate the data in order to find initial mass of filter papers:

$$f(x) = \frac{A2 + (A1 - A2)}{1 + \exp\left(\dfrac{x - x_0}{dx}\right)}$$
(4.1)

An example of a graph used for initial filter paper mass determination is shown in Fig. 4.5.
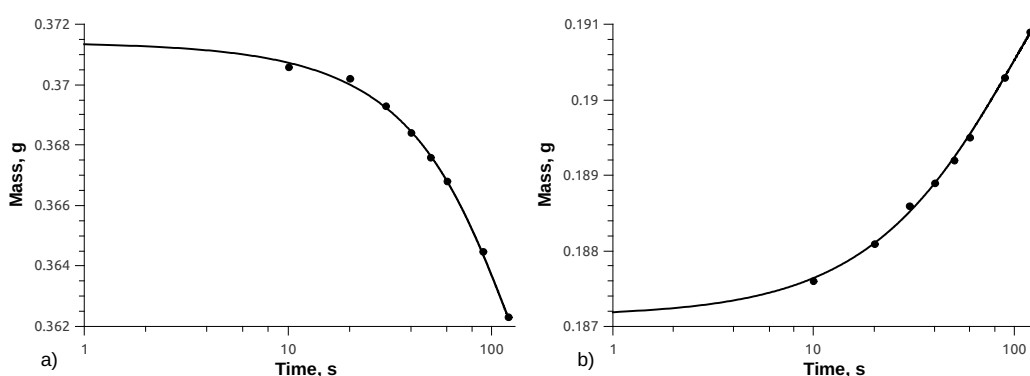
Fig. 4.5 Determination of initial mass of filter paper through sigmoidal function fit. a) Wet filter paper loosing humidity b) dry filter paper absorbing humidity

After calculation of filter paper water content, its suction could be found using the following equation [119]:

$$s = \begin{cases} 10^{6.05 - 2.48 \log(w)} & for \, w < 47.1 \\ 10^{4.84 - 0.0622\,w} & for \, w \leq 47.1 \end{cases}$$
(4.2)

where s is suction in kPa and w is water content in percent.

Filter paper is capable of measuring suctions between 0-30 and 30000 kPa [120], [121]. Average humidity and temperature in the laboratory where present experiments were carried out were 50% and 24º C respectively. These conditions impose a suction of 95011 kPa, so it was necessary to use an additional method of suction measurement to cover the range above 30000 kPa. For this purpose WP4C model chilled-mirror psychrometer, produced by Decagon Devices, Inc., was employed (Fig 4.6).
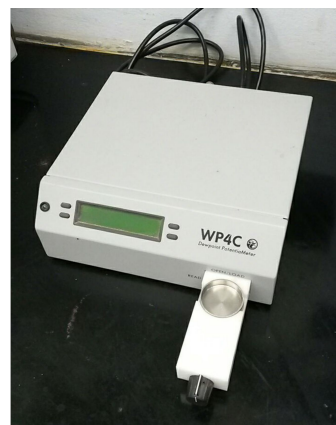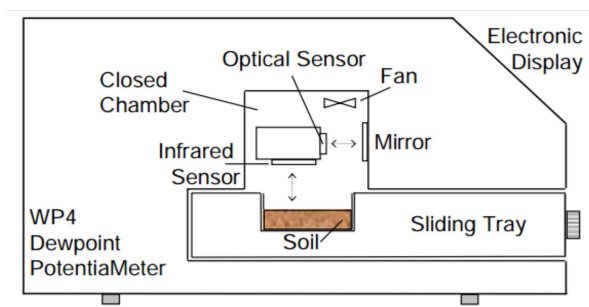
Fig. 4.6 WP4 dewpoint potentiometer

The measuring method of a dewpoint potentiometer is based on the principle of equilibrating the suctions of the water in a soil sample with the water vapor above the sample in a sealed chamber. The suction is measured with the aid of chilled-mirror dewpoint technique. The mirror is placed above soil sample. A Peltier cooling device is used to cool the mirror until the formation of dew and then to heat the mirror to evaporate the dew. An optical sensor detects the condensation of the dew on the mirror, while its temperature, and the temperature of the soil sample is registered. These temperatures are used to determine RH of the air in the chamber and consequently total suction. A fan is used to accelerate vapor equilibrium, which reduces the time of the test to 5-15 minutes. The speed of the test depends mainly on the initial temperature and water content of soil sample. Dewpoint potentiometer allows for measuring of suctions between 1 – 300 MPa, the precision below 1 MPa is very low, which generates very scattered results [118].

4.7.
Unconfined compression and Brazilian tensile tests

To determine the strength of the soil specimens unconfined compression test (UCS test) and diametrical compression test (Brazilian test) were carried out. These tests provide a simple way of evaluating compressive and tensile strengths of soil.

Brazilian test is an indirect method for the determination of the tensile strength of materials. It consists in diametrical compression of a cylindrical specimen, which induces tensile stress normal to the loading direction. It is

assumed that the failure occurs at the center of the cylinder, where the tensile stress is the highest, and that radial compressive stress has no influence on the result of the test [122]. The length-to-diameter ratio of the specimen should range from 0.5 to 1 and test duration should be 1-10 min [123]. Schematic representation of Brazilian test is shown in Fig. 4.7b.

After weighing wet filter paper in SWRC test, one specimen of each pair was subject to diametrical compression. During the weighing procedure of the filter paper, which took two minutes, the sample was placed back into sealed plastic container to avoid moisture loss. Then its length and diameter were measured using a digital caliper. The test was carried out immediately afterwards. In this manner the influence of water content, and subsequently suction, on the tensile strength of the specimens could be evaluated. A similar procedure was used by Jaquin et al [74].

The tensile strength of soil subject to Brazilian test can be calculated as follows:

$$\sigma_t = \frac{F}{\pi \cdot d \cdot L} \tag{4.3}$$

σ_t – tensile strength,

F – applied load,

d – specimen diameter,

L – specimen length.
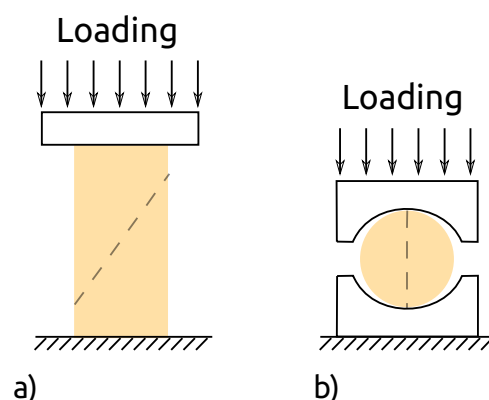
Fig. 4.7 Schematic configuration of a) Unconfined strength test b) Brazilian tensile test. Dashed lines indicate failure planes

There were six 50 x 100 mm UCS cylindrical specimens for each soil density, so by analyzing the results of Brazilian tests, a suction (water content) range of interest was chosen. Within this range six water content values were defined,

minimum water content being as of air dried samples. After compaction the UCS specimens were dried or moistened until they reached target mass corresponding to chosen water content. Two filter papers were placed at the top and bottom of each specimen, one protective and one for matric suction measurement. Finally the specimens were wrapped in several layers of PVC film in such a way that the ends of the specimen could be unwrapped independently. This enabled weighing the top filter paper while the bottom one retained its initial mass. All the specimens were placed inside a Styrofoam cooler box for moisture equilibration. The period of moisture equilibration was estimated by the time of complete air drying of one specimen and was equal to two-three weeks. Change of water content of K30 and K40 specimens with time while drying is shown in Fig. 4.8. The mass of the specimens stabilized after 12 days.
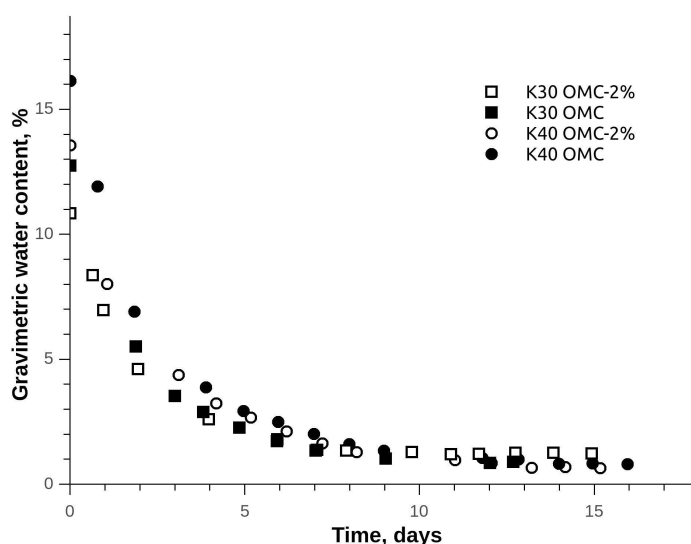
Fig. 4.8 Drying of UCS specimens

After the specimens achieved moisture equilibrium, UCS tests could be carried out. The PVC wrapping was removed, the filter papers weighed and the specimens' dimensions and mass recorded. The test configuration is shown schematically in Fig. 4.7a.

According to the recommendations for UCS tests, the specimens should have height-to-diameter ratio of 2-2.5, the largest particle should not exceed one tenth of specimen diameter [124]. If irregular, upper and lower surfaces of the cylinder should be capped with a thin layer of fine soil or mortar. The speed of loading frame displacement should be between 0.5-2% of sample's height per minute. Displacement and load cell readings should be recorded during the test, which is stopped when the load begins to decrease or when the strain reaches 15%.

When calculating compressive stress, area correction should be made. The following formulas were used:

$$\sigma = \frac{F}{A_c} \qquad (4.4)$$

σ – compressive stress,

A_c – cprrected cross sectional area of the specimen.

$$A_c = \frac{A_i}{1 - \varepsilon_a} \qquad (4.5)$$

A_i – initial cross sectional area of the specimen,

ε_a – axial strain.
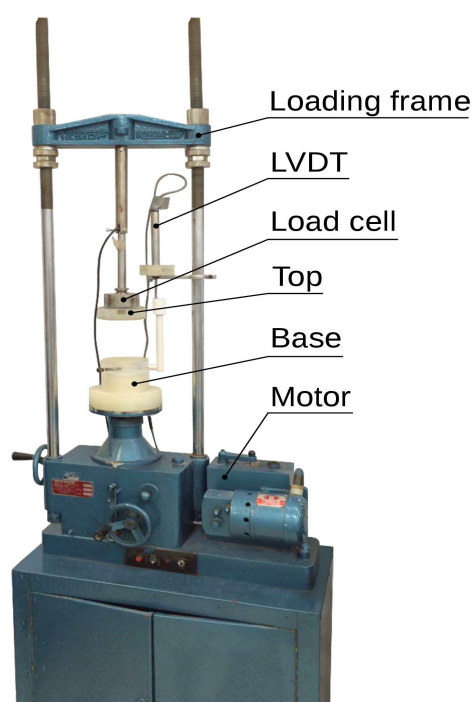
Fig. 4.9 Triaxial rig used for UCS and Brazilian tests

A triaxial test rig with loading capacity of ten tons-force produced by Ronald Top, LTDA was used for UCS and Brazilian tests. The equipment is shown in Fig. 4.9. The control of the displacement speed of the loading is done by a gear system. The speed used for the tests was 0.3 mm/min. The instrumentation consisted of a load cell that had a capacity of 100 kN and precision of 1 N, and LVDT with 50 mm gauge length and resolution of 0.01 mm. HBM data acquisition system and CatmanEasy software were used for data logging.

After the failure of each UCS specimen, a small quantity of soil was taken from its interior and its suction determined in dewpoint potentiometer. Another

portion of the specimen was taken for water content determination. The suction vs. water content data obtained from UCS samples by filter paper and dewpoint potentiometer methods was incorporated into SWRCs.

4.8.
Triaxial tests

In order to predict unsaturated soil strength using both Eqs. 3.15 and 3.17, saturated shear strength parameters, such as effective cohesion (c') and effective angle of friction (φ'), should be determined. This was done by the means of confined drained tests on isotropically consolidated samples (CID).

Triaxial tests were carried out using a Wykeham Farrance brand Bishop-Wesley triaxial apparatus with water pressure cell and a loading frame with displacement control. The triaxial cell was adapted for 1.5" diameter specimens and could operate continuously at pressures up to 1000 kPa. The displacement rate was controlled with the aid of a gear system. Loading frame had a capacity of 10 tons-force. The instrumentation consisted of a 50 kN load cell with 0.1 kN resolution, a LVDT with 20 mm gauge and a resolution of 0.01 mm, a pressure transducer of 1700 kPa capacity and a bellofram type volumetric transducer of Imperial College design. The equipment is shown in Fig. 4.10.
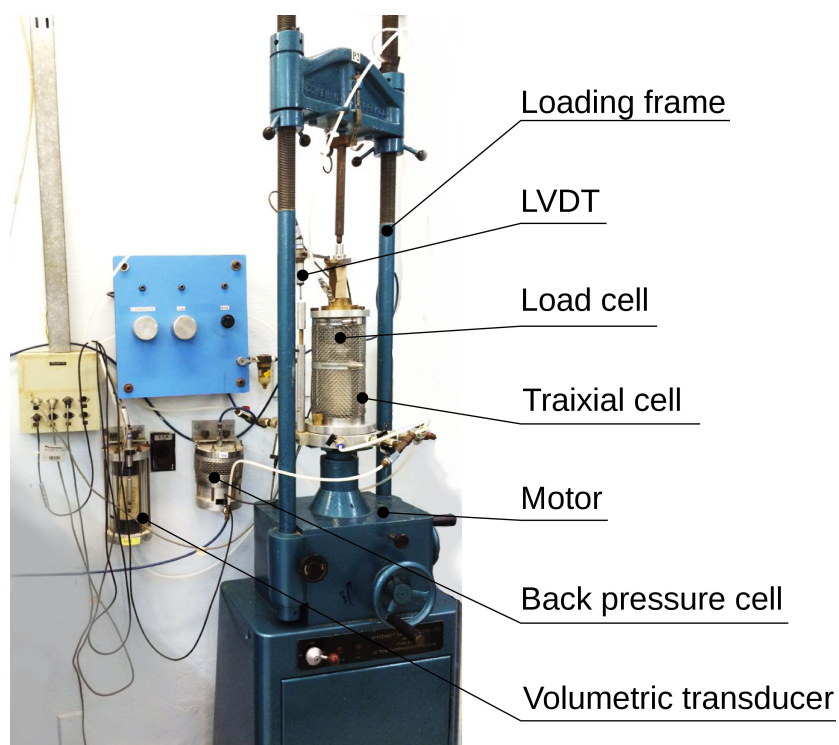
Fig. 4.10 Triaxial apparatus

Three specimens compacted to each dry density were tested for each soil mix. In order to be used in triaxial cell they were reduced to 38 mm in diameter and 72 mm in height. The tests were performed according to the recommendations reported by Head [125].

The saturation of the specimens was made by alternating increments of back pressure and percolation. Back pressure increments were of 50 kPa, while a differential of 10 kPa between cell pressure and back pressure was maintained. After stabilization of volumetric transducer readings, the pressure on the bottom of the specimen was increased by 5 kPa, thus creating a pressure gradient and making the water percolate from the base to the top of the specimen expelling air bubbles. This procedure was repeated until Skempton's pore pressure coefficient B reached 0.95:

$$B = \frac{\Delta u}{\Delta \sigma_3} \qquad (4.6)$$

where Δu is the increment in pore pressure and $\Delta \sigma_3$ is the increment of cell pressure.

The specimens were consolidated isotropically at confining pressures of 100, 200 and 300 kPa respectively. After 8-hour consolidation period, an adequate test speed for a drained test was determined as follows. The graph of volume change

vs. square root of time was plotted as shown in Fig. 4.11.
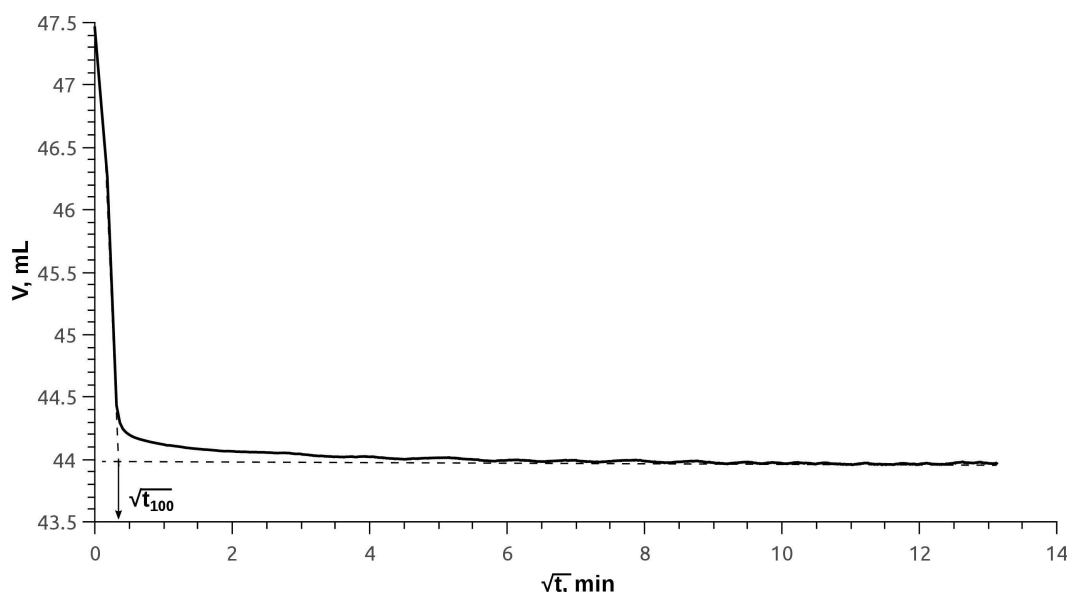
Fig. 4.11 Isotropic consolidation of K10 specimen, confining pressure of 200 kPa. Graphical determination of t_{100}

Initial linear portion of the graph was extended until the intersection with the horizontal line corresponding to the stabilization of the volume readings. The point of the intersection indicates the time of the end of consolidation t_{100}. Then the time to failure t_f for CD test was calculated:

$$t_f = 8.5 \cdot t_{100} \tag{4.7}$$

If $t_f < 120$ min, then $t_f = 120$ min should be adopted. Maximum axial displacement rate r_d during shearing was determined as follows:

$$r_d = \frac{\varepsilon_f L_i}{t_f} \tag{4.8}$$

where ε_f is the strain at failure and L_i is the initial height of the specimen. The resulting shearing speed was such that the duration of all conducted triaxial tests ranged between 6 and 8 hours.

In order to calculate deviator stress area correction due to barreling of the specimen was made:

$$A_c = \frac{1 - \varepsilon_{vol}}{1 - \varepsilon_a} A_i \tag{4.9}$$

$$\sigma_1 - \sigma_3 = \frac{P(1 - \varepsilon_a)}{A_i(1 - \varepsilon_{vol})} \tag{4.10}$$

where

$$\varepsilon_a = \frac{\Delta L}{L_i} \tag{11}$$

$$\varepsilon_{vol} = \frac{\Delta V}{V_i} \tag{12}$$

A_c – corrected area,

ε_a – axial strain,

ε_{vol} – volumetric strain,

V – volume of the specimen,

V_i – initial volume of the specimen,

Trail triaxial tests were carried out using K10 mix compacted in Proctor test. The graph of deviator stress vs. axial strain in shown in Fig. 4.12 and effective stress envelope in p'-q space is shown in Fig. 4.13.
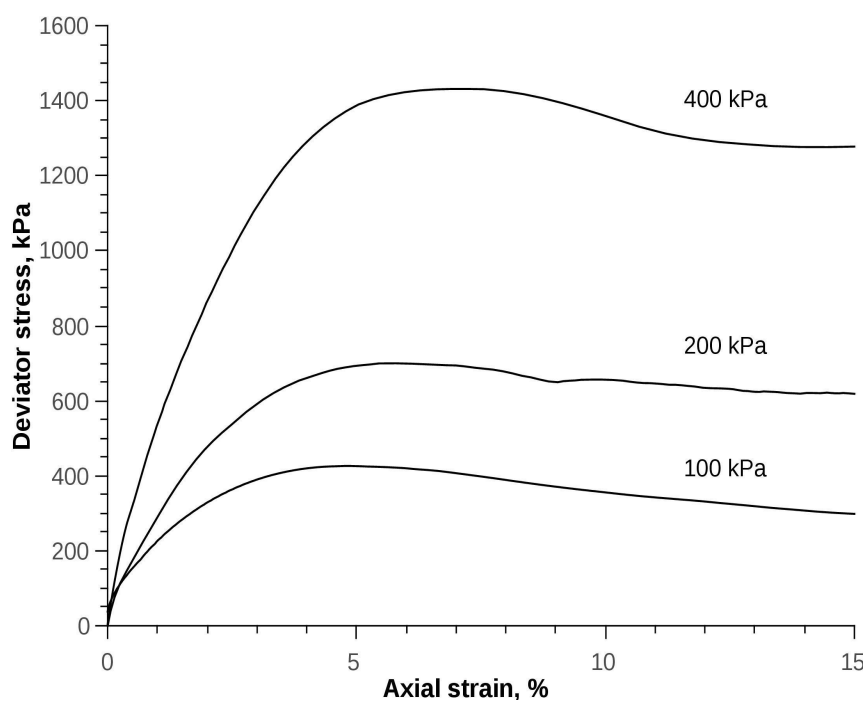
Fig. 4.12 Stress-strain data from CID triaxial test on dynamically compacted K10 mix
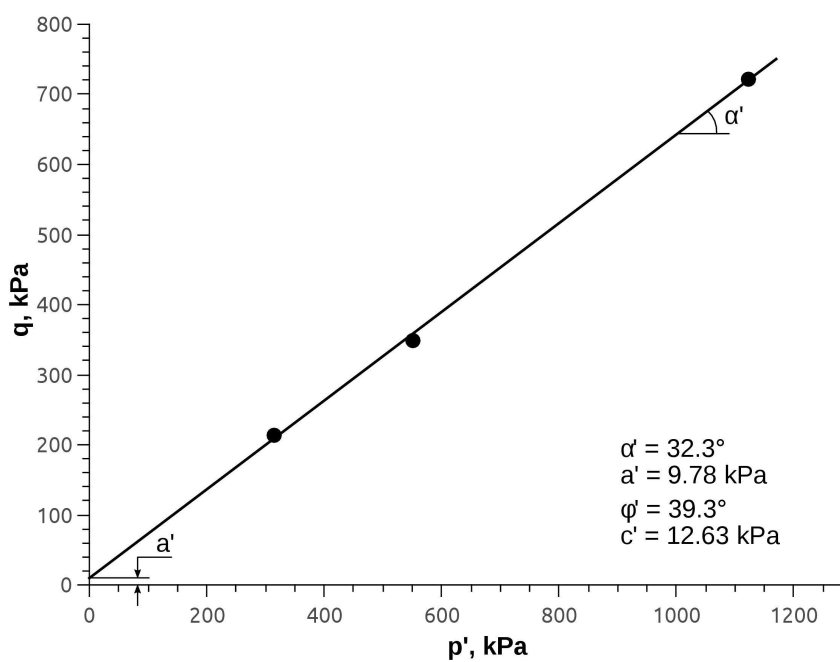
Fig. 4.13 Effective stress envelope for dynamically compacted K10 mix

Initially it was planned to consolidate the specimens at 100, 200 and 400 kPa, however it was decided to avoid high cell pressures and the value of 300 kPa was chosen instead of 400 kPa for subsequent tests.

5
Results and discussion

In the following section the results of the experiments carried out are presented and their implications for the objectives of the present study are discussed.

5.1.
Properties of kaolinitic clay

Kaolinitic clay used in this work was acquired from Monte Pascoal Ldta and comes from a deposit in Prada, Bahia state. Raw mineral is processed firstly by removing impurities coarser than 74 μm with the aid of sieving and hydrocyclones. Then it is submitted to magnetic separation in order to eliminate iron oxides and hydroxides, which is further accomplished by bleaching with sodium dithionite ($N_2S_2O_4$) [126]. SEM micrographs of kaolinitic clay before and after processing are shown in Fig. 5.1.
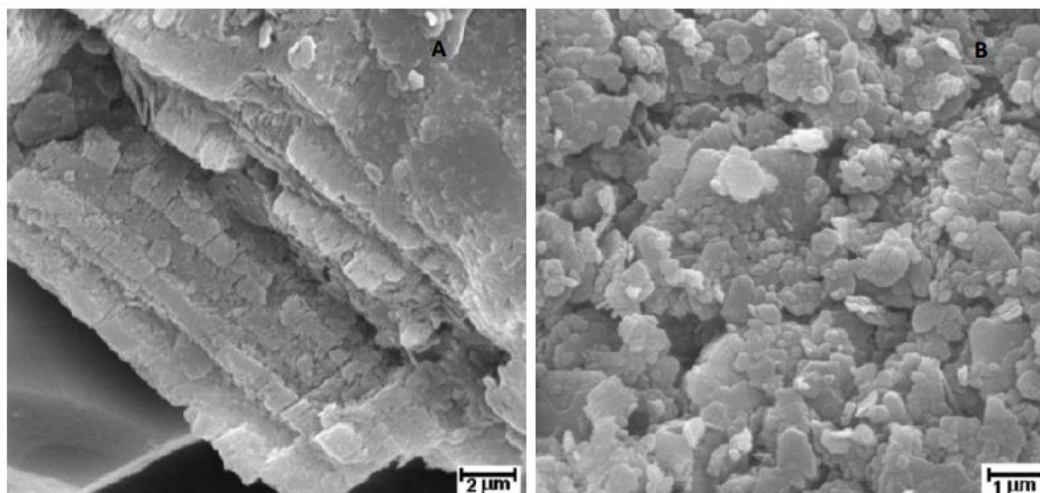
Fig. 5.1 SEM image of kaolinitic clay before (A) and after processing (B) [126]

Kaolinitic clay has an appearance similar to talcum or mica, so X ray analysis is necessary to certify its composition. X ray diffraction is a technique used to identify crystalline formations present in a studied material. It is based on the

analysis of the diffraction pattern of X ray beam directed at a small portion of the material analyzed. According to the distances between the structural units of the crystals present, obtained diffractogram indicates peaks characteristic of crystal basal spacings. X ray diffraction test of the kaolinitic clay used in the present study was carried out by Pessôa [127].
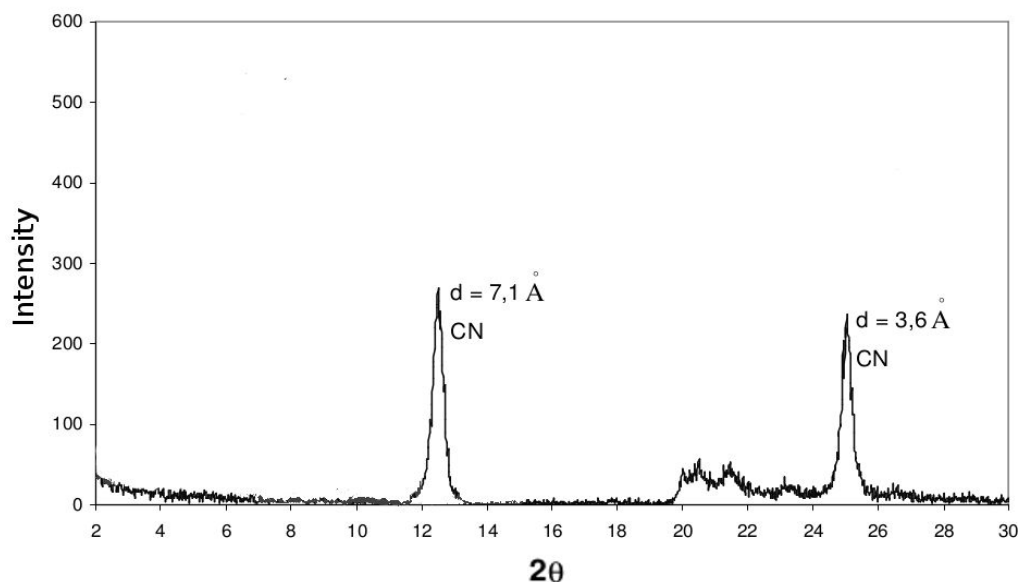
Fig. 5.2 X ray diffractogram of powdered kaolinitic clay [127]

A powdered specimen of kaolin was subject to X ray beam scan at angles ranging from 0 to 30º at a speed of 0.02º per second. The resulting diffractogram is shown in Fig. 5.2. The peaks at 7.1 Å and 3.6 Å can be observed, which is characteristic of kaolinite [29], [31].

5.2.
Characterization tests

Material characterization consisted in the determination of the particle size distributions of mix components and soil mixes, their respective specific gravities and consistency limits. Granulometric tests of building sand were made according to NBR 7181 [128] with an extended set of sieves. Wet sieving was performed, revealing that the sand contained negligible percentage of fines. Particle size analysis of quartz powder and kaolinitic clay was made through sedimentation. Densimeter calibration and calculation were carried out following the procedure

described by Head [93].
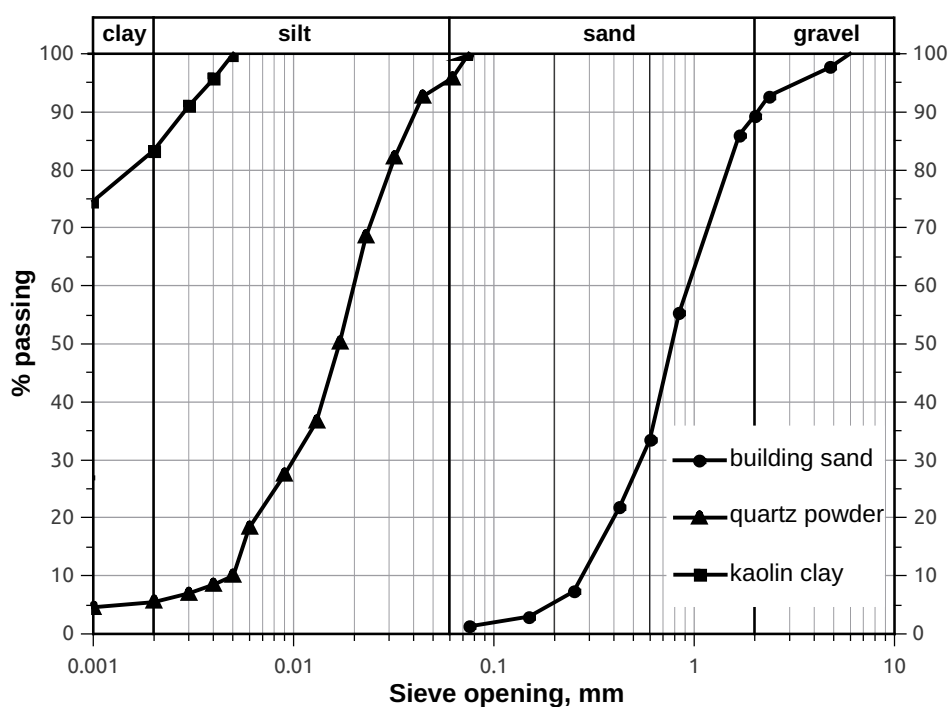
Fig. 5.3 Particle size distribution of mix components

After the completion of granulometric tests of the components, the mix proportions could be calculated. The inert fraction, building sand and quartz powder were blended in a proportion 6:1 in dry mass. This proportion was chosen after trial calculations. The aim was to produce an inert fraction that, when blended with the kaolinitic clay, could ensure the PSD that falls into recommended range. Before blending, building sand was passed through #4 sieve, thus maximum particle size was 4.75 mm. Maintaining the same inert fraction, kaolinitic clay was added in quantities to produce the desired four soil mixes. The PSDs of the resulting soils are shown in Fig. 5.4. The details of the granulometric composition of the mixes are presented in Table 5.1. The PSDs of the soil mixes was verified through determination of fines content. The produced materials were stored in the room with controlled humidity and temperature.

Table 5.1 Granulometric composition of the soil mixes

Soil mix denomination	Clay, %	Silt, %	Sand, %
Building sand	0	0	100
Quartz powder	5.47	90.3	4.23
Kaolinitic clay	83.3	16.7	0
K10	10	13.3	76.7
K20	20	13.8	66.2
K30	30	14.2	55.8
K40	40	14.7	45.3
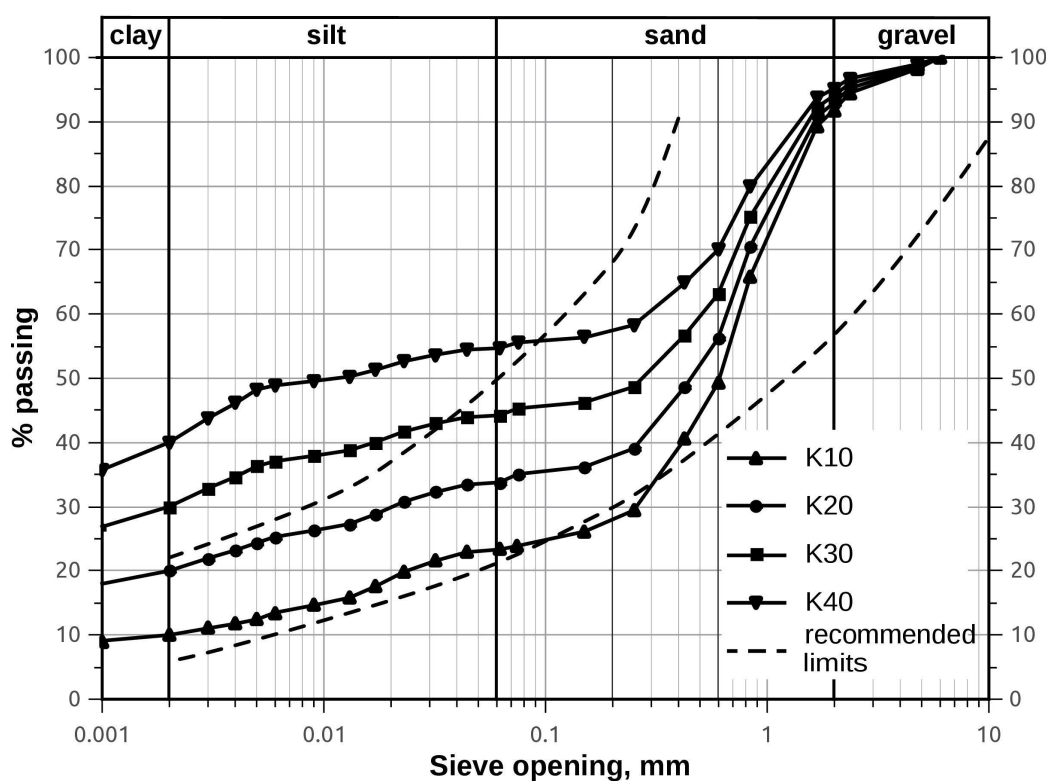
Fig. 5.4 Particle size distributions of four soil mixes and the narrowest recommended limits from [88]

Specific gravity was determined according to NBR 6508 [129] using the soil passed through #40 sieve, which yield more homogeneous material. Consistency limits tests were carried out according to ABNT norms [130], [131]. Liquid limit was determined in Casagrande apparatus. The summary of the tests' results is presented in Table 5.2.

Table 5.2 Specific gravity and Atterberg limits of soil mixes and mix components

Material	Gs	LL, %	PL, %	PI, %
Sand	2.69	-	-	-
Quartz powder	2.67	-	-	-
Kaolin	2.63	70	44	26
K10	2.68	20	15	5
K20	2.68	32	17	15
K30	2.67	40	22	18
K40	2.66	57	35	22

5.3.
Standard Proctor compaction

Standard Proctor compaction was performed for the four soil mixes in order to determine approximate parameters for static compaction tests, such as water content and dry density ranges. The procedure was carried out according to NBR 7182 [132]. Initial amount of water was added to each soil mix and the moisture was allowed to equilibrate during 24 hours. The compaction was carried out with material reuse, which was considered acceptable as in earth construction the quantity of soil clods and large aggregates should be reduced to minimum. The energy input of this compaction method is 574 kJ/m^3. Proctor compaction curves for the four soil mixes are presented in Fig. 5.5 and the test results are summarized in Table 5.3.
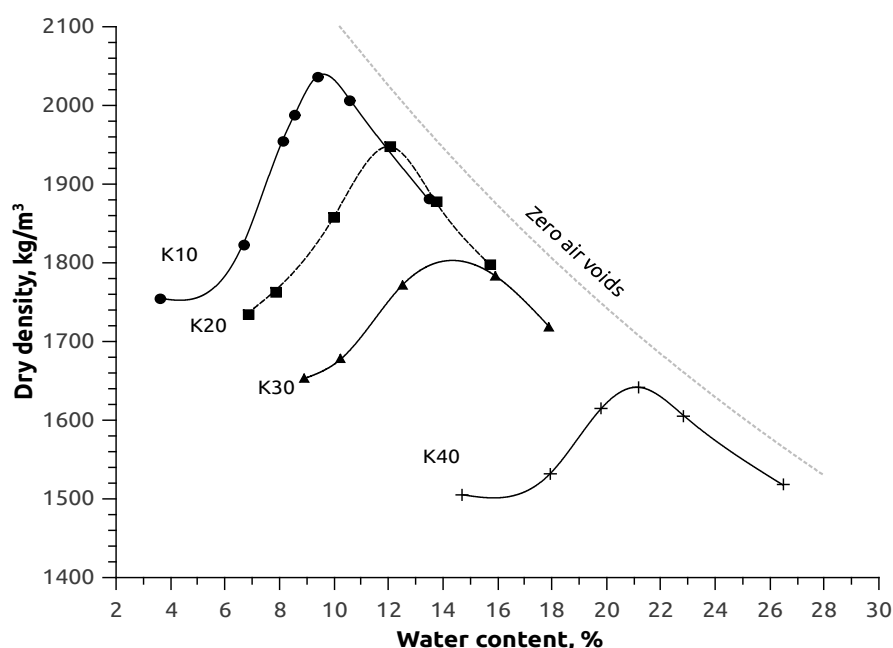
Fig. 5.5 Standard Proctor compaction curves for all soil mixes

Table 5.3 Standard Proctor compaction results

Soil mix	OMC, %	Max. dry density, kg/m^3	Water content range, %
K10	9.6	2040	5 – 13.5
K20	12	1940	6.5 – 15.5
K30	14	1800	9 - 18
K40	21	1640	16 - 26

5.4.
Static compaction

For the static compaction test five or six 200 g batches of each dry soil were taken, mixed with different quantities of water, according to moisture content limits indicated by Proctor tests, and stored in sealed bags for at least 24 hours for humidity equilibration. Then the contents of the bags were placed into mini CBR mold and compacted statically at a constant displacement speed of 2 mm/min up to static load of 15 MPa or until the first signs of consolidation appeared. The compaction energy was calculated by integration of load-displacement curves and was divided by the specimen volume at each point of the curve in order to obtain energy density values. The results obtained were similar to the ones

reported be Reddy and Jagadish [106]. No wet-of-optimum part of the curve was observed. Optimum moisture content therefore was defined as the point of transition between compaction and consolidation. The static compaction curves were produced for different constant energy inputs and constant pressures. The curves for energy density equivalent to one of the Proctor test were plotted for the sake of comparison of the efficiency of the static and dynamic compaction methods for the studied soils mixes (Fig. 5.6). For statically compacted soils OMCs were defined with the precision of +/-0.5%, as it was impossible to verify the exact point of the start of consolidation for all the energy inputs.

Static compaction was more efficient for all studied soil mixes, except K10. However, for quantitative conclusion to be made, the molds used for both static and dynamic compaction test should be the same. In the case of present research, 50 mm x 130 mm mini CBR mold was used for static compaction in order to reduce material consumption and facilitate sample production for strength tests. Considering the final thickness of one compacted layer, the lateral to cross sectional area ratio for mini CBR mold is 2.67, while for standard Proctor mold it is 1.69. Thus, the friction between soil and the mold in the performed static compaction test causes higher energy dissipation compared to Proctor test.
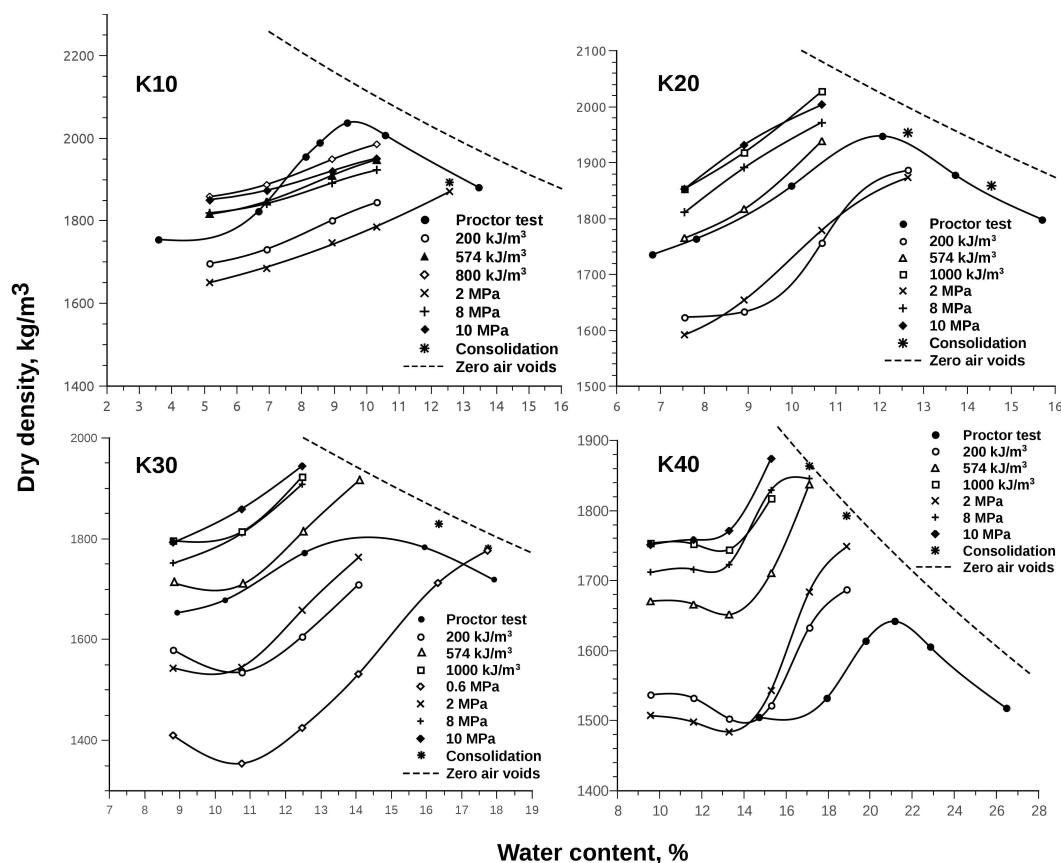
Fig. 5.6 Static compaction curves for different energy densities and static pressures

The relations between energy inputs and static compaction pressures in the static compaction tests were studied. Energy density – pressure curves were plotted and showed quasi-linear and bilinear shapes (Fig 5.7). Their inclination depended on the water content of the soil. To further illustrate this behavior, the curves for constant maximum compaction pressures of 2 and 8 MPa were plotted in energy density-water content space (Fig. 5.8).

Based on the literature review and experimental data obtained in the present study it can be concluded that the shape of the static compaction curves depends on the conditions of the experiment such as characteristics of the equipment and the rate of strain. If the equipment is such that it allows water to drain and compaction speed is slow enough or the soil is permeable enough, the shape of the curves should be similar to the ones presented here and by Reddy and Jagadish [106]. In this case, OMC can be defined as the point of transition between compaction, when only air is displaced from soil, and consolidation, when water starts to be expelled. Otherwise, at a certain moisture content the soil reaches near-saturation and further increase of compaction force generates equal increase in the pore pressure, providing a compaction curve similar in shape to

that of Proctor test.

Dynamic compaction is normally done by application of fixed energy and static compaction is defined by maximum pressure. For the results of these two tests to be comparable, the energy applied during static compaction should be calculated and energy density of both tests obtained.
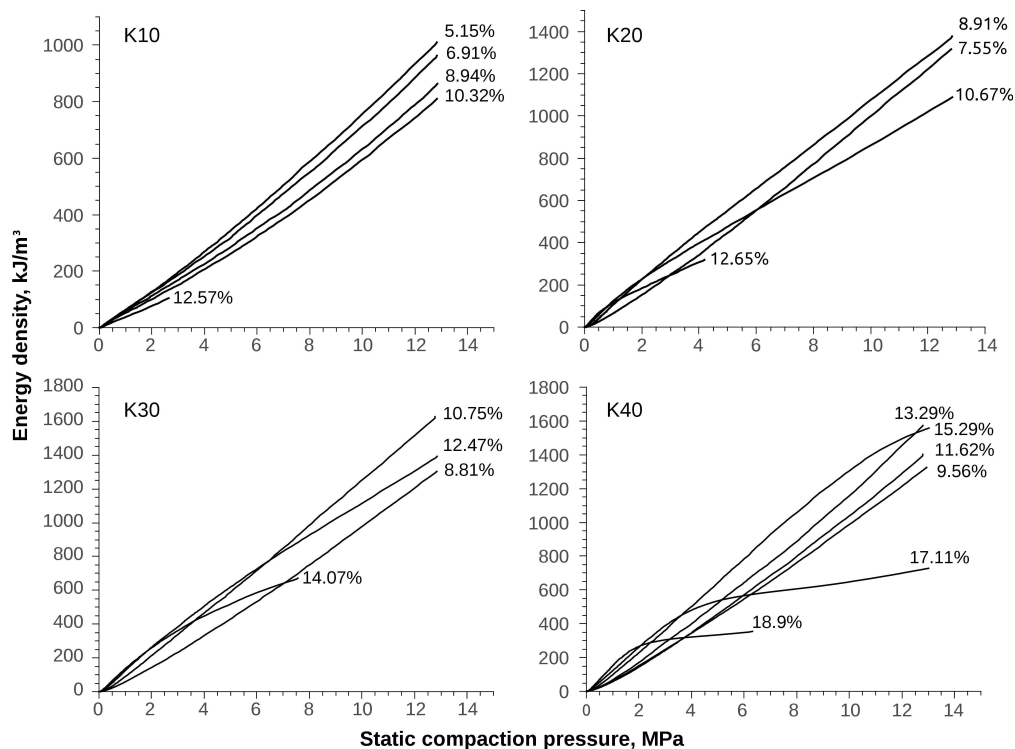
Fig. 5.7 Relations between energy density and compaction pressure for different moisture contents

Static compaction of wetter soils is more efficient, which can be used to enhance the performance of manual presses. If the pressure is applied slowly, higher densities can be achieved without affecting CEB quality. Feasibility studies should be made, as the drying time of resulting blocks also increases.
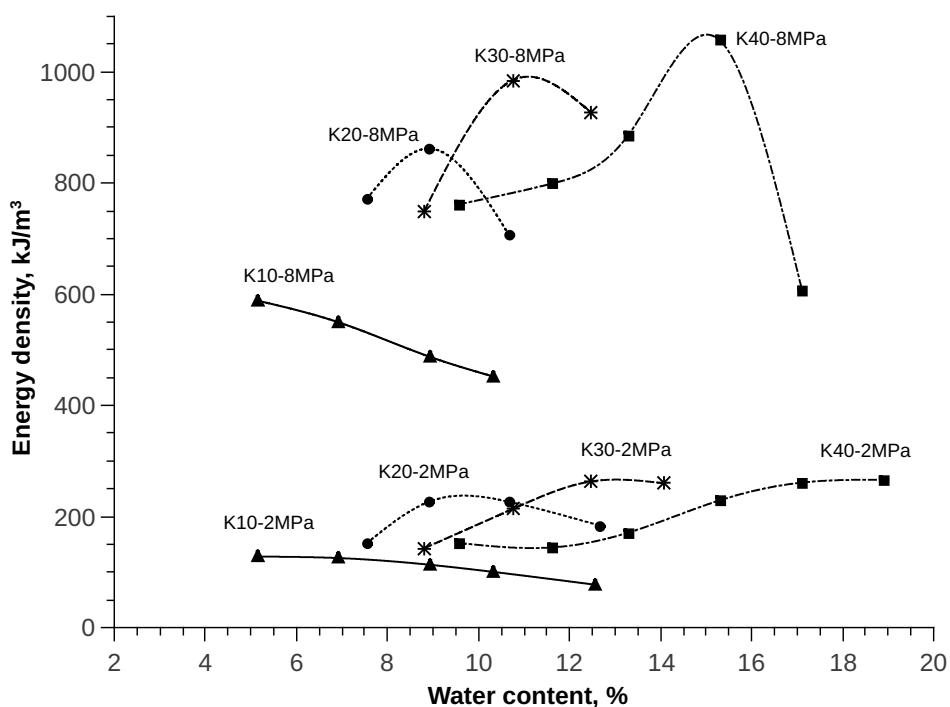
Fig. 5.8 Relations between energy density and water content for constant maximum compaction pressures

According to the results of static compaction tests, the values of densities and water contents for the production of the specimens were chosen. All the samples were compacted by applying the same maximum static pressure of 10 MPa. For each soil mix a half of the specimens were produced at static OMC and the other half at OMC-2%, which resulted in two different densities. The summary of the nomenclature used to refer to the samples and such characteristics as water content on compaction (w), dry density (ρ_d), void ratio (e) and porosity (n) are represented in Table 5.4.

Table 5.4 Characteristics of compacted samples

Mix	Name	w, %	ρ_d, kg/m^3	e	n	Max. static pressure, MPa
K10	K10 OMC-2% K10 OMC	9.6 11.6	1940 1970	0.38 0.36	0.28 0.26	10
K20	K20 OMC-2% K20 OMC	9.2 11.2	1945 2020	0.38 0.33	0.27 0.25	10
K30	K30 OMC-2% K30 OMC	10.5 12.5	1845 1945	0.45 0.37	0.31 0.27	10
K40	K40 OMC-2% K40 OMC	13 15	1755 1855	0.52 0.43	0.34 0.30	10

5.5.
Soil water retention curves

Soil water retention curves of the compacted specimens are shown in Figs. 5.9-5.12. The results were grouped in the same graphs for each soil mix. The data obtained from suction measurements on 50 x 25 mm specimens and 50 x 100 mm specimens with filter paper and dewpoint potentiometer is indicated separately. The measurements of matric suction made with filter are in close agreement with those of total suction made using dewpoint method. This was expected as distilled water was used in sample production and no ions were introduced into the soil. Under present experimental conditions it was possible to measure suctions up to 25000 kPa with filter paper. The data obtained with this method on air dry samples was excluded, as average suction developed in the soil considering temperature and RH in the laboratory was approximately 95000 kPa. Suctions below 1000 kPa measured with dewpoint method were also excluded, as they diverged significantly from filter paper measurements. Unfortunately chilled-mirror psychrometer was not available when K10 mix was tested, thus only filter paper data is presented.

All the soils showed bimodal structure. First air entry value was under about 5 kPa and second air entry value varied between 2500 and 5500 kPa depending on clay content and density. For the same soil mix the increase in dry density didn't affect significantly SWRCs, the difference is more pronounced for the suctions lower then second air entry value. A method modified from that proposed by Vanapalli et al. [55] was used to determine second air entry suction. It was defined as an intersection of the extension of constant slope parts of the curve before and after second air entry. Residual desaturation started above 10000 kPa. In air dry state the specimens retained less than 1.7% of water by volume and less than 1% by weight. The air entry values and the suctions of transition to residual desaturation zone for all specimens are presented in Table 5.5.
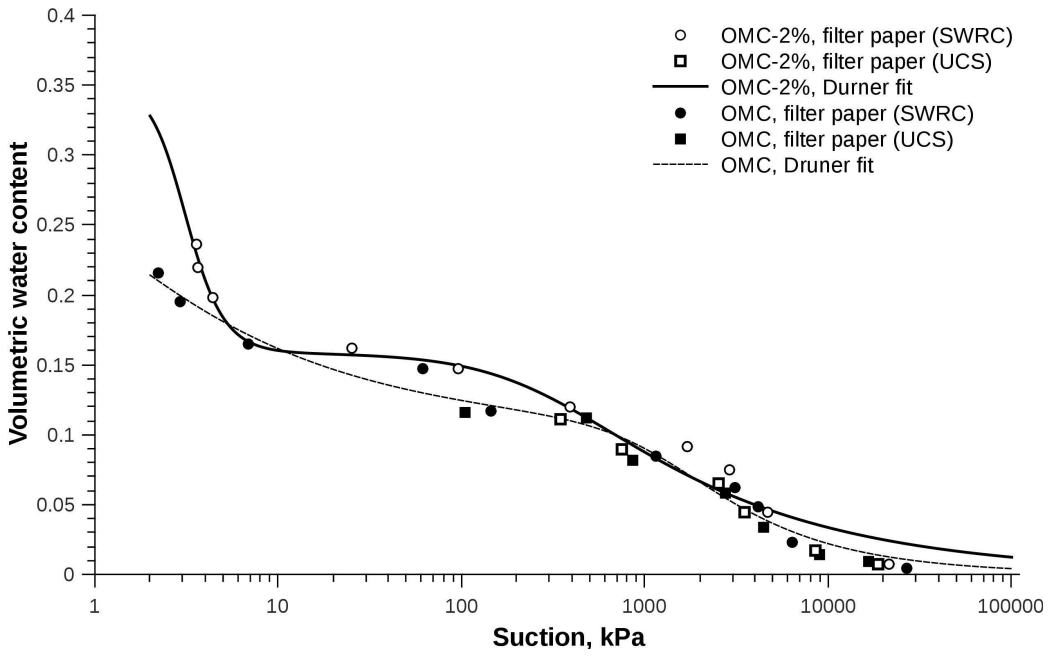
Fig. 5.9 SWRCs for K10 mix

Fig. 5.10 SWRCs for K20 mix

116

PUC-Rio - Certificação Digital Nº 1112056/CA
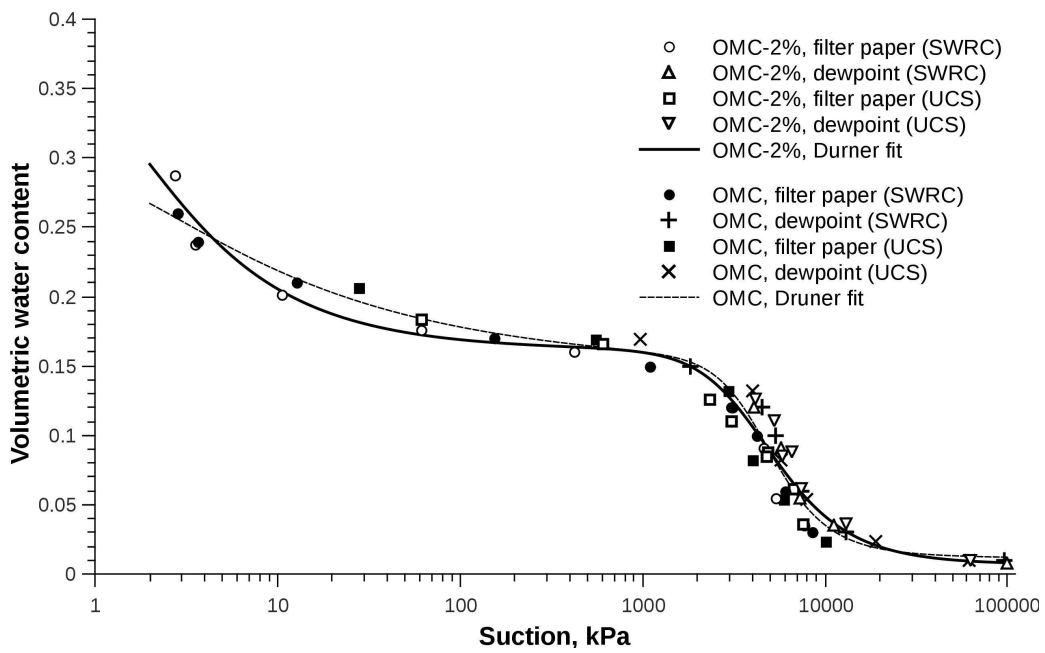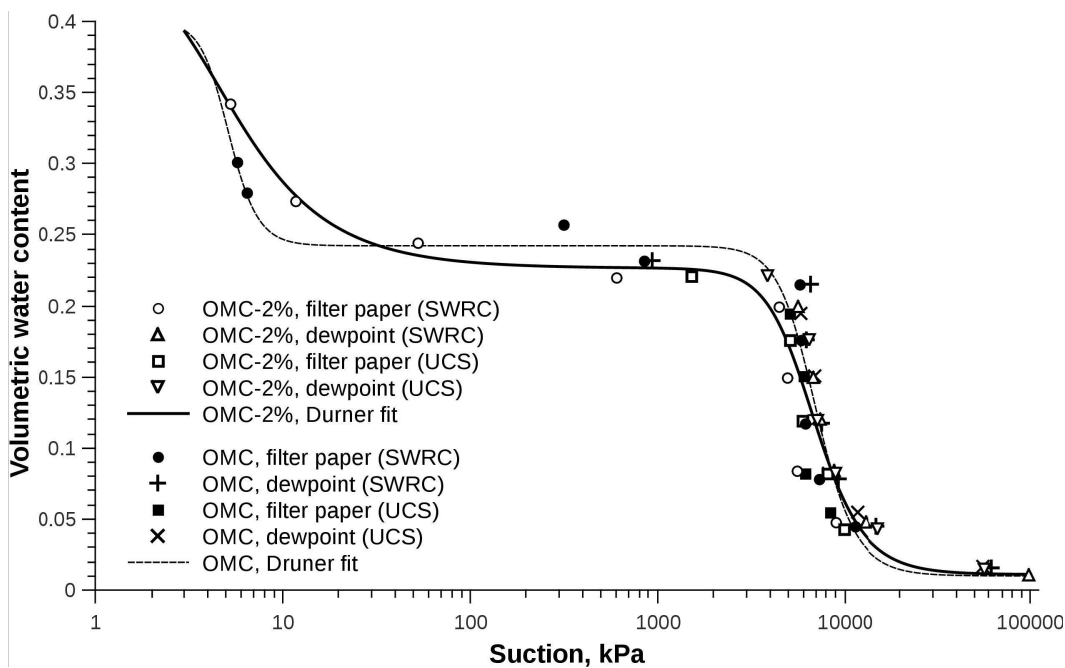
Fig. 5.11 SWRCs for K30 mix
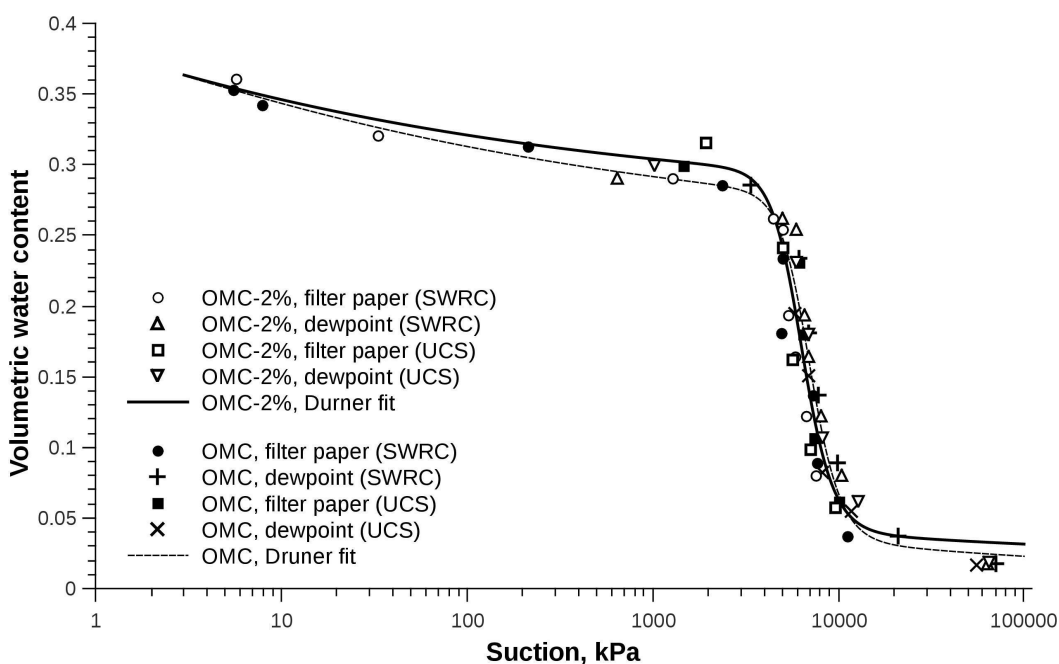
Fig. 5.12 SWRCs for K40 mix

From presented SWRCs it can be noted that the greater is soil's clay content the slower is the desaturation of macropores, i.e. until second air entry suction is reached. On the contrary, the desaturation of micropores is faster for the specimens with higher clay content, which is indicated by the steeper slope of the transition zone of the curve.

Table 5.5 Characteristics of SWRC specimens

Specimen	Dry density, kg/m^3	e	1st air entry value, kPa	2nd air entry value, kPa	Start of residual desaturation, kPa
K10 OMC-2%	1940	0.38	2.5	2580	15000
K10 OMC	1970	0.36	2	3390	14000
K20 OMC-2%	1945	0.38	2.5	2520	15000
K20 OMC	2020	0.33	2.5	2850	12500
K30 OMC-2%	1845	0.45	5	5100	13700
K30 OMC	1945	0.37	5	5350	11800
K40 OMC-2%	1755	0.52	5	4710	10300
K40 OMC	1855	0.43	5	4735	10200

Second air entry values were higher for K30 and K40 mixes than for K10 and K20. For the same clay content higher densities lead to higher air entry values. Similar behavior was reported by Vanapalli et al. [55] and Sheng [133] (Fig. 5.13). Birle et al. [134] studied the influence of dry density on the shape of SWRCs of statically compacted clay. The authors observed a greater degree of saturation at the same suction values for denser specimens. In high suction range SWRCs were independent of the void ratio, the fact also confirmed in the present study. This kind of behavior can be explained by the findings of Cuisinier and Laloui [135], who studied combined effects of suction and mechanical loading on the fabric of unsaturated aggregated silt. The research showed that mechanical loading affected mainly the macropores, while there was only a slight increase in the volume of micropores. The SWRCs for all mixes used in the present study are almost identical for suctions above 10000 kPa due to the fact that the same kaolinitic clay was used for their production, therefore the curves reflect the behavior of the same clay aggregates. The difference is attributed to increasing clay content, thus increasing residual water content.
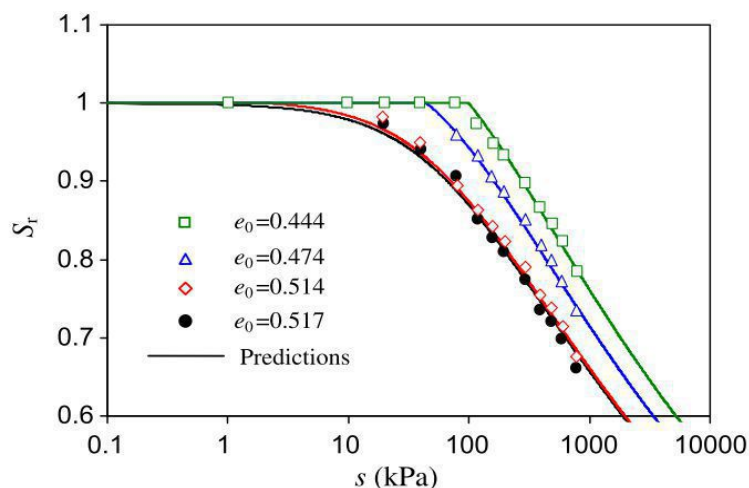
Fig. 5.13 SWRCs of a compacted till at various void ratios [55]

Initially experimental data was obtained in terms of gravimetric water content. Then volumetric water content was calculated as follows:

$$\theta = \frac{m_{wet} - m_{dry}}{\rho_w V_i} \tag{5.1}$$

m_{wet} – wet mass of the specimen,

m_{dry} – dry mass of the specimen,

V_i – initial volume of the specimen.

SWRCfit, developed by Seki [63], was used for the fitting of experimental data, being the only software found to be able to work with bimodal soils. SWRCfit is an open source software written in *GNU Octave* programming language. It is capable of fitting soil water retention data using there unimodal models: Brooks and Corey, van Genuchten and Kosugi; and two bimodal: Durner and Seki. The input data, i.e., the soil water retention curve, should be prepared as a text file with two columns. The first column is suction and the second column is volumetric water content. The user interacts with the program via command line interface, where initial estimates of saturated and residual water contents can be defined. It can be either chosen for the algorithm to find the best fit θ_s and θ_r, or to use initial values as constants. Two available bimodal formulas for SWRC were tested on the experimental data and Durner's model (Eq. 3.12), that presented better results, was chosen.

The algorithm for determining the initial estimate of Durner model parameters is as follows. The estimate is first performed by fitting certain numbers of the data points in the low suction region with van Genuchten equation to calculate the

effect of large pores (parameters α_2, n_2). By subtracting the van Genuchten curve from all data plots and fitting the subtracted curve to the van Genuchten equation, the effect of the small pores (parameters α_2, n_2) is calculated. The best fit θ_s and θ_r is estimated using coefficient of determination R^2 as a criterion:

$$R^2 = 1 - \frac{\sum_i (y_i - f_i)^2}{\sum_i (y_i - \bar{y})^2}$$

(5.2)

y_i – measured values,

f_i – predicted values,

$\bar{y}$ – mean of the observed data.

It is widely recognized that R^2 is not adequate for estimating goodness of fit of nonlinear regression [136]. R^2 is based on the assumption that a linear model is used, for nonlinear models the value of R^2 no longer has to be between 0 and 100%. Taking into consideration this limitation of *SWRCfit*, a script was written in Python programming language that cycled through the values of θ_s and θ_r in a given interval. Each iteration of the cycle invoked an instance of *SWRCfit* and resulting equation was checked for Root Mean Squared Error (RMSE), which is adequate for non-linear regression:

$$RMSE = \sqrt{\frac{\sum_{i=1}^{n} (f_i - y_i)}{n}}$$

(5.3)

The best fit parameters were chosen according to the smallest RMSE value.

Saturated volumetric water content was calculated as follows:

$$\theta_S = 1 - \frac{\rho_d}{G_s \rho_w}$$

(5.4)

However, it wasn't possible to account for the initial portions of SWRCs using the calculated values of θ_s. Actual saturated water contents were greater than theoretical ones due to soil expansion. It was impossible to reach or check for the saturation of SWRC samples. Therefore, a range of θ_s values was used to find the best fit, the lower limit determined by Eq. 5.4. Checked interval of θ_r values was always from 0 to the smallest experimental result for a given dataset. The resulting parameters of Durner model for each specimen density are presented in Table 5.17. In general, better fitting results were obtained for the soils with lower clay contents. R^2 and RMSE values are presented for each resulting set of model

parameters. It can be noted that the fits with lower RMSEs also have higher R^2 values.

By studying the changes in SWRCs depending on the soil composition and density, it is possible to develop a methodology that allows to produce an engineered soil with desired retention properties. Due to its low strength in comparison to industrialized construction materials, engineers are reluctant to use unstabilized soil in structural elements. However, rammed earth or CEBs can serve as nonstructural walls that can regulate indoor climate of buildings. For this, daily fluctuations of air humidity should be studied. Then a soil can be specially selected or an available soil can be modified to perform a desired moisture regulating function such as absorbing or releasing humidity when specific RH limits are reached. This can be particularly useful in improving either conditions of people that are subject to high humidity environments in the workplace or the quality of air-conditioned spaces that tend to have very low RH. While the application of the material used in the present study for abovementioned purposes is hardly feasible, the experiments carried out provide an insight of how to regulate moisture absorption behavior of compacted soil by changing its composition and density.

Table 5.6 Parameters of Durner fit for θ_s calculated using Eq. 5.4 and for best value for the interval given between parentheses

Specimen	θ_s	θ_r	w_1	α_1	n_1	α_2	n_2	R^2	RMSE
K10 OMC-2%	0.28	0	0.43405	0.27546	5.6890	0.0035357	1.4350	0.98108	0.00979977
	0.35 (0.29..0.35)	0	0.54743	0.34108	4.6549	0.0035284	1.4352	0.98118	0.00977869
K10 OMC	0.26	0	0.60394	0.93582	1.4520	8.2256e-04	1.7921	0.98344	0.00816468
	0.3 (0.27..0.3)	0	0.65817	1.7275	1.4226	8.0199e-04	1.8100	0.98378	0.00808185
K20 OMC-2%	0.27	0.004	0.39840	0.19676	2.2451	2.7393e-04	2.3872	0.95494	0.01412124
	0.39 (0.27..0.4)	0.007	0.59643	0.59643	1.7788	2.5939e-04	2.5211	0.95926	0.01344134
K20 OMC	0.25	0.008	0.38180	0.10852	1.5762	2.3382e-04	3.0191	0.97062	0.01215697
	0.31 (0.24..0.35)	0.01	0.53602	0.83555	1.3875	2.3264e-04	3.2195	0.97369	0.01150434
K30 OMC-2%	0.31	0.01	0.25655	0.085688	14.627	1.6931e-04	3.4944	0.91434	0.02447772
	0.45 (0.31..0.45)	0.011	0.50928	0.28756	2.1809	1.6397e-04	3.6814	0.92150	0.02343193
K30 OMC	0.27	0.01	0.14096	0.0031637	37.287	1.4971e-04	4.6628	0.88034	0.02889372
	0.3 (0.27..0.35)	0.013	0.22698	0.15523	14.042	1.5338e-04	4.5541	0.88416	0.02842557
K40 OMC-2%	0.34	0.017	0.11240	0.030744	6.9330	1.6259e-04	4.7960	0.92837	0.02604337
	0.42 (0.35..0.47)	0.016	0.37236	4.8744	1.1735	1.6433e-04	5.6178	0.93190	0.02539219
K40 OMC	0.3	0.015	0.13912	2.3840e-04	48.313	1.4058e-04	5.0647	0.93856	0.02560193
	0.4 (0.3..0.4)	0.01	0.38820	1.5472	1.1638	1.4908e-04	5.6732	0.95472	0.02204743

5.6.
Brazilian tests

The results of diametrical compression tests are shown in Fig. 5.15. Average test duration was around four minutes. Time to failure reduced with increasing density and decreasing water content. Typical failure mode of the samples in Brazilian tests is shown in Fig. 5.14.
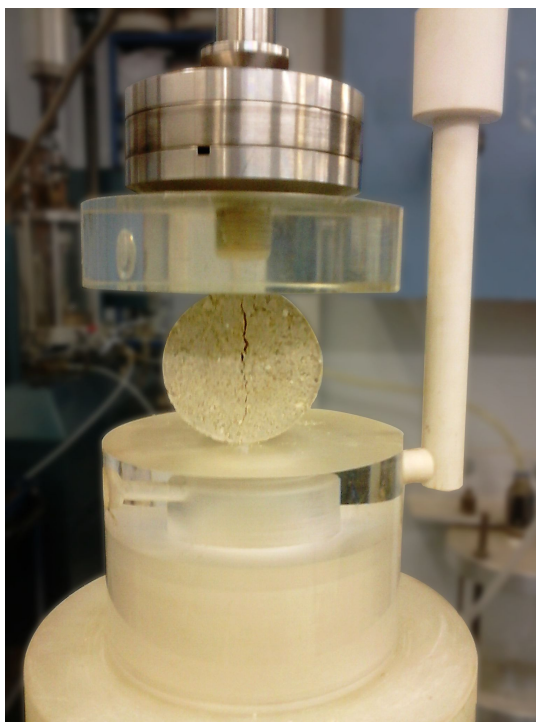
Fig. 5.14 Typical failure mode of the samples in Brazilian test

The relationships between the tensile strengths of the specimens, suctions and water contents on testing were plotted for each mix. Filter paper measurements were carried out on intact specimens before Brazilian tests, while dewpoint potentiometer suctions were obtained from crushed specimens. Nonetheless, there is a close agreement between the suction values measured in these two methods. This can be explained by the fact that at high suctions, especially after second air entry value is exceeded, the macropores are almost dry and the air starts to enter the micropores, i.e. drying of clay aggregates occurs. At this level of desaturation water is discontinuous and is found in adsorbed state. Thus, during shear the changes in suctions are localized and overall value doesn't change.

A similar trend in tensile behavior was observed for all soils. As expected,

near-saturated specimens had negligible tensile strength. With drying it increased until a peak value was reached. With respect to suction, the tensile strength reached its maximum approximately at the second air entry value. After that the strength started to decrease until the beginning of residual desaturation zone at about 10000 kPa. The rate of this decrease was higher for the soils with higher clay content. After soil reached residual desaturation, tensile strength seemed to stabilize. Despite having only two data points for each specimen density with suction higher than 10000 kPa, all the soils behaved in this manner. For convenience, the value of the strength at high suctions is called residual strength from here on.

For all soil mixes, denser specimens had greater tensile strengths for the same values of suction. The exception is the zone between saturation and second air entry value for K10 and K20 mixes, where no significant difference in the behavior of the specimens of different densities could be noted. In general, soil tensile strength increased with the addition of clay. The difference between peak and residual strength also increased with increasing clay content. In this sense, more clayey soils were more sensitive to the changes in suction, which can be expected, as they are able to retain more water.

Beckett [30] reviewed ten papers that investigated relationships between water content and tensile strength of compacted soils through Brazilian test. All the studies, with the exception of Mullins and Panayiotopoulos [137], observed steady in tensile strength with increasing suction. The same trend was reported by Jaquin et al. [74] for unsaturated rammed earth samples.

The behavior of compacted soil studied by Mullins and Panayiotopoulos [137] was similar to one observed in the present study. The authors investigated the tensile strengths of the mixes of sand and 0.5-8% of kaolin. The samples showed an increase in tensile strength with reducing water content until 5% by weight, where tensile strengths rapidly reduced. This moisture corresponded approximately to second air entry suction of the studied soils. Benessiuti et al. [138] and Villar et al. [139] also observed peaks in tensile strength of compacted residual soils following the increase in suction.
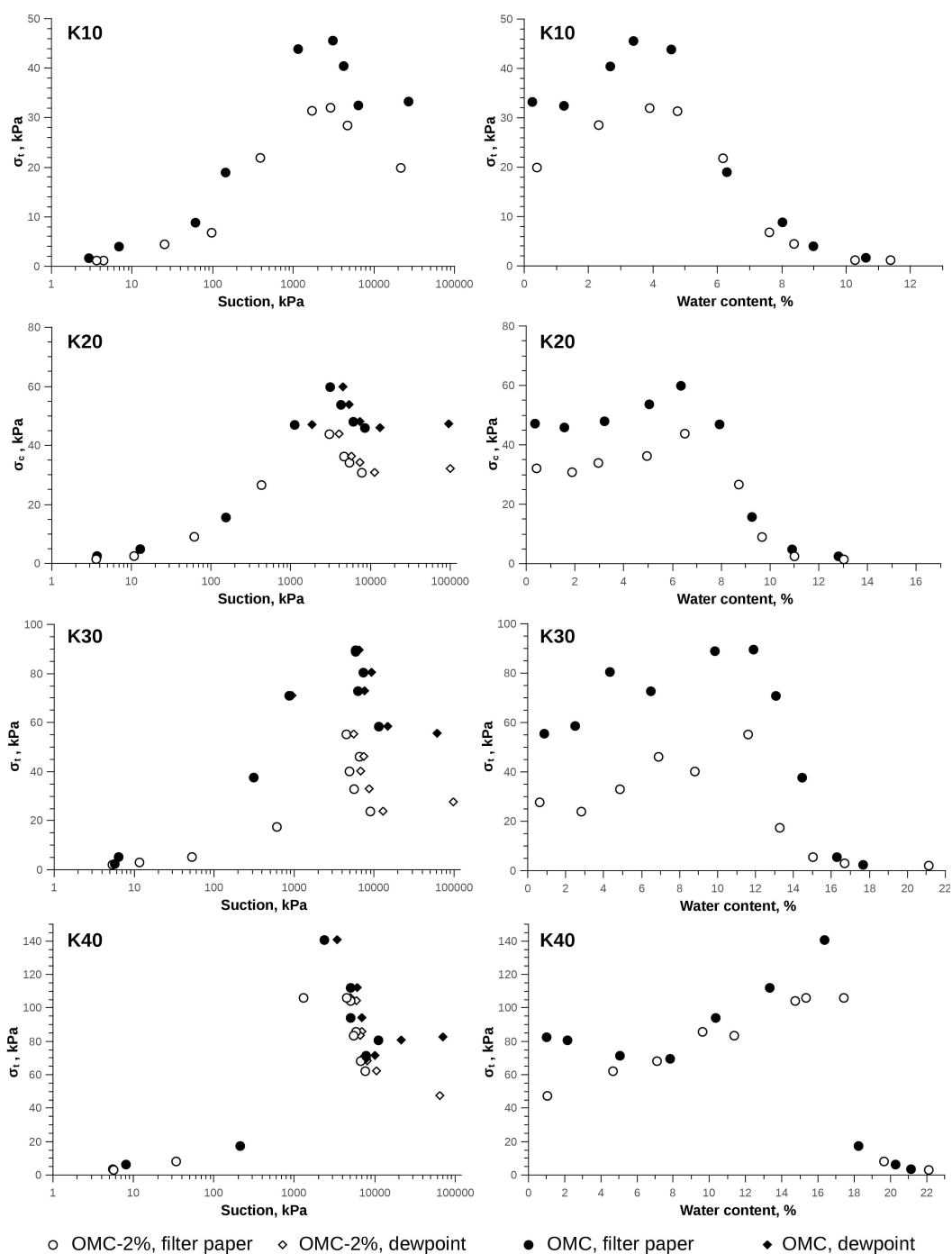
Fig. 5.15 Results of Brazilian tests in terms of suction and water content for all soil mixes

For better understanding the results of Brazilian tests were plotted using the same scale combined with SWRCs in Fig 5.21.

5.7.
Unconfined compression tests

After analyzing the results of the first Brazilian tests, it was decided to choose

the water contents of UCS specimens as to cover the range of suctions from before second air entry value until air dry state to verify if there is a similar peak in UCS following the increase in suction. The results of unconfined compression tests are shown in Figs. 5.17 and 5.18. The values of UCS with respect to suction and water content are presented in Fig. 5.17, while stress-strain curves for all tested specimens can be found in Fig. 5.18. Average time to failure was around 7-9 minutes. Typical failure mode of UCS samples is shown in Fig. 5.16.
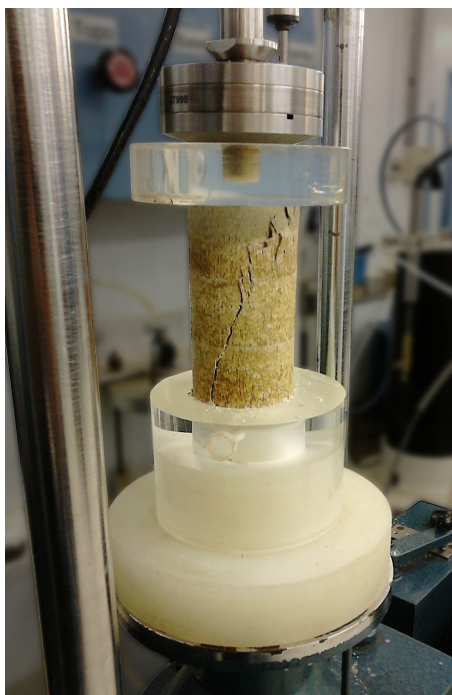
Fig. 5.16 Typical failure mode of UCS specimens

In the case of UCS samples filter paper measurements were carried out before the tests and total suction was obtained using the material taken from failed specimens. Again, the results showed good correlation, which indicated little change in suction during the tests for the range of values covered by chilled-mirror psychrometer.

With respect to the increase in suction (and decrease in water content), unconfined compressive strength of the specimens followed exactly the same trend observed in diametrical compression tests. UCS increased until the suction reached approximately second air entry. Though it is difficult to estimate exactly, peak strength occurred between the suctions equal to 1000 and 5000 kPa. Then UCS decreased until becoming constant at about 10000 kPa, i.e. the start of residual desaturation zone. Again, the drop in strength had steeper slope as clay

content increased and UCS was higher for higher clay contents and densities for the same soil mix.
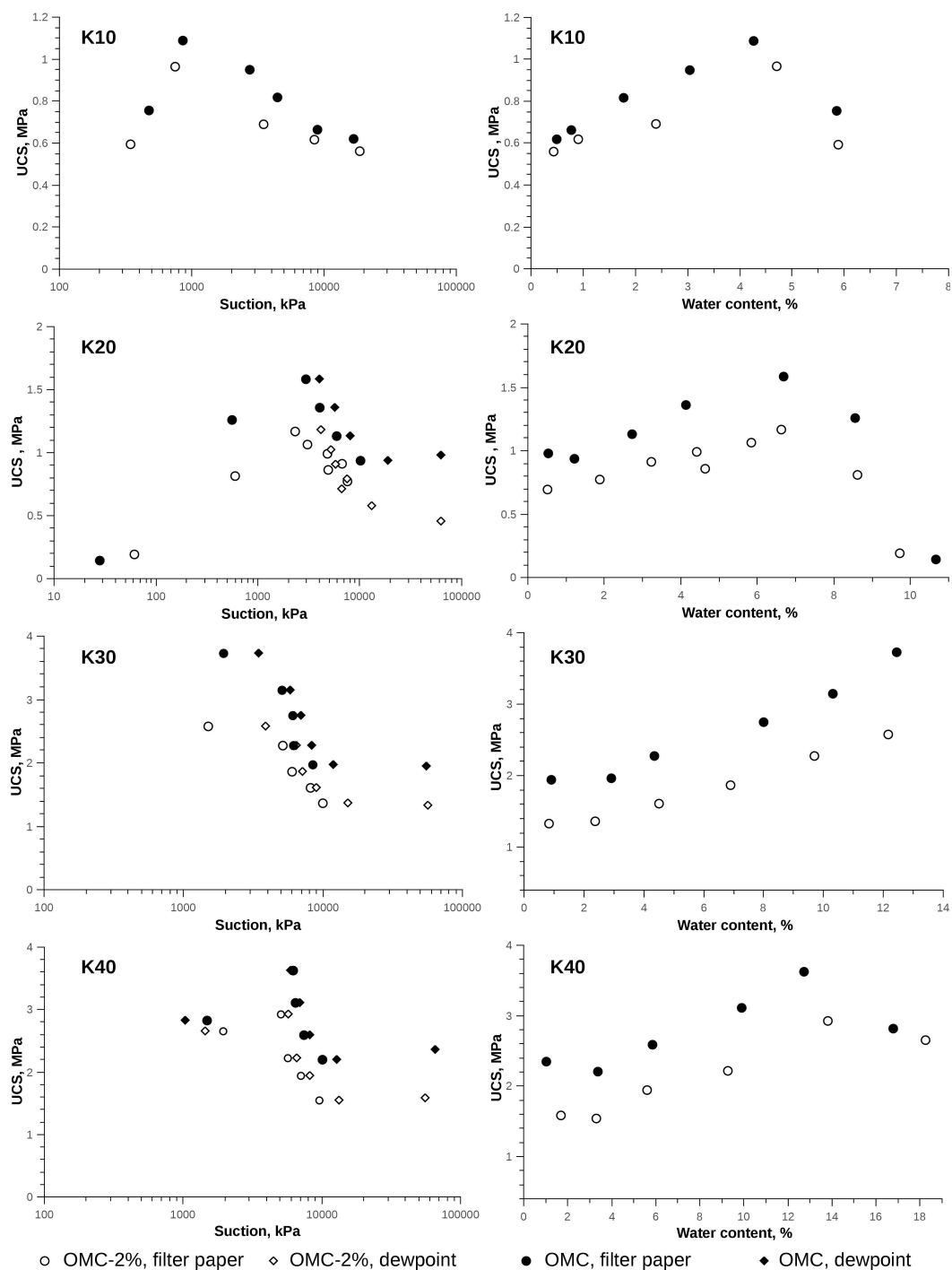
Fig. 5.17 The results of UCS tests in terms of suction and water content for all soil mixes
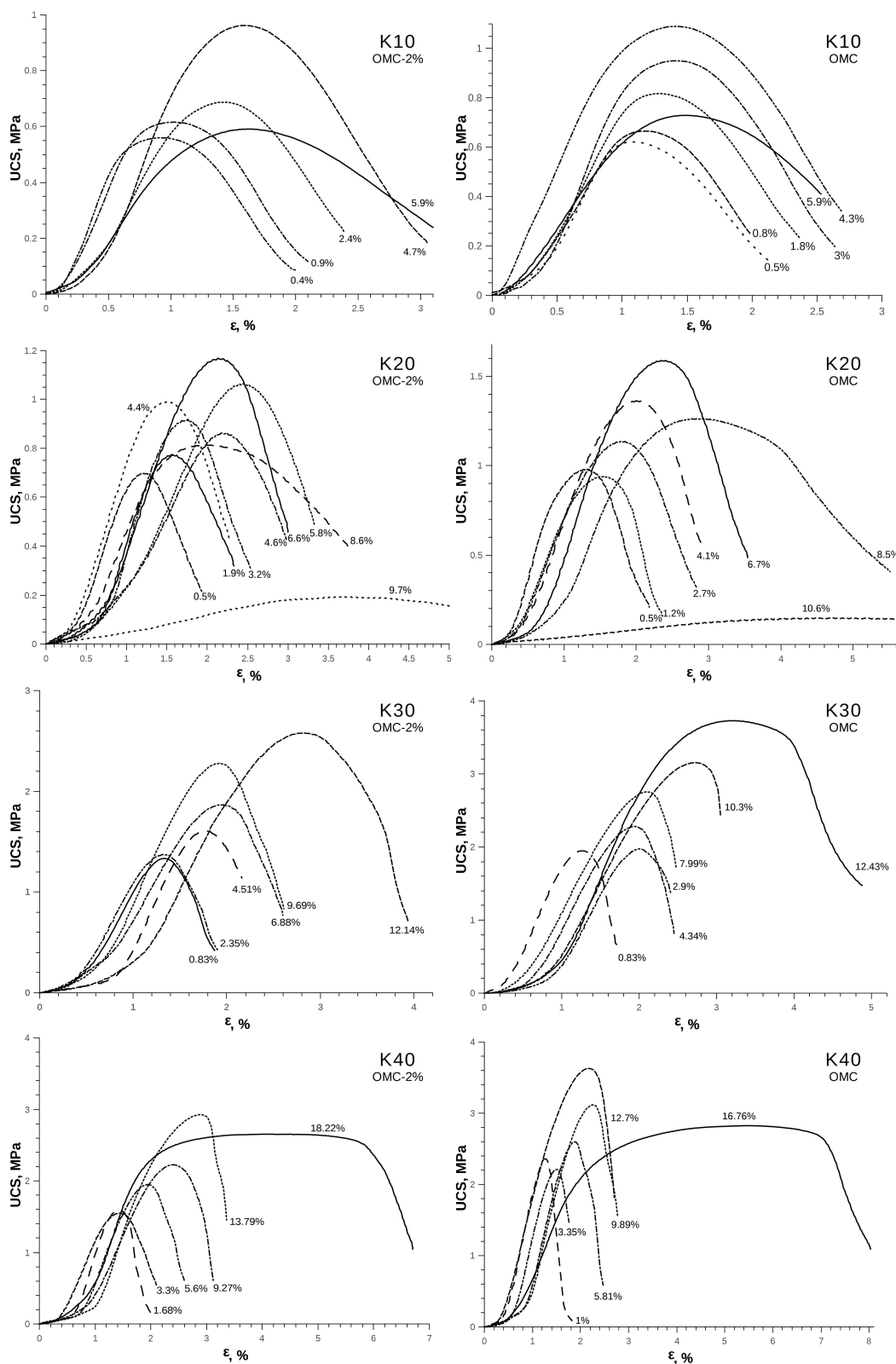
Fig. 5.18 Stress – strain curves for UCS specimens. Water content on testing is indicated near each curve

With some exceptions in K10 and K20 mixes, axial deformation on failure of UCS specimens increased following increase in water content. The specimens with the greatest water contents presented ductile behavior, which is most

noticeable for K30 and K40 mixes. While the majority of the specimens had well defined failure planes, similar to shown in Fig. 5.16, the ones with high moisture contents presented considerable barreling.

Elastic modulus was determined for each specimen as an average slope of the linear portion of the stress-strain curve according to ASTM D3148-96 [140]. For this a linear function was fitted to the data that represented a straight region of every curve. R^2 of all the functions was higher than 0.99. An example of the determination of Young's modulus for three K10 samples is shown Fig. 5.19.
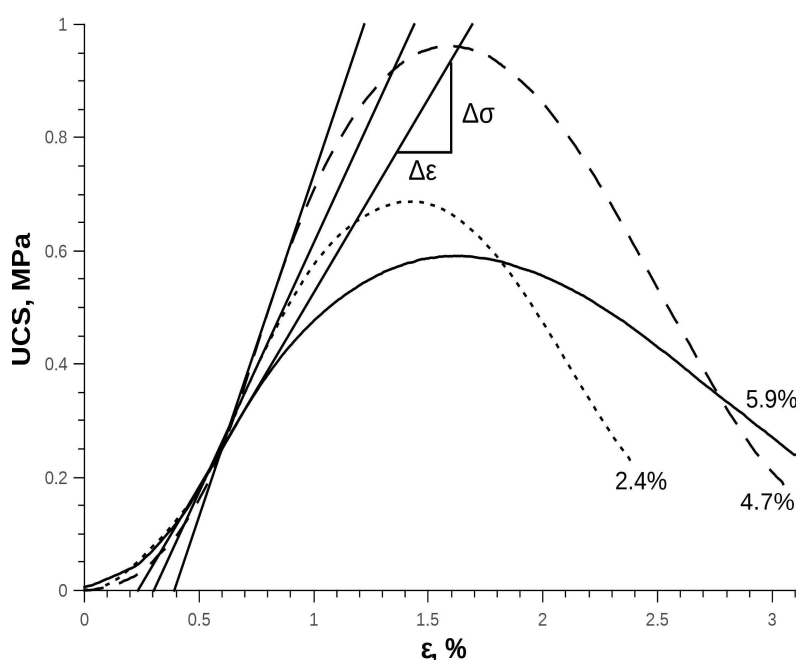
Fig. 5.19 Determination of Young's modulus for three samples of K10 mix compacted at 9.6% (OMC-2%). Water contents on testing are indicated near to stress-strain curves

Calculated elastic moduli are presented in Table 5.7 together with corresponding suctions and water contents. Obtained data was plotted against suction for all tested specimens (Fig. 5.20). In general, Young's modulus was higher for the soils with higher clay content. For some groups of specimens, like K10 OMC and K20 OMC, elastic moduli followed a similar trend as UCS values, i.e. increasing until a certain suction, and then decreasing. For K40 OMC Young's modulus steadily increased with suction. In general, the data is too scattered for conclusions about any existing trend to be made. Bui et al. [114] and Jaquin et al. [74] observed an increase in elastic modulus of rammed earth in unconfined compression following an increase in suction, which is consistent with suction hardening behavior reported in the literature.

Table 5.7 Values of Young's modulus for tested UCS specimens

Specimen	s, kPa *	w, %	E, MPa	Specimen	s, kPa *	w, %	E, MPa
K10 OMC-2%	343.5	5.88	68.6	K30 OMC-2%	56600.0	0.83	168.9
	746.6	4.70	120.6		12520.3	2.35	166.8
	3453.8	2.39	87.9		6553.0	6.88	160.8
	8390.5	0.90	106.0		5786.5	9.69	203.0
	18481.1	0.43	123.6		2691.6	12.14	185.5
K10 OMC	16581.6	0.48	103.9		8482.8	4.51	194.6
	848.8	4.26	119.5	K30 OMC	55210.0	0.89	238.8
	2743.4	3.04	138.1		10092.7	2.90	198.9
	4399.1	1.77	104.8		7197.4	4.34	203.6
	8905.9	0.77	86.6		6510.5	7.99	200.8
	472.4	5.85	77.8		5441.1	10.30	203.0
K20 OMC-2%	3216.9	6.62	96.3		2693.4	12.43	252.9
	62180.0	0.51	100.4	K40 OMC-2%	55660.0	1.68	242.1
	4142.1	5.82	76.6		7610.6	5.60	203.5
	5728.1	4.62	67.0		6115.6	9.27	171.8
	7058.9	3.21	116.5		5374.8	13.79	231.9
	10297.4	1.88	103.3		11416.5	3.30	178.6
	598.3	8.61	82.7		1684.3	18.23	221.1
	5295.6	4.41	103.8		65350.0	1.00	311.2
	60.9	9.70	7.4		11418.9	3.35	282.5
K20 OMC-2%	4866.7	4.13	116.4	K40 OMC	7789.2	5.82	287.9
	62020.0	0.51	143.9		6683.3	9.89	273.7
	14549.2	1.20	100.9		6068.1	12.70	264.8
	6951.7	2.71	102.5		1253.2	16.76	163.8
	552.4	8.55	102.1				
	3470.0	6.67	125.9	* suction values given as an average of filter paper and dewpoint potentiometer measurements, when available			
	27.9	10.66	3.7				
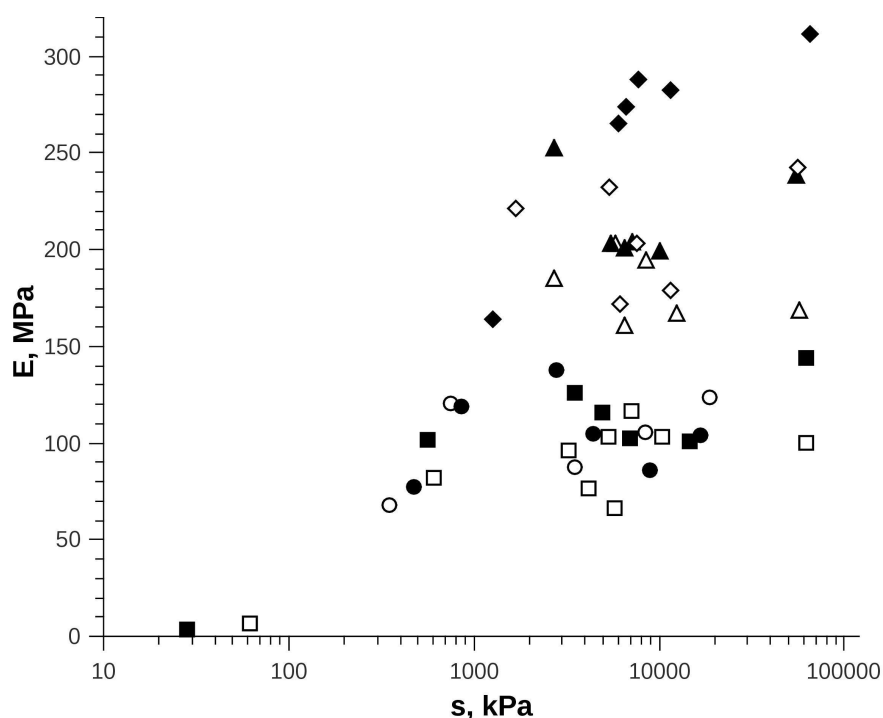
Fig. 5.20 Relationships between elastic moduli of all tested specimens and suction

For better understanding of the relationships between UCS, tensile strength and suction, experimental results were plotted in Fig 5.21 using the same scale. As the trends in the behavior of the specimens seemed to be related to specific zones of SWRCs, the curves were superimposed over the results of the strength tests. For clarity, average suction values were used instead of showing data obtained in filter paper and dewpoint potentiometer tests separately.

It can be noted that in transition zone of desaturation water content seems to be related to soil strength. As clay content of the soil mixes increases, the slope of the portion of SWRCs between second air entry and residual zone becomes steeper. Similarly, the decrease in strength in the same zone of SWRCs is greater for the soils with higher clay contents. Assuming that at suction equal to second air entry value all the water in clay aggregates is found in adsorbed state, the soil specimens behave according to Grim's hypothesis [51]. The author suggested that maximum strength of a clay-sand mix is attained when all the water present in the material is in "rigid" state, i.e. adsorbed by clay fraction.
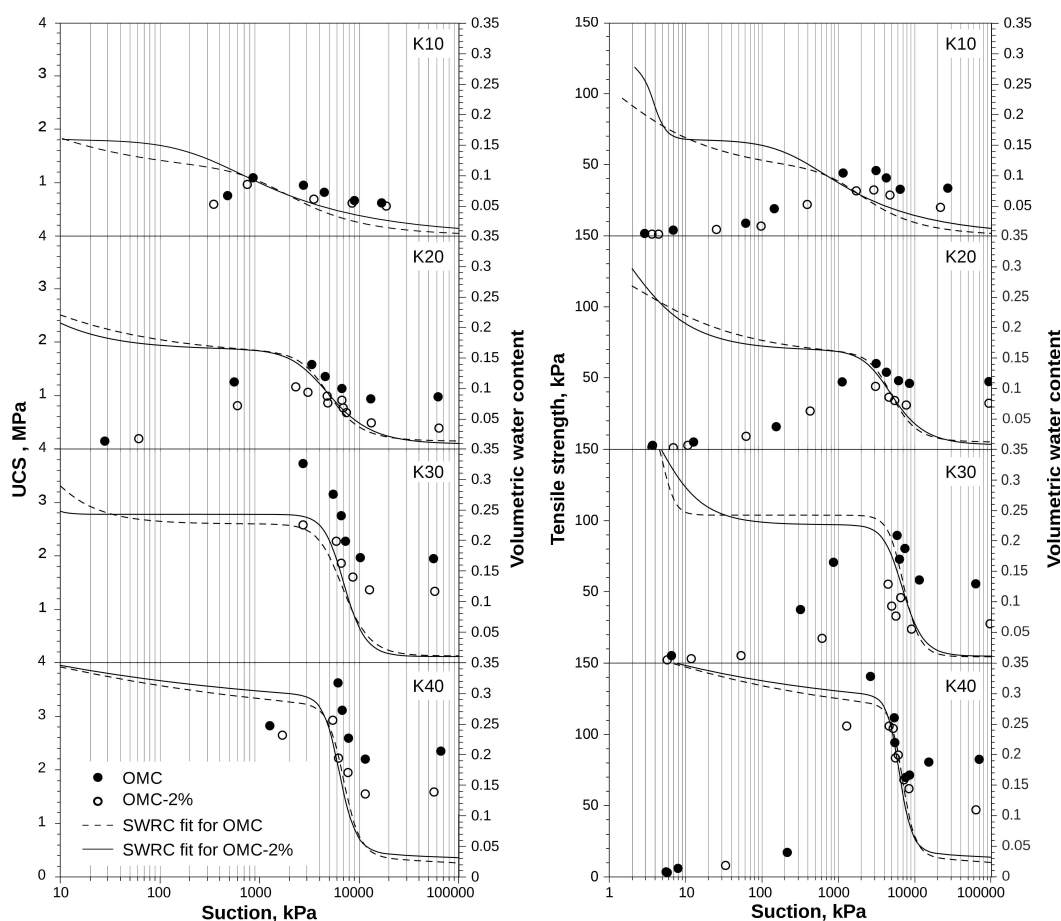
Fig. 5.21 Superposition of SWRCs with the results of UCS and Brazilian tests

From the point of view of the performance as construction materials, it is important to know how climatic conditions affect the strength of the studied soil mixes. According to Kelvin's equation, RH = 90% and t = 0º C result in suction equal to 13270 kPa. This means that if relative humidity on site doesn't exceed 90%, all the soils used in this study will remain in residual state of desaturation, i.e. their strength unaffected by the changes in climatic conditions. Considering the temperature of 0º C, the increase of RH from 90% to 95%, that amounts to suction equal to 6500 kPa, will provoke the increase in the strength of the studied soil mixes up to approximately maximum value. In the worst-case scenario, RH might reach 99% and the suction 1270 kPa. Under these circumstances, all the soil specimens will still be stronger than in residual desaturation state. This findings are opposite of the behavior reported by Beckett and Augarde [64]. The authors observed significant reduction of soil strength following the increase in RH, while the materials used in the present study become stronger with the increase of RH up to 99%.
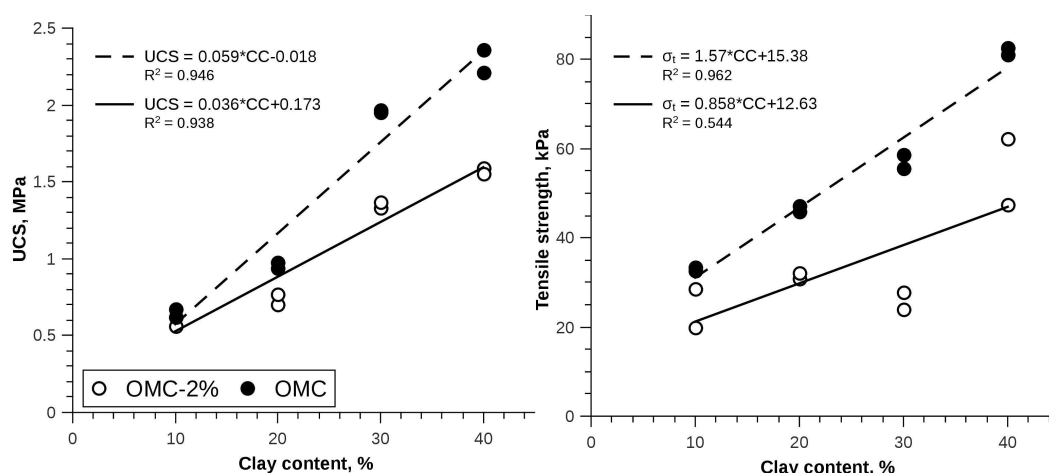
Fig. 5.22 Influence of clay content on the strength of tested specimens with residual water content

It is evident that clay content is the main factor that influence the behavior of the studied soils. The relationship between clay content and residual compressive and tensile strength of the soil mixes compacted at OMC and OMC-2% is shown in Fig. 5.22. The following linear trend can be observed for OMC-2% specimens:

$$UCS = 0.59\,CC - 0.018 \tag{5.5}$$

UCS – unconfined compressive strength in MPa,

CC – clay content in percent.

$$\sigma_t = 1.57\,CC + 15.38 \tag{5.6}$$

σ_t – tensile strength in kPa.

For OMC specimens the trend is as follows:

$$UCS = 0.036\,CC + 0.173 \tag{5.7}$$

$$\sigma_t = 0.858\,CC + 12.63 \tag{5.8}$$

Eqs. 5.5-5.8 can serve as a rough estimate of residual strength of the soil mixes produced with the same components that were used in the present research. Moreover, the use of the given formulas must be restricted to clay content limits of 10-40%. Inert fraction with no clay added would have negligible strength, while at high clay contents the soil strength would tend to become constant as the influence of sand and silt would gradually decrease. This kind behavior was reported by Grim [51], who observed the stabilization of the strength of as-compacted sand-clay mixtures with clay content as low as 8-12%.
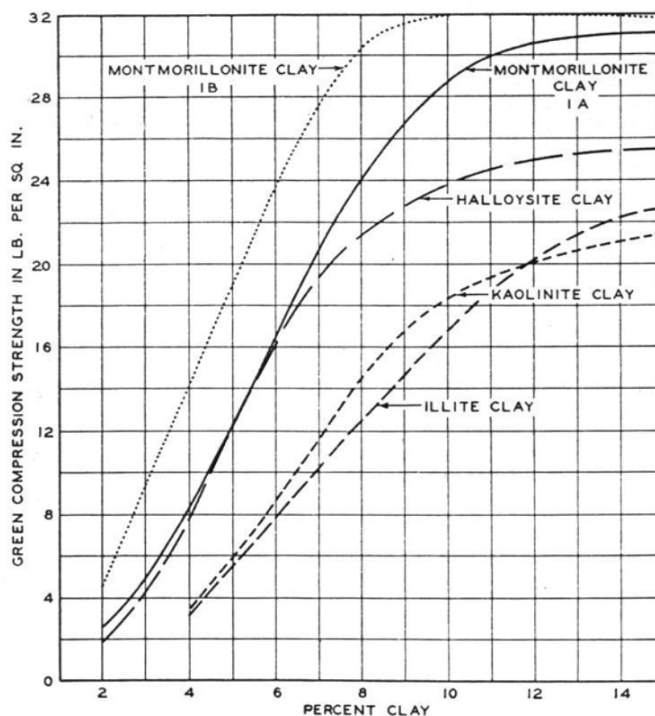
Fig. 5.23 Influence of clay content on the unconfined compressive strength of as-compacted sand-clay mixes [51]

Dry density is cited by many authors as a possible indicator of the strength of earthen construction materials [13], [46], [91]. In the present study this was verified to be true if the composition of the soil is the same, which is consistent with the findings of Kouakou and Morel [104]. However, for the soils with different clay contents, lower density is probably a sign if higher clay content. This can lead to greater soil strength, given the same compactive effort.

| ○ K10 OMC-2% | ● K10 OMC | □ K20 OMC-2% | ■ K20 OMC |
| △ K30 OMC-2% | ▲ K30 OMC | ◇ K40 OMC-2% | ◆ K40 OMC |
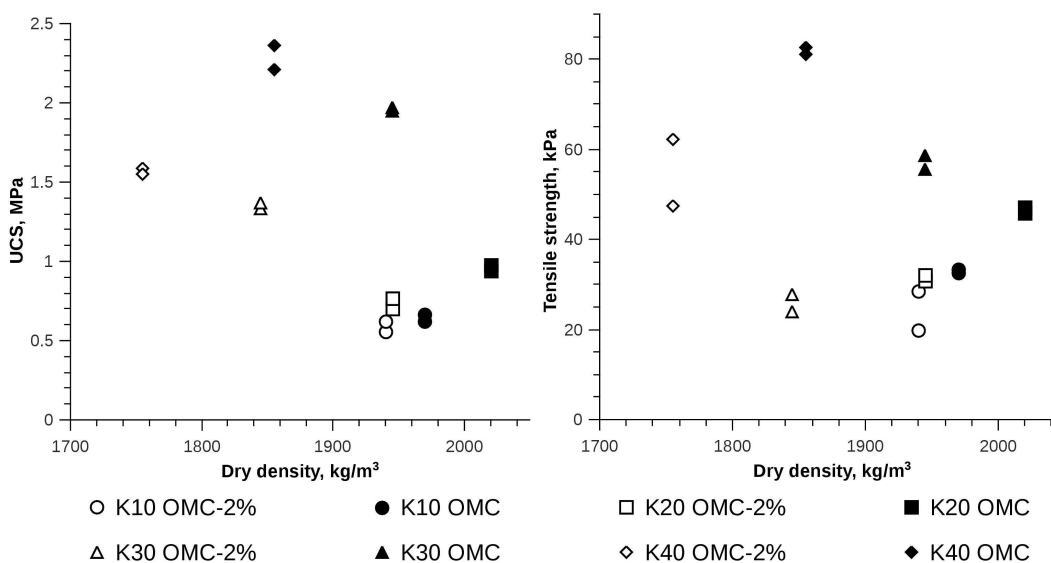
Fig. 5.24 Influence of dry density on the residual strength of tested specimens

5.8.
Triaxial tests

Deviator stress vs. axial strain data obtained in triaxial tests was is presented in Fig. 5.25. As the recommendations for the test speeds were followed, the tests were considered drained. From the graphs peak deviator stress (σ'_1-σ'_3) values were taken for each specimen.

These values were used to calculate p' and q as follows:

$$p' = \frac{\sigma'_1 + \sigma'_3}{2} \tag{5.9}$$

$$q = \frac{\sigma'_1 - \sigma'_3}{2} \tag{5.10}$$

Obtained p' and q were plotted and effective stress envelopes were found through linear fitting. Effective angle of internal friction of soil φ' and cohesion intercept c' were calculated as:

$$\sin\varphi' = \tan\alpha' \tag{5.11}$$

$$c' = \frac{a'}{\cos\varphi'} \tag{5.12}$$

where a' and α' are effective stress parameters in p'-q space.

For each soil mix the denser specimens showed higher strength. As expected, the angle of internal friction decreased with increasing clay content while cohesion intercept increased. Effective stress parameters obtained in triaxial tests together with initial void ratios are presented in Table 5.8.
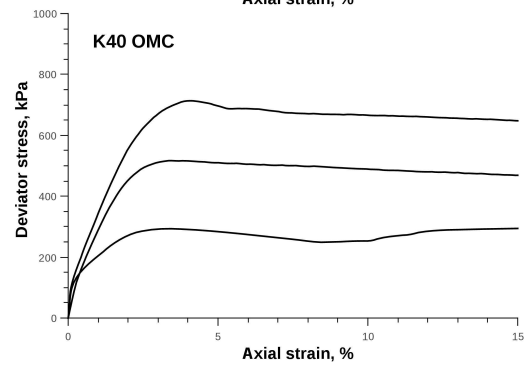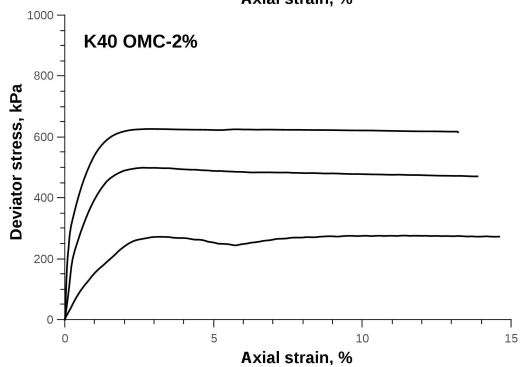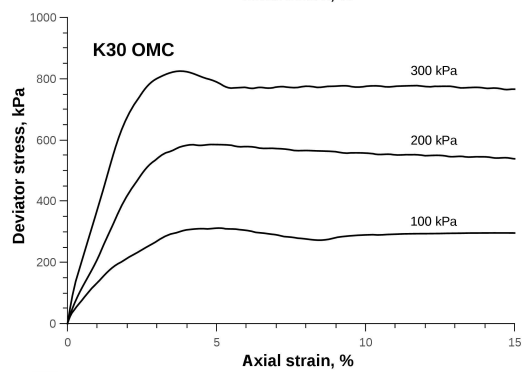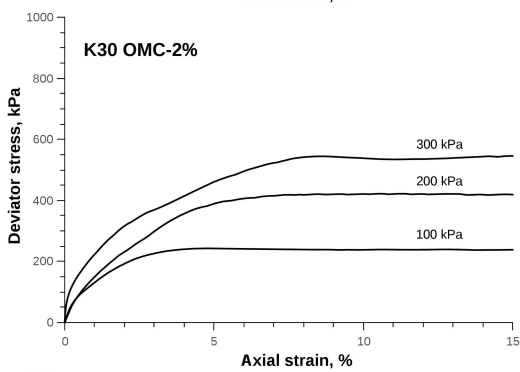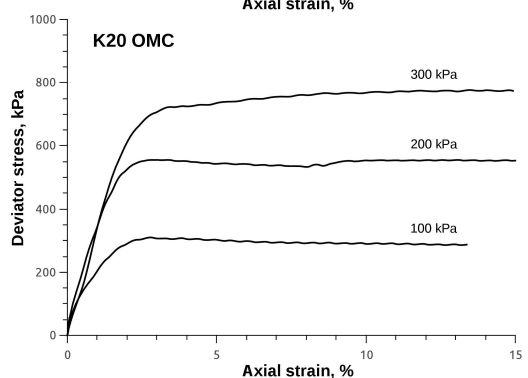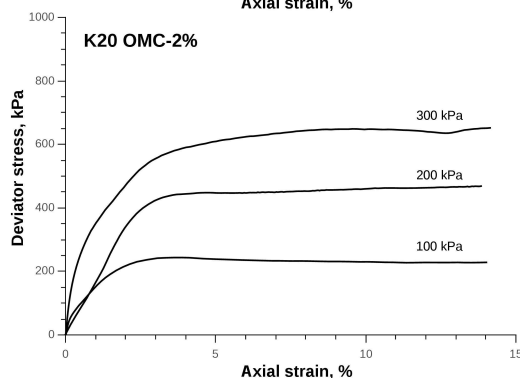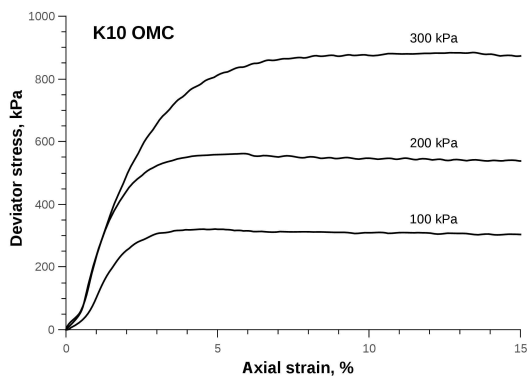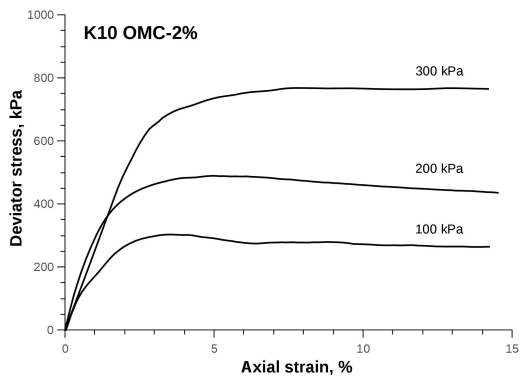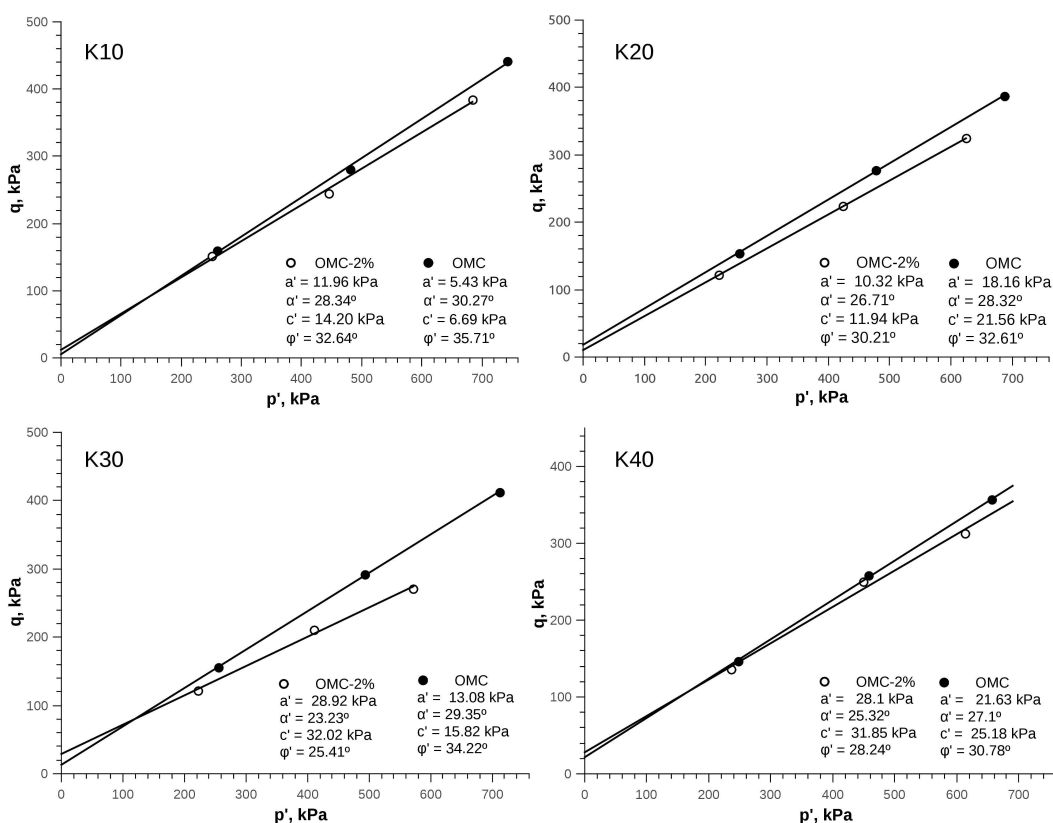
Fig. 5.26 Effective stress envelopes for all soil mixes

Table 5.8 Effective stress parameters obtained in triaxial tests

Specimen	e (initial)	a', kPa	α', °	c', kPa	φ', °
K10 OMC-2%	0.38	11.96	28.34	14.20	32.64
K10 OMC	0.36	5.43	30.27	6.69	35.71
K20 OMC-2%	0.38	10.32	26.71	11.94	30.21
K20 OMC	0.33	18.16	28.32	21.56	32.61
K30 OMC-2%	0.45	28.92	23.23	32.02	25.41
K30 OMC	0.37	13.08	29.35	15.82	34.22
K40 OMC-2%	0.52	28.06	25.32	31.85	28.24
K40 OMC	0.43	21.63	27.10	25.18	30.78

5.10.
Prediction of unconfined compressive strength

Some of the existing criteria for the prediction of unsaturated soil strength were reviewed in Section 3.5.2. There are a number of studies applied for geotechnical engineering that attempt to use some of these criteria for the

prediction of UCS of soils. In the field of earth construction, in spite of dealing with the same material, the interpretation of the experimental data has been restricted to almost exclusively using linear functions to describe various aspects of soil behavior. On the other hand, in recent years there has been a growing understanding that unsaturated soil mechanics may be the key to understanding the strength of the earthen construction materials.

For any strength criterion to be successfully used by earth construction community, the necessary parameters for its application should be possible to be determined using simple tests. In this respect, the empirical method of calculation of Bishop's effective stress parameter χ proposed by Khalili and Khabbaz [66] is of interest. In order to verify its applicability for the prediction of the strength of CEBs, the data obtained in SWRC, UCS and triaxial tests was used.

The values of χ were obtained applying Bishop's effective stress criterion for unsaturated soils to unconfined compression tests.

Assuming that $s = u_a - u_w$:

$$q = a' + (p + s\,\chi)\tan\alpha' \tag{5.13}$$

$$\chi = \frac{q - a'}{\tan\alpha'} - p \tag{5.14}$$

$$\chi = \frac{q - c'\cos\varphi'}{\sin\varphi'} - p \tag{3.15}$$

In unconfined compression $\sigma_3 = 0$, thus:

$$\chi = \frac{\sigma_1\left(\dfrac{1}{\sin\varphi'} - 1\right) - 2c'\cot\varphi'}{2s} \tag{5.16}$$

where $\sigma_1 = \text{UCS}$.

The values of χ were calculated using suctions measured in both filter paper and dewpoint potentiometer tests. The results were plotted in Fig. 5.27. Some of the values are greater than one, which is not possible according to the original theory. Blight [54] pointed out that at low suctions values of the parameter χ greater than 1 can occur during shear loading and compression of compacted silt, clay and clay-shale. The author stated that theoretical explanation of this phenomenon is based on the fact that the curvature of the liquid bridges between soil grains changes when soil desaturates and becomes re-saturated, leading to the increase in effective stress.
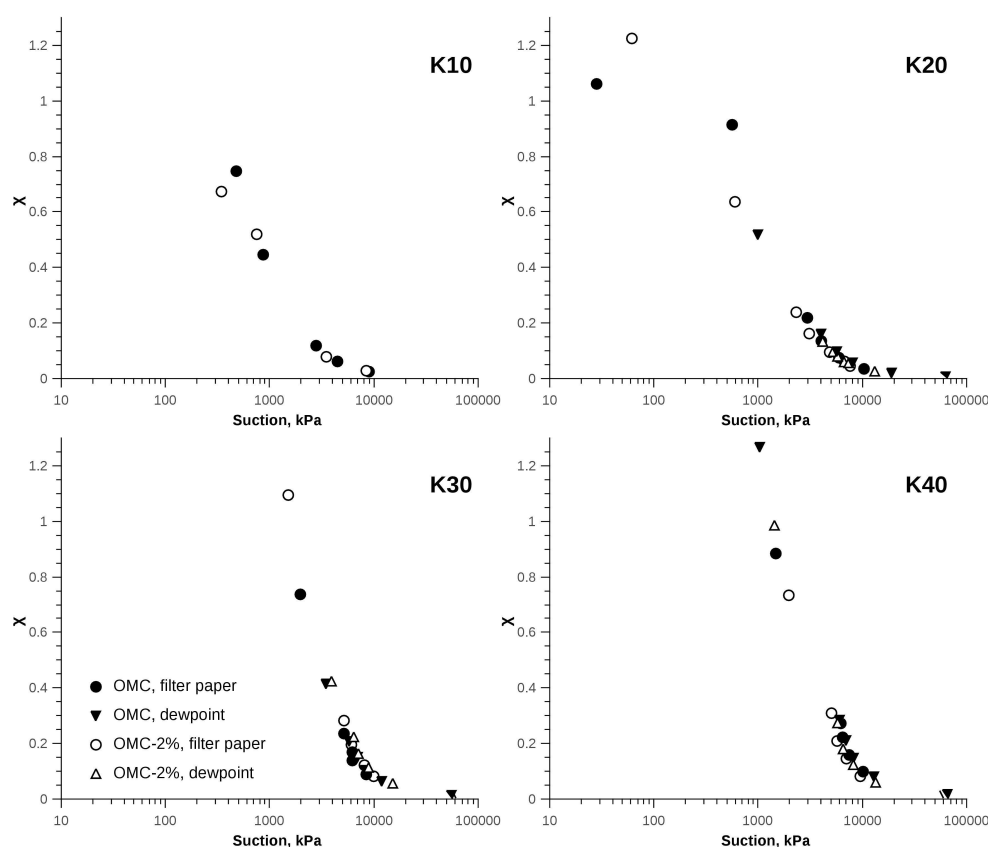
Fig. 5.27 Values of χ for all tested specimens

The values of χ, and consequently the contribution of suction to the effective stress, decrease exponentially with increasing suction in the same manner for all soil mixes. χ vs. suction curve apparently undergoes a change in shape around 2000-3000 kPa. This is more visible on a log-log scale as shown in Fig. 5.28. This change in shape of χ-s curve might be explained by bimodal nature of the soil.
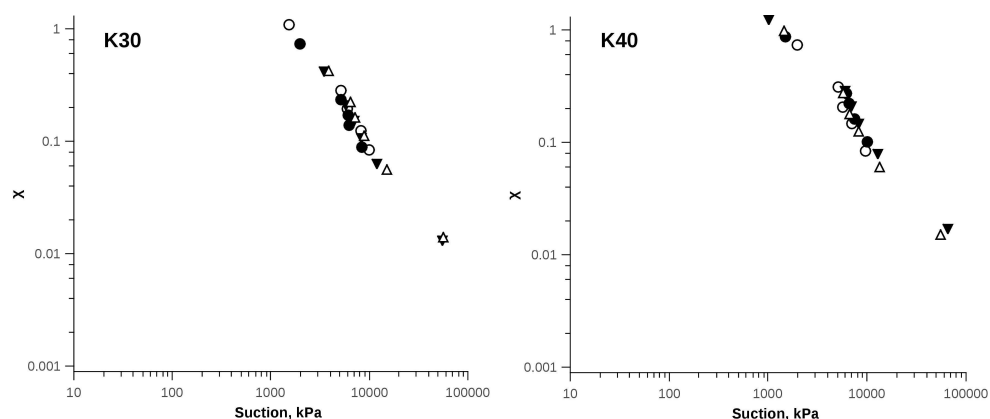
Fig. 5.28 χ vs suction for K30 and K40 mixes, log-log scale

The values of χ were plotted against suction normalized by second air entry values of the corresponding groups of UCS specimens. The result is shown in Fig. 5.29. A power function of the following form was used to fit the experimental

data:

$$\chi = A \left(\frac{s}{s_{air}} \right)^{n} \qquad (5.17)$$

where A and n are constants and s_{air} - second air entry suction. Eq. 5.17 is similar to that proposed by Khalili and Khabbaz [66].

Taking into consideration the shape of χ-s curves and double porosity of the soils, the data corresponding to the suction greater than second air entry value was excluded from subsequent calculations. The fitting procedure was repeated for a number of UCS vs. suction datasets, namely:

- data for all tested specimens;

- data for all the specimens of each soil mix;

- data for the specimens of each density (OMC and OMC-2%)

Curve fitting was carried out with the aid of *SciPy* library, available for *Python* programming language. The particular routine used was *scipy.optimize.curve_fit* – a non-linear least squares fit algorithm that uses Levenberg-Marquardt method of adjustment. The routine requires as input a user-defined fitting function, an initial guess for fit parameters, the x-axis and the y-axis data. The function was defined as $y = Ax^{n}$ and for the initial guess the values of A and n for the dataset containing all UCS results were used. The fit parameters obtained in this manner for all datasets are summarized in Table 5.9.
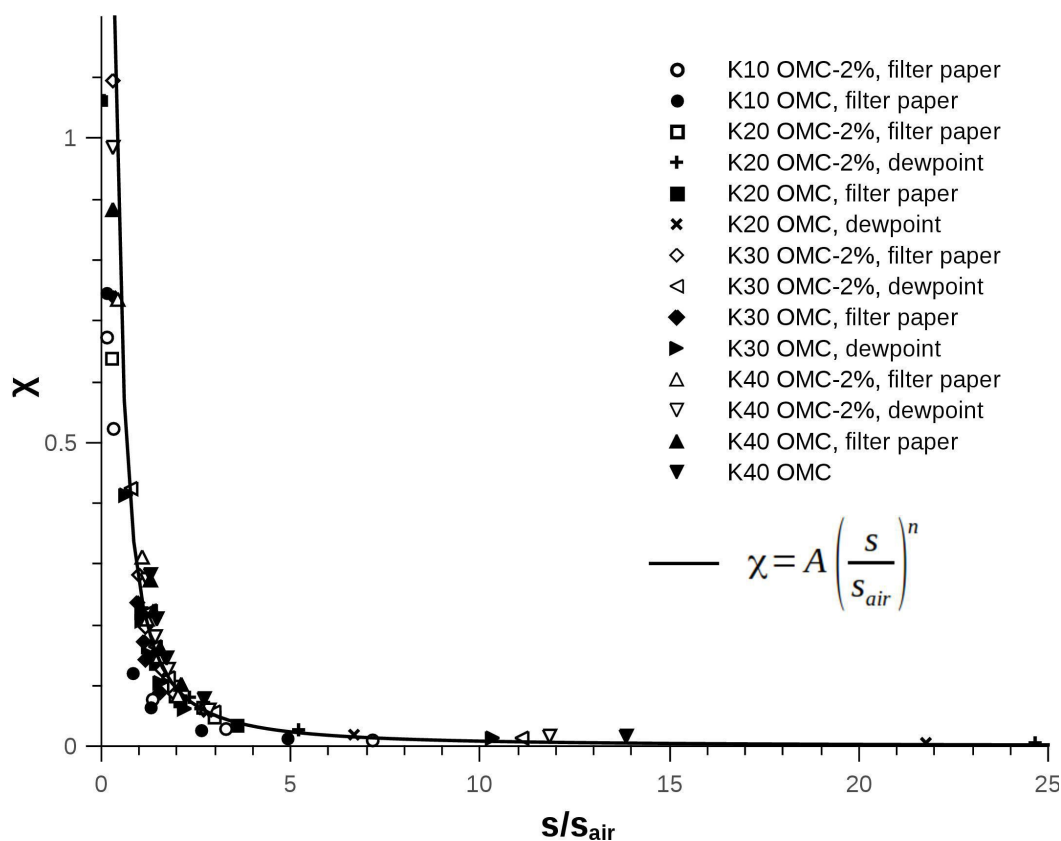
Fig. 5.29 χ vs. normalized suction. Power function fit for all UCS data corresponding to s ≥ s_{air} is shown

Table 5.9 Fit parameters A and n for Eq. 5.17 calculated for different datasets

Dataset	A	n	RMSE
K10 OMC-2%	0.1097	-1.1269	0.00004944
K10 OMC	0.0892	-1.2637	0.00061845
K10, all specimens	0.0986	-1.1899	0.00599251
K20 OMC-2%	0.2175	-1.2401	0.00749154
K20 OMC	0.2318	-1.3648	0.00726024
K20, all specimens	0.2274	-1.3126	0.00765059
K30 OMC-2%	0.2829	-1.6340	0.01435349
K30 OMC	0.2137	-1.6746	0.01455669
K30, all specimens	0.2462	-1.6250	0.02546641
K40 OMC-2%	0.3471	-1.9316	0.01898090
K40 OMC	0.4351	-1.9610	0.01224460
K40, all specimens	0.3596	-1.7194	0.02442607
All mixes	0.2656	-1.5068	0.03615841

To validate the use of Eq. 5.17, the RMSEs of the following formula, derived from Eq. 5.16 and Eq. 5.17, against experimental data were calculated:

$$UCS = \frac{2A\left(\dfrac{s}{s_{air}}\right)^{n} s + 2c'\cot\varphi'}{\left(\dfrac{1}{\sin\varphi'} - 1\right)} \qquad (5.18)$$

It was hypothesized by Khalili and Khabbaz [66] that the unique relationship proposed by the authors (Eq. 3.16) for the empirical determination of χ could be used to calculate effective stress in different soils. This hypothesis was verified for the case of the present study in the following way. For each group of samples with the same composition and density three versions of Eq. 5.18 were used. The difference between them was in the values of A and n (presented in Table 5.9):

- calculated using the data for the group of samples in question,
- calculated using the data for all the specimens of the same mix,
- calculated for the data for all the specimens for all mixes.

The resulting RMSEs are shown in Table 5.10 and the curves for all the checked equations are plotted in Fig. 5.30 together with the experimental data.

Table 5.10 Results of the validation of Eq. 5.17

Dataset	RMSE calculated for Eq. 5.18 using A and n for:		
	Same mix and dry density	Same mix	All specimens
K10 OMC-2%	0.0052	0.0955	0.2304
K10 OMC	0.7075	0.8187	1.8876
K20 OMC-2%	0.0830	0.0988	0.1426
K20 OMC	0.1665	0.1499	0.2353
K30 OMC-2%	0.3302	0.4070	0.2865
K30 OMC	0.5564	0.5751	0.7061
K40 OMC-2%	0.4768	0.4405	0.4342
K40 OMC	0.7149	0.6977	0.9660
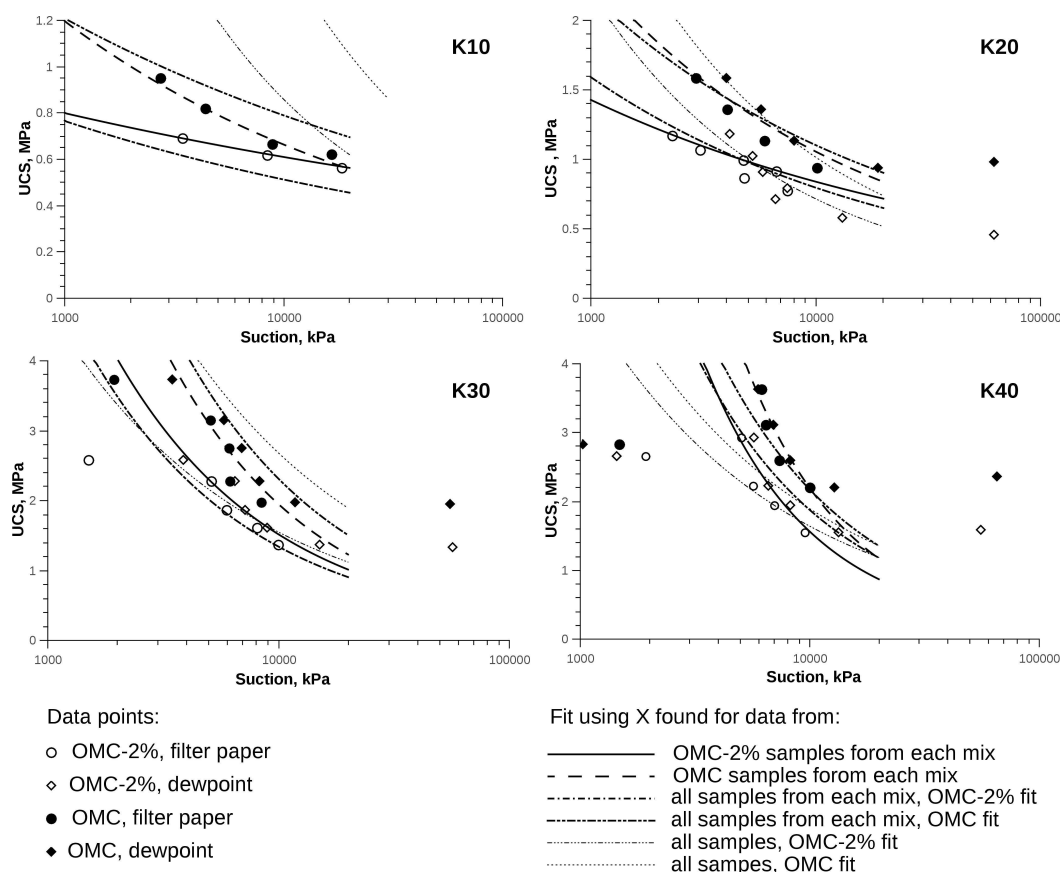
Fig. 5.30 UCS prediction using values of X calculated from different datasets

In can be noted from Fig. 5.30 that the values of effective stress parameter χ defined using Eq. 5.17 and the parameters A and n calculated for all soil mixes can give a rough estimate of UCS, with the exception of K10 mix. The best fit was achieved for K30 mix. Regardless of the method of A and n determination, it was not possible to predict UCS of the specimens in air dry state. Thus the use of Eq. 5.17 should be restricted to the suction values ranging between second air entry and the start of residual desaturation.

The values of residual UCS were excluded from the datasets and the validation of Eq. 5.17 preformed once again. The data for K10 samples was also dismissed, as the exact measurements of suction in air-dry state are not available. The results are presented in Table 5.11. As expected, a better correlation could be achieved this time.

Table 5.11 Results of the validation of Eq. 5.17 for datasets not including residual UCS values

Dataset (without air dry samples)	RMSE calculated for Eq. 5.18 using A and n for:		
	Same mix and dry density	Same mix	All specimens
K20 OMC-2%	0.0736	0.0703	0.0758
K20 OMC	0.0950	0.1044	0.1527
K30 OMC-2%	0.1744	0.2877	0.1707
K30 OMC	0.2681	0.4120	0.6878
K40 OMC-2%	0.2379	0.2944	0.3639
K40 OMC	0.2363	0.3591	0.8445

Taking into consideration the limitations of Eq. 5.17, the following can be proposed for the prediction of UCS of the specimens used in this study:

$$UCS = \begin{cases} \dfrac{2A\left(\dfrac{s}{s_{air}}\right)^n s + 2c'\cot\varphi'}{\left(\dfrac{1}{\sin\varphi'} - 1\right)} & \text{for } s_{air} \le s \le s_{res} \\[4ex] \dfrac{2A\left(\dfrac{s_{res}}{s_{air}}\right)^n s_{res} + 2c'\cot\varphi'}{\left(\dfrac{1}{\sin\varphi'} - 1\right)} & \text{for } s > s_{res} \end{cases} \qquad (5.19)$$

where s_{res} is the suction of the start of residual desaturation.

Eq. 3.19 was also used to calculate φ^b for UCS data obtained in this research. It was confirmed that for the methodology used in the present study Eqs. 3.19 and 5.16 are equivalent and $\chi = \tan\varphi^b/\tan\varphi'$. The values of φ^b are plotted for average suctions for all tested specimens in Fig. 5.31.
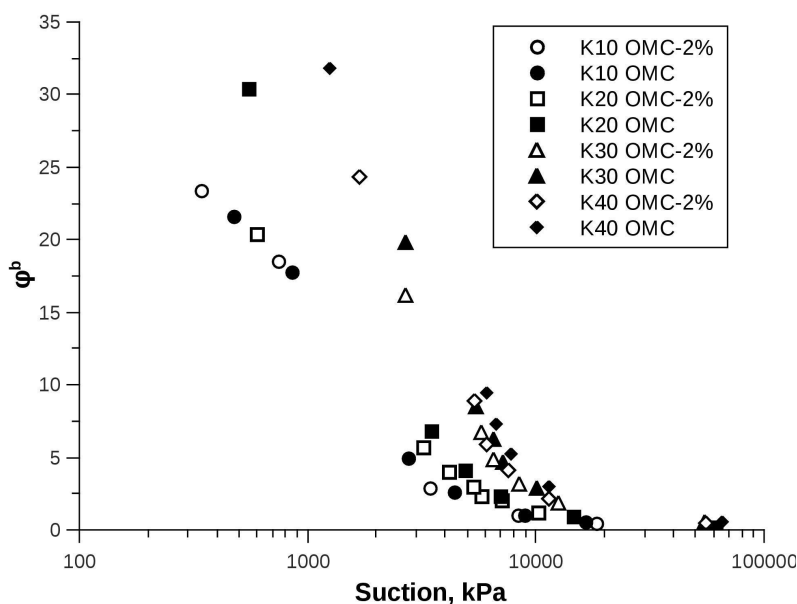
Fig. 5.31 Values of φ^b for average suctions for all tested specimens

Using Eq. 5.18 with the best fir A and n parameters for each sample density, an evaluation of the influence of suction on the UCS of the studied mixes was made with respect to changes in clay content. UCS of the specimens produced with all soil mixes at OMC and OMC-2% was calculated for the suctions of 5000, 7500 and 10000 kPa. The results are shown in Fig. 5.32.
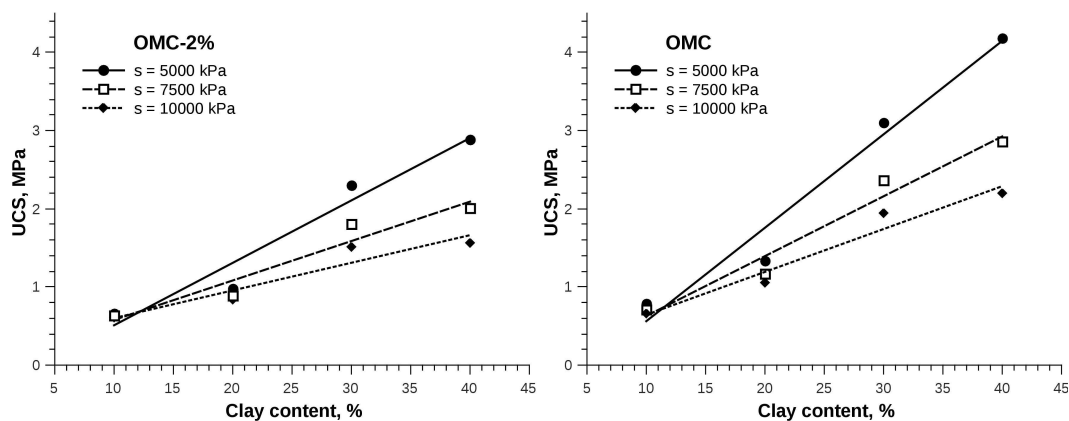
Fig. 5.32 Influence of clay content and suction on the UCS of the specimens compacted at OMC-2% and OMC

The influence of suction on the unconfined compressive strength of the specimens increases with the addition of clay. For all soil mixes this influence increases with the increase in dry density.

6
Conclusions

In the present study the effect of suction and clay content on the strength of compressed earth blocks was evaluated. CEBs were represented by statically compacted cylindrical specimens. Artificial soil mixes were used in order to facilitate the control of particle size distributions. Building sand and quartz powder were chosen to represent inert fraction and kaolinitic clay was employed as an active fine fraction.

To verify the influence of clay content on the strength of the CEBs the specimens containing 10, 20, 30 and 40% of clay were tested. Mixes containing 10 and 20% percent of fine fraction were in agreement with the existing PSD recommendations for CEBs. The other two mixes had clay contents higher than recommended. By using these soil mixes it was investigated if the existing specifications based on PSD could guarantee stronger materials.

Compaction curves obtained in static compaction tests had a shape which didn't allow to determine optimum moisture content in its traditional sense. Instead OMC was defined as the boundary between compaction and consolidation. Two compaction water contents, corresponding to static OMC and OMC-2%, were used for each mix in order to produce specimens with different densities. A number of studies used Proctor compaction tests to determine OMC for CEB production. It was shown that this approach can lead to erroneous results, as static and dynamic compaction are not directly comparable.

Soil water retention curves were obtained using a combination of filter paper and dewpoint potentiometer techniques. All the specimens demonstrated bimodal structure having two air entry values. This is hypothesized that this fact was a consequence of the compaction method used, as it is difficult to break clay aggregates in static compaction. In comparison to the majority of natural soils, the studied samples had very low residual moisture contents, which influenced their strength.

The shape of SWRCs was greatly influenced by clay content, while the

changes in density had little effect. In general the value of the air entry suction increased with the addition of clay and increasing density. It is hypothesized that by analyzing the behavior of SWRCs with respect to different PSD and densities it is possible to develop a methodology that would allow the production of earthen materials specially designed to improve indoor climate of buildings.

The influence of suction and clay content on compressive and tensile strengths of statically compacted specimens was studied by conducting UCS and Brazilian tests. The desired values of suction were inferred by regulating water content of the specimens. A trend opposite to the findings reported in the majority of relevant studies was observed. Instead of steady increase, both unconfined compressive and tensile strengths had a peak corresponding to suction approximately equal to second air entry value. Following the increase in suction, the strength dropped until reaching a more or less constant value. This happened approximately at the transition to residual desaturation zone. This behavior can be explained by the dessication of clay aggregates that may provoke fissures and consequently reduce material strength.

The specimens with higher clay content had higher values of UCS and tensile strength. Thus existing recommendations for choosing soil PSD didn't apply to the material used. It can be concluded that granulometry only is not sufficient for the evaluation of soil suitability for construction purposes.

The specimens with greater densities had higher strength only for the same clay content. In general, an inverse trend was observed, as for the same compactive effort, the soils with lower densities were stronger due to greater amount of fine fraction.

The findings showed that unsaturated behavior of compacted soils is complex and the conclusions have to be made with caution. The characteristics of the earthen construction materials depend strongly on their structure, i.e. on the type of compaction and water content on production. Thus the unsaturated behavior of rammed earth may significantly differ from that of CEBs. Taking into consideration equal popularity of the two construction methods, more research should be dedicated to compressed earth blocks.

Finally, an attempt to predict UCS of the studied samples was made using effective stress equation for unsaturated soils. The applicability of the empirical method of the determination of unsaturated effective stress parameter using soil

air entry value was also evaluated. For this triaxial tests were performed in order to obtain saturated effective stress parameters for the specimens of all densities and clay contents. Unsaturated effective stress parameter was calculated using experimental data form UCS tests using Bishop's equation. It was concluded that for the results of the present study the empirical equation for the calculation of χ is applicable only for the suctions ranging from second air entry value to the start of residual desaturation zone. It was proposed to complement the equation with the condition that for the suctions higher than approximately the boundary between transition and residual zones UCS continues constant.

For the future studies it is proposed to:

- Evaluate the behavior of CEBs with other types of clay minerals,

- Study the influence of the type of compaction on unsaturated strength of the same materials,

- Evaluate the effect of changing proportions of inert fraction components and the shape of sand grains,

- Provide a comprehensive methodology that would allow to create specially designed earthen materials that can be used to improve the quality of indoor air,

- Check the applicability of unsaturated effective stress criterion and the empirical method of the determination of unsaturated effective stress parameter for a compacted soil that doesn't have a decrease in strength following the increase in suction.

7
References

[1]   F. Pacheco-Torgal and S. Jalali, "Earth construction: Lessons from the past for future eco-efficient construction," *Constr. Build. Mater.*, vol. 29, pp. 512–519, Apr. 2012.

[2]   F. P. Torgal and S. Jalali, *Eco-efficient Construction and Building Materials*. London: Springer, 2011.

[3]   Paola Sassi, *Strategies for Sustainable Architecture*. New York: Taylor & Francis, 2006.

[4]   G. J. Treloar, C. Owen, and R. Fay, "Environmental assessment of rammed earth construction systems," *Struct. Surv.*, vol. 19, no. 2, pp. 99–105, 2001.

[5]   A. Alcorn, "Embodied Energy and CO2 Coefficients for NZ Building Materials," Wellington, 2001.

[6]   A. Manzano-Ramíres, J. P. Piñón, and K. Ghavami, "Characterization of Clay for Human Habitat," in *International Symposium on Earthen Structures*, 2007, no. August, pp. 22–24.

[7]   G. Minke, *Building with earth*. Basel: Birkhäuser, 2006.

[8]   A.-T. Nguyen, Q.-B. Tran, D.-Q. Tran, and S. Reiter, "An investigation on climate responsive design strategies of vernacular housing in Vietnam," *Build. Environ.*, vol. 46, no. 10, pp. 2088–2106, Oct. 2011.

[9]   H. Houben, "Ecological and energy-saving advantages and benefits of building with earth," in *Environmental Aspects of Construction with Waste Materials*, 1996.

[10] P. J. Walker, "Strength and Erosion Characteristics of Earth Blocks and Earth Block Masonry," *J. Mater. Civ. Eng.*, no. October, pp. 497–506, 2004.

[11] S. Deboucha and R. Hashim, "A review on bricks and stabilized compressed earth blocks," *Sci. Res. Essays*, vol. 6, no. 3, pp. 499–506, 2011.

[12] P. G. Hammond and C. Jones, "Inventory of Carbon & Energy (ICE) Version 2.0," 2011.

[13] H. Houben and H. Guillaud, *Earth construction*. London: Intermediate

Technology Publications, 1994.

[14]   S. Pollock, *Ancient Mesopotamia*. Cambridge University Press, 1999.

[15]   H. Niroumand and M. Jamil, "The Earth Refrigerators as Earth Architecture," vol. 1, pp. 187–190, 2011.

[16]   K. Ghavami, "Materiais e Tecnologias não Convencionais para o Século XXI," in *I Congresso Luso-Brasileiro de Materiais de Construção Sustentáveis*, 2014.

[17]   Vahid Ghobadian, *Climatic Analysis of Traditional Iranian Buildings*. Tehran: Tehran University Press, 1995.

[18]   D. Easton, *The Rammed Earth House*. White River Junction: Chelsea Green Pub. Co., 1996.

[19]   A. Heath, P. Jaquin, P. Walker, and M. Lawrence, "Render-induced cracking of earth masonry," *Struct. Build.*, 2011.

[20]   R. Rael, *Earth Architecture*. New York: Princeton Architectural Press, 2010.

[21]   S. Sheweka, "Using Mud Bricks as a Temporary Solution for Gaza Reconstruction," *Energy Procedia*, vol. 6, pp. 236–240, Jan. 2011.

[22]   A. M. Assallay, C. D. F. Rogers, I. J. Smalley, and I. F. Jefferson, "Silt: 2–62 μm, 9–4 φ," *Earth Sci. Rev.*, vol. 45, pp. 61–88, 1998.

[23]   N. Samtani and E. Nowatzki, "Soils and Foundations. Reference Manual," 2006.

[24]   B. Das, *Advanced Soil Mechanics*, Third Edit. London: Taylor & Francis Group, 2008.

[25]   T. W. Lambe and R. V. Whitman, *Soil Mechanics*. New York: John Wiley & Sons, Ltd, 1969.

[26]   J. C. Santamarina, G. Tech, G. C. Cho, and S. Korea, "Soil behaviour : The role of particle shape," in *The Skempton Conference*, 2004, pp. 1–14.

[27]   J. K. Mitchell and K. Soga, *Fundamentals of Soil Behavior*. New York: Wiley, 2005.

[28]   M. R. Cox and M. Budhu, "A practical approach to grain shape quantification," *Eng. Geol.*, vol. 96, no. 1–2, pp. 1–16, Jan. 2008.

[29]   R. Grim, *Clay Mineralogy*, Second Edi. New York, 1968.

[30]   C. Beckett, "The Role of Material Structure in Compacted Earthen Building Materials: Implications for Design and Construction," Durham University, 2011.

[31] H. Murray, *Applied clay mineralogy*. Amsterdam: Elsevier, 2007.

[32] W. Powrie, *Soil Mechanics: concepts and Applications*, Second Edi. Oxford: Spon Press, 2008.

[33] "Kaolinite image." [Online]. Available: http://webmineral.com/specimens/picshow.php?id=1283&target=Kaolinite. [Accessed: 20-Oct-2014].

[34] R. E. Grim, "Clay Mineralogy: The clay mineral composition of soils and clays is providing an understanding of their properties.," *Science*, vol. 135, no. 3507, pp. 890–8, Mar. 1962.

[35] M. Division, "Clay mineralogy and chemistry of halloysite and alunite deposits in the Turplu area, Balikesir, Turkey," *Clays Clay Miner.*, vol. 55, no. 1, pp. 18–35, Feb. 2007.

[36] "Montmorillonite image." [Online]. Available: ttp://webmineral.com/specimens/picshow.php?id=1285. [Accessed: 20-Oct-2014].

[37] "Illite image." [Online]. Available: http://webmineral.com/specimens/picshow.php?id=1284. [Accessed: 20-Oct-2014].

[38] "Chlorite image." [Online]. Available: http://www.petrotech-assoc.com/images/Chlorite_1.jpg. [Accessed: 20-Oct-2014].

[39] M. N. Çaġatay, "Palygorskite in the Eocene Rocks of the Dammam Dome, Saudi Arabia," *Clays Clay Miner.*, vol. 38, no. 3, pp. 299–307, 1990.

[40] R. Brewer and J. Sleeman, *Soil Structure and Fabric*. Adelaide, Australia: CSIRO Publishing, 1988.

[41] V. Osipov, V. Sokolv, and N. Rumyantseva, *Mikrostrukrura Glinistih Porod*. Moscow: Nedra, 1989.

[42] A. Tarantino, "A water retention model for deformable soils," *Géotechnique*, vol. 59, no. 9, pp. 751–762, Jan. 2009.

[43] S. Olivella, E. E. Alonso, J. Vaunat, and J.-M. Pereira, "A microstructurally based effective stress for unsaturated soils," *Géotechnique*, vol. 60, no. 12, pp. 913–925, Jan. 2010.

[44] P. Jaquin, D. G. Toll, D. Gallipoli, and C. E. Augarde, "The strength of unstabilised rammed earth materials," *Géotechnique*, vol. 59, no. 5, pp. 487–490, Jan. 2009.

[45] D. Gallipoli, A. W. Bruno, C. Perlot, and N. Salmon, "Raw earth construction: is there a role for unsaturated soil mechanics?," in

PUC-Rio - Certificação Digital Nº 1112056/CA

Unsaturated Soils: Research & Applications, 2014, pp. 55–62.

[46] D. Ciancio, P. Jaquin, and P. Walker, "Advances on the assessment of soil suitability for rammed earth," *Constr. Build. Mater.*, vol. 42, pp. 40–47, May 2013.

[47] K. P. Panayiotopoulos, "Packing of Sands - A Review," *Soil Tillage Res.*, vol. 13, pp. 101–121, 1989.

[48] C. Voivret, F. Radjai, J. Delenne, and M. S. El Youssoufi, "Multiscale Force Networks in Highly Polydisperse Granular Media," *Phys. Rev. Lett.*, vol. 102, 2012.

[49] J. C. Santamarina, "Soil Behavior at the Microscale: Particle Forces," in *Proc. Symp. Soil Behavior and Soft Ground Construction, in honor of Charles C. Ladd*, 2001, no. October, pp. 1–32.

[50] D. G. Toll, S. D. N. Lourenço, P. C. Fisher, D. Gallipoli, a. Congreve, and C. E. Augarde, "Formation and evolution of water menisci in unsaturated granular media," *Géotechnique*, vol. 62, no. 3, pp. 193–199, Mar. 2012.

[51] R. Grim and F. Cuthbert, "The bonding action of clays," *Univ. Illinois Bull.*, vol. 42, no. 50, p. 64, 1946.

[52] A. Gens, "47th Rankine Lecture. Soil - environment interactions in geotechnical engineering," *Géotechnique*, vol. 60, no. 1, pp. 3–74, 2010.

[53] D. G. Fredlund and A. Xing, "Equations for the soil-water characteristic curve," *Can. Geotech. J.*, vol. 31, no. 3, pp. 521–532, 1994.

[54] G. E. Blight, *Unsaturated Soil Mechanics in Geotechnical Practice*. London: Taylor & Francis Group, 2013.

[55] S. K. Vanapalli, D. G. Fredlund, and D. E. Pufahl, "The influence of soil structure and stress history on the soil-water characteristics of a compacted till," *Geotechnique*, vol. 49, no. 2, pp. 143–159, 1999.

[56] R. H. Brooks and A. T. Corey, "Hydraulic properties of porous media." Colorado State University, Fort Collins, 1964.

[57] M. T. Van Genuchten, F. J. Leiji, and S. R. Yates, "The RETC Code for Quantifying the Hydraulic Functions of Unsaturated Soils," Ada, Oklahoma, 1991.

[58] M. T. Van Genuchten, "A closed-form equation for predicting the hydraulic conductivity of unsaturated soils," *Soil Sci. Soc. Am. J.*, vol. 44, no. 5, pp. 892–898, 1980.

[59] K. Kosugi, "Three-parameter lognormal distribution model for soil water retention," *Water Resour. Res.*, vol. 30, no. 4, pp. 891–901, 1994.

[60] W. Durner, "Hydraulic conductivity estimation for soils with heterogeneous pore structure," *Water Resour. Res.*, vol. 30, no. 2, pp. 211–223, 1994.

[61] Rudiyanto, M. Sakai, M. T. van Genuchten, A. A. Alazba, B. I. Setiawan, and B. Minasny, "A complete soil hydraulic model accounting for capillary and adsorptive water retention, capillary and film conductivity, and hysteresis," *Water Resour. Res.*, 2015.

[62] R. Haverkamp and J. Y. Parlange, "Predicting the Water-Retention Curve From Particle-Size Distribution: 1. Sandy Soils Without Organic Matter," *Soil Sci.*, vol. 6, pp. 325–339, 1986.

[63] K. Seki, "SWRC fit – a nonlinear fitting program with a water retention curve for soils having unimodal and bimodal pore structure," *Hydrol. Earth Syst. Sci. Discuss.*, vol. 4, pp. 407–437, 2007.

[64] C. T. S. Beckett and C. Augarde, "The Effect of Relative Humidity and Temperature on the Unconfined Compressive Strength of Rammed Earth," *Unsaturated Soils Res. Appl.*, pp. 1–23, 2012.

[65] A. W. Bishop, "The principle of effective stress," *Tecknish Ukebl.*, vol. 106, pp. 859–863, 1959.

[66] N. Khalili and Khabbaz M, "A unique relationship for Chi for the determination of the shear strength of unsaturated soils," *Géotechnique*, vol. 48, no. 5, pp. 681–687, 1998.

[67] D. G. Fredlund, N. R. Morgenstern, and R. A. Widger, "The shear strength of unsaturated soils," *Can. Geotech. J.*, vol. 15, no. 3, pp. 313–321, 1978.

[68] S. K. Vanapalli, D. E. Pufahl, and D. G. Fredlund, "Interpretation of the shear strength of unsaturated soils in undrained loading conditions," in *Proceedings of the 52nd Canadian Geotechnical Conference*, 1999, pp. pp. 643–650.

[69] S. K. Vanapalli, D. G. Fredlund, D. E. Pufahl, and A. W. Clifton, "Model for the prediction of shear strength with respect to soil suction," *Can. Geotech. J.*, vol. 33, no. 3, pp. 379–392, 1996.

[70] N. Lu and W. J. Likos, "Suction Stress Characteristic Curve for Unsaturated Soil," *J. Geotech. Geoenvironmental Eng.*, vol. 132, no. 2, pp. 131–142, 2006.

[71] X. Li, H. Wen, B. Muhunthan, and J. Wang, "Modeling and Prediction of the Effects of Moisture on the Unconfined Compressive and Tensile Strength of Soils," *J. Geotech. Geoenvironmental Eng.*, vol. 141, no. 7, 2015.

[72] S. Assouline, "Modeling the Relationship between Soil Bulk Density and the Water Retention Curve," *Vadose Zo. J.*, vol. 5, no. 2, p. 554, 2006.

[73] N. Khalili, R. Witt, L. Laloui, L. Vulliet, and A. Koliji, "Effective stress in double porous media with two immiscible fluids," *Geophys. Res. Lett.*, vol. 32, no. August, pp. 2–6, 2005.

[74] P. A. Jaquin, C. E. Augarde, and L. Legrand, "Unsaturated characteristics of rammed earth," in *Unsaturated Soils: Advances in Geo-Engineering*, 2008, no. 1995, pp. 417–422.

[75] N. Lu, M. Asce, and W. J. Likos, "Suction Stress Characteristic Curve for Unsaturated Soil," no. February, pp. 131–142, 2006.

[76] N. Lu, "Is Matric Suction a Stress Variable?," *J. Geotech. Geoenvironmental Eng.*, vol. 134, no. 7, pp. 899–905, 2008.

[77] J. F. Kennedy, Ed., *Building Without Borders: Sustainable Construction for The Global Willage*. New Society Publishers, 2004.

[78] R. Rael, "Tebogo Home for Handicapped Children," 2008. [Online]. Available: http://eartharchitecture.org/index.php?/archives/955-Tebogo-Home-for-Handicapped-Children.html.

[79] "The Beehive Enigma," *Saudi Aramco World*, vol. 18, no. 6, pp. 8 – 9, 1967.

[80] L. Alter, "How To Live Without Air Conditioning: Syrian Beehive Houses," 2009. [Online]. Available: http://www.treehugger.com/sustainable-product-design/how-to-live-without-air-conditioning-syrian-beehive-houses.html.

[81] T. Morton, F. Stevenson, B. Taylor, and N. Smith, "Low cost earth brick construction," 2005.

[82] V. Bokalders and M. Block, *The Whole Building Handbook*. London: Earthscan.

[83] P. Jaquin, "Humidity regulation in earth buildings," in *Ramboll Technical Forum*, 2009.

[84] S. Liuzzi, M. R. Hall, P. Stefanizzi, and S. P. Casey, "Hygrothermal behaviour and relative humidity buffering of unfired and hydrated lime-stabilised clay composites in a Mediterranean climate," *Build. Environ.*, vol. 61, pp. 82–92, Mar. 2013.

[85] A. M. Memari, S. V. Grossenbacher, and L. D. Iulo, "Structural Testing of High Thermal Mass Walls Used in Sustainable Designs," *Struct. Congr. 2008*, pp. 1–9, Oct. 2008.

[86] P. Vega, A. Juan, M. Ignacio Guerra, J. M. Morán, P. J. Aguado, and B. Llamas, "Mechanical characterisation of traditional adobes from the north of Spain," *Constr. Build. Mater.*, vol. 25, no. 7, pp. 3020–3023, Jul. 2011.

[87] M. R. Hall and D. Allinson, "Evaporative drying in stabilised compressed earth materials using unsaturated flow theory," *Build. Environ.*, vol. 45, no. 3, pp. 509–518, Mar. 2010.

[88] M. C. J. Delgado and Ignacio Cañas Guerrero, "The selection of soils for unstabilised earth building: A normative review," *Constr. Build. Mater.*, vol. 21, no. 2, pp. 237–251, Feb. 2007.

[89] V. Maniatidis and P. Walker, "A Review of Rammed Earth Construction - DTi Partners in Innovation Project 'Developing Rammed Earth for UK Housing,'" 2003.

[90] V. S. Burroughs, "Quantitative criteria for the selection and stabilisation of soils for rammed earth wall construction," University of New South Wales, 2001.

[91] M. Hall and Y. Djerbib, "Rammed earth sample production: context, recommendations and consistency," *Constr. Build. Mater.*, vol. 18, no. 4, pp. 281–286, May 2004.

[92] H. Houben, V. Rigassi, and P. Garnier, *Compressed earth blocks production equipment*, Second Edi. Brussels: CRATerre-EAG, 1996.

[93] K. H. Head, *Manual of Soil Laboratory Testing Volume 1: Soil Classification and Compaction Tests*, Third Edit. Dunbeath: Whittles Publishing, 2006.

[94] R. L. Sloane and T. R. Kell, "The fabric of mechanically compacted kaolin," in *Fourteenth National Conference on Clays and Clay Minerals*, 1966, no. 1932.

[95] O. M. D. E. Oliveira, "Estudo sobre a resistência ao cisalhamento de um solo residual compactado não saturado," Universidade de São Paulo, 2004.

[96] A. R. Bagherieh, N. Khalili, G. Habibagahi, and A. Ghahramani, "Drying response and effective stress in a double porosity aggregated soil," *Eng. Geol.*, vol. 105, no. 1–2, pp. 44–50, 2009.

[97] D. G. Toll, "The Influence of Fabric on the Shear Behaviour of Unsaturated Compacted Soils," in *Advances in Unsaturated Geotechnics*, 2000, vol. 639798, pp. 222–234.

[98] D. G. Toll and B. H. Ong, "Critical-state parameters for an unsaturated residual sandy clay," *Géotechnique*, vol. 53, no. 1, pp. 93–103, 2003.

[99] S. P. Wright, P. J. Walden, C. M. Sangha, and J. N. Langdon, "Observations on soil permeability, moulding moisture content and dry density relationships," *Q. J. Eng. Geol.*, vol. 29, no. 3, pp. 249–255, 1996.

[100] U. S. Army Corps of Engineers, "Soil Compaction Investigation Report No. 1. Compaction Studies on Clayey Sands Technical Memorandum No. 3.271," Vicksburg, Mississippi, 1949.

[101] V. Maniatidis and P. Walker, "Structural Capacity of Rammed Earth in Compression," *J. Mater. Civ. Eng.*, vol. 20, no. March, pp. 230–239, 2008.

[102] M. Olivier, "Le matériau terre Essai de compactage statique pour la fabrication de briques de terre compressées," pp. 37–43, 1986.

[103] W. J. Turnbull, "Compaction and strength tests on soils," Vicksburg, Mississippi, 1950.

[104] C. H. Kouakou and J. C. Morel, "Strength and elasto-plastic properties of non-industrial building materials manufactured with clay as a natural binder," *Appl. Clay Sci.*, vol. 44, no. 1–2, pp. 27–34, Apr. 2009.

[105] W. D. Lawson, C. Kancharla, and P. W. Jayawickrama, "Engineering Properties of Unstabilized Compressed Earth Blocks," in *Geo-Frontiers 2011: Advances in Geotechnical Engineering*, 2011, pp. 2679–2688.

[106] B. V. V. Reddy and K. S. Jagadish, "The static compaction of soils," *Géotechnique*, vol. 43, no. 2, pp. 337–341, 1993.

[107] A. R. A. G. Pinto, "Fibras de curauá e sisal como reforço em matrizes de solo," Pontifícia Universidade Católica do Rio de Janeiro, 2008.

[108] M. Olivier, "Discussion: The static compaction of soils," *Géotechnique*, vol. 45, no. 0, pp. 363–367, 1995.

[109] A. Mesbah, J. C. Morel, and M. Olivier, "Comportement des sols fins argileux pendant un essai de compactage statique : détermination des paramètres pertinents," *Mater. Struct.*, vol. 32, pp. 687–694, 1999.

[110] A. Tarantino and E. De Col, "Compaction behaviour of clay," *Géotechnique*, vol. 58, no. 3, pp. 199–213, Jan. 2008.

[111] Q.-B. Bui, J.-C. Morel, S. Hans, and N. Meunier, "Compression behaviour of non-industrial materials in civil engineering by three scale experiments: the case of rammed earth," *Mater. Struct.*, vol. 42, no. 8, pp. 1101–1116, Oct. 2008.

[112] J.-C. Morel, A. Pkla, and P. Walker, "Compressive strength testing of compressed earth blocks," *Constr. Build. Mater.*, vol. 21, no. 2, pp. 303–309, Feb. 2007.

[113] J. E. E. Aubert, A. Fabbri, J. C. C. Morel, and P. Maillard, "An earth block with a compressive strength higher than 45MPa!," *Constr. Build. Mater.*, vol. 47, pp. 366–369, 2013.

[114] Q.-B. Bui, J.-C. Morel, S. Hans, and P. Walker, "Effect of moisture content on the mechanical characteristics of rammed earth," *Constr. Build. Mater.*, vol. 54, pp. 163–169, Mar. 2014.

[115] H. Nowamooz and C. Chazallon, "Finite element modelling of a rammed earth wall," *Constr. Build. Mater.*, vol. 25, no. 4, pp. 2112–2121, Apr. 2011.

[116] C. T. S. Beckett and C. E. Augarde, "Development of microstructure in compacted earthen building materials," in *Unsaturated Soils*, 2011, pp. 139–144.

[117] ASTM International, "ASTM D5298-94, Standard Test Method for Measurement of Soil Potential (Suction) Using Filter Paper." West Conshohocken, PA, 1994.

[118] R. Bulut and E. C. Leong, "Indirect Measurment of Suction," in *Laboratory and Field Testing of Unsaturated Soils*, A. Tarantino, E. Romero, and Y.-J. Cui, Eds. Springer Science, 2009, pp. 21–32.

[119] R. J. Chandler, M. S. Crilly, and G. Montgomery-Smith, "A Low-cost Method Of Assessing Clay Desiccation For Low-rise Buildings," *Proc. Inst. Civ. Eng. - Civ. Eng.*, vol. 92, no. 2, pp. 82–89, 1992.

[120] F. A. M. Marinho, "Medição de sucção com o método do papel filtro," in *X Congresso Brasileiro de Mecânica dos Solos e Engenharia de Fundações*, 1994, pp. pp. 515–522.

[121] K. V. Bicalho, A. C. Chrystello, K. F. Cupertino, a J.-M. Fleureau, and Antonio G. Correia, "Study of suction-water content calibrations for the Whatman No. 42 filter paper," in *From Fundamentals to Applications in Geotechnics*, 2015, vol. 42, no. 42, pp. 2071–2077.

[122] C. Fairhurst, "On the validity of the 'Brazilian' test for brittle materials," *Int. J. Rock Mech. Min. Sci.*, vol. 1, pp. 535–546, 1964.

[123] ASTM, "ASTM D3967 - 08 Standard Test Method for Splitting Tensile Strength of Intact Rock Core Specimens." 2008.

[124] ASTM, "D 2166-00 Standard Test Method for Unconfined Compressive Strength of Cohesive Soil." 2000.

[125] K. H. Head, *Effective Stress Tests, Volume 3, Manual of Soil Laboratory Testing*, 2nd ed. John Wiley & Sons, 1998.

[126] L. C. Bertolino, M. L. Torem, R. Scorzelli, and A. Rossi, "Caracterização

Mineralógica e Beneficiamento do Caulim de Prado (BA)," *HOLOS*, vol. 5, no. 0, pp. 83–92, 2012.

[127] T. O. A. Pessôa, "Avaliação da Influência da Mineralogia , Índice de Vazios e Teor de Umidade em Propriedades Térmicas de Solos," Pontifícia Universidade Católica do Rio de Janeiro, 2006.

[128] ABNT, "NBR 7181 - Solo - análise granulométrica." 1984.

[129] ABNT, "NBR 6508 - Solo - determinação da massa específica dos grãos." 1984.

[130] ABNT, "NBR 6459 - Solo - determinação do limite de liquidez." 1984.

[131] ABNT, "NBR 7180 - Solo - determinação do limite de plasticidade." 1984.

[132] ABNT, "NBR 7182 - Solo - ensaio de compactação." 1986.

[133] D. Sheng, "Review of fundamental principles in modelling unsaturated soil behaviour," *Comput. Geotech.*, vol. 38, no. 6, pp. 757–776, 2011.

[134] E. Birle, D. Heyer, and N. Vogt, "Influence of the initial water content and dry density on the soil–water retention curve and the shrinkage behavior of a compacted clay," *Acta Geotech.*, vol. 3, no. 3, pp. 191–200, Apr. 2008.

[135] O. Cuisinier and L. Laloui, "Fabric evolution during hydromechanical loading of a compacted silt," *Int. J. Numer. Anal. Methods Geomech.*, vol. 28, no. 6, pp. 483–499, 2004.

[136] A.-N. Spiess and N. Neumeyer, "An evaluation of R2 as an inadequate measure for nonlinear models in pharmacological and biochemical research: a Monte Carlo approach," *BMC Pharmacol.*, vol. 10, no. 1, 2010.

[137] C. E. Mullins and K. P. Panayiotopoulos, "The strength of unsaturated mixtures of sand and kaolin and the concept of effective stress," *J. Soil Sci.*, vol. 35, pp. 459–468, 1984.

[138] M. F. Benessiuti, G. D. P. Bernardes, P. Ivo, and M. Camarinha, "Influência da sucção matricial na resistência à tração de solos residuais de gnaisse compactados," in *COBRAMSEG 2010*, 2010.

[139] L. F. S. Villar, T. M. P. de Campos, and J. G. Zornberg, "Relação Entre a Resistência a Tração Obtida via Ensaio Brasileiro, a Sucção e Índices Físicos de um Solo," in *VI Simpósio Brasileiro de Solos Não Saturados*, 2007, pp. 421–432.

[140] ASTM International, "ASTM D3148-96, Standard Test Method for Elastic Moduli of Intact Rock Core Specimens in Uniaxial Compression." Conshohocken, USA, 2002.